

Ph.D Thesis

Preparation and Study of Optical Properties of CdS, CdS-TiO₂ and CdS-Au Nanocomposites for Photonic Applications



Mathew S

**International School of Photonics
Cochin University of Science and Technology**

**Preparation and Study of Optical Properties
of CdS, CdS-TiO₂ and CdS-Au Nanocomposites for
Photonic Applications**

Ph. D. Thesis submitted to

Cochin University of Science and Technology

In partial fulfilment of the requirements for the award of the Degree of

Doctor of Philosophy

Mathew. S.

Reg. No: 3391



**International School of Photonics
Faculty of Technology
Cochin University of Science and Technology
Cochin -682022, Kerala, India**

February 2015

Preparation and Study of Optical Properties of CdS, CdS-TiO₂ and CdS-Au Nanocomposites for Photonic Applications

Ph D thesis in the field of Photonics

Author:

Mathew S.
Research Fellow
International School of Photonics
Cochin University of Science & Technology
Cochin -682022, Kerala, India
mathewphys@gmail.com

Research Advisor:

Dr. C. P. Girijavallbhan
Emeritus Professor
International School of Photonics
Cochin University of Science & Technology
Cochin -682022, Kerala, India
vallabhan@cusat.ac.in, gvallabhan@gmail.com

International School of Photonics
Cochin University of Science & Technology
Cochin -682022, Kerala, India
www.photonics.cusat.edu

February 2015

Cover image: *Selected image of prepared Nanostructure*

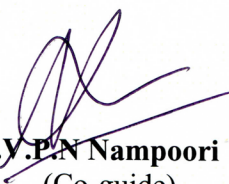
*Dedicated to God Almighty,
my parents and sister, teachers and
well-wishers*

**INTERNATIONAL SCHOOL OF PHOTONICS
COCHIN UNIVERSITY OF SCIENCE AND TECHNOLOGY
COCHIN -682022, KERALA, INDIA**

Certificate

This is to certify that the thesis entitled “**Preparation and Study of Optical Properties of CdS, CdS-TiO₂ and CdS-Au Nanocomposites for Photonic Applications**” submitted by **Mr. Mathew. S.**, is an authentic record of research work carried out by him under my guidance and supervision in partial fulfilment of the requirement of the degree of Doctor of Philosophy of Cochin University of Science and Technology, under the Faculty of Technology and has not been included in any other thesis submitted previously for the award of any degree.

*Kochi-682022
25 - 02- 2015*


Dr. Y.P.N Nampoore
(Co-guide)


Dr. C.P. Girijavallabhan
(Supervising guide)

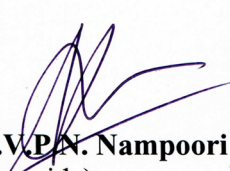
Phone: +91 484 2575848 Fax: 0091-484-2576714.
Email: vallabhan@cusat.ac.in, gvallabhan@gmail.com

INTERNATIONAL SCHOOL OF PHOTONICS
COCHIN UNIVERSITY OF SCIENCE AND TECHNOLOGY
COCHIN -682022, KERALA, INDIA

Certificate

This is to certify that the thesis entitled “**Preparation and Study of Optical Properties of CdS, CdS-TiO₂ and CdS-Au Nanocomposites for Photonic Applications**” submitted by **Mr. Mathew. S**, has incorporated all the relevant corrections and modifications suggested by the audience during the pre-synopsis seminar and recommended by the Doctoral Committee.

Kochi-682022
25- 02- 2015


Dr. V.P.N. Nampoori
(Co-guide)


Dr. C.P. Girijavallabhan
(Supervising guide)

Phone: +91 484 2575848 Fax: 0091-484-2576714.
Email: vallabhan@cusat.ac.in, gvallabhan@gmail.com

Declaration

I, Mathew.S, do hereby declare that the thesis entitled "Preparation and Study of Optical Properties of CdS, CdS-TiO₂ and CdS-Au Nanocomposites for Photonic Applications" is a genuine record of research work done by me under the supervision of Dr. C.P. Girijavallabhan, Professor, International School of Photonics, Cochin University of Science and Technology, Kochi-22, India and it has not been included in any other thesis submitted previously for the award of any degree.

Kochi- 682022
25- 02- 2015



Mathew.S

Acknowledgements

I am indebted to many individuals who have provided assistance and support during the period of this research.

First and foremost, I would like to express my sincere gratitude to my supervisor Dr. C.P.Girjavallabhan, Emeritus Professor, International School of Photonics (ISP), for giving me an opportunity to work under his guidance. His inspiration, encouragement, constant support and valuable suggestions have gone a long way in the completion of my work. His extraordinary attention to detail and endless efforts in reviewing this thesis and many manuscripts are highly appreciated.

I would like to thank Prof. V. P. N. Nampoory, Professor Emeritus, International School of Photonics, for his encouragement and constructive remarks in the course of my Ph D studies. His inspiration, encouragement, constant support and valuable suggestions have gone a long way in the completion of my work.

I would like to thank Prof. P. Radhakrishnan, Professor Emeritus, International School of Photonics, for his encouragement and constructive remarks in the course of my Ph D studies. His inspiration, encouragement, constant support and valuable suggestions have gone a long way in the completion of my work.

My sincere thanks goes to Dr. M. Kailasnath, Director, ISP, for his wholehearted support and advice during my doctoral work.

I gratefully thank Dr. V. M. Nandakumaran, Dr. Sheenu Thomas and all other teachers of both ISP and Centre of Excellence in Lasers and Optoelectronic Sciences (CELOS) for the support provided during the years of my Ph D.

My special and sincere thanks to Prof. Jayesh Bellare, Biswajeet Singh India, for helping me in doing characterization work and also for helpful discussions and valuable technical support.

Sincere thanks go to my colleagues Boni Samuel, Adrine Correya, Mr. K. J. Thomas, Dr. Lyjo K. Joseph, Dr. Sheeba Rajesh, Dr. Litty Irimpan, Dr. Manu Punnen John for the support and encouragement that they have provided in all my activities.

I would like to acknowledge other co-scholars of the ISP, in particular, Mr. J. Linesh, Pradeep Chandran, Mr. Libish T.M, Dr. Sony T George, Mr. Linslal, Mr. Bobby Mathews, Mr Bejoy Varghese, Mr. Nideep T K, Sudeesh K, Divya Sasi, Tintu, Aparna Subhash, Sr. Rosmin, Indu Sebastian, Sunitha Sebastian, Sithara and, for all their support

and for creating a very vibrant environment. The group has been a source of friendship as well as good advice and collaboration.

I would like to thank Lab, library and administrative staff of the ISP for the assistance extended during the tenure.

I greatly acknowledge, Mr. Emil Joy and Mr. Shamkumar for their support and encouragement to carry out my Ph. D.

I am also grateful to my parents, sister and uncle whose unfailing support and encouragement allowed me to complete this research program.

Thanks to the Almighty God

Mathew.S

*“The Light shines in the darkness and the darkness
has not overcome it.”*

John 1:5 (The Holy Bible)

Preface

Nanophotonics can be regarded as a fusion of nanotechnology and photonics and it is an emerging field providing researchers opportunities in fundamental science and new technologies. In recent times many new methods and techniques have been developed to prepare materials at nanoscale dimensions. Most of these materials exhibit unique and interesting optical properties and behavior. Many of these have been found to be very useful to develop new devices and systems such as tracers in biological systems, optical limiters, light emitters and energy harvesters. This thesis presents a summary of the work done by the author in the field by choosing a few semiconductor systems to prepare nanomaterials and nanocomposites. Results of the study of linear and nonlinear optical properties of materials thus synthesized are also presented in the various chapters of this thesis. CdS is the material chosen here and the methods and the studies of the detailed investigation are presented in this thesis related to the optical properties of CdS nanoparticles and its composites

The contents of the thesis are described in the following sections.

Chapter 1 provides an introduction to the foundation of nanophotonics. Nanoscale interactions of matter and light are described. Detailed descriptions of optical properties of semiconductor nanocrystals are depicted in this chapter. A brief description of properties of CdS is also included.

Chapter 2 provides an outlook of experimental methods like z-scan, single beam second harmonic generation technique and preparation technique that are adopted in this thesis work. Various characterization techniques such as X-ray diffraction, Photoluminescence, Optical absorption, Transmission electron microscope, Scanning electron microscope, Energy-Dispersive Spectroscopy, etc. are also described.

Chapter 3 consists of preparation of CdS, Au, TiO₂ nanoparticles. From the optical study, excitation wavelength dependence of fluorescence behavior is observed in the case of CdS nanoparticles. Possible mechanism for this behavior is also illustrated. Four bands of emission is observed in the case of TiO₂ colloidal nanoparticles and the mechanism for this emission is also described.

Chapter 4 depicts the second-order nonlinear optical properties of a nanostructured CdS thin film by optical second harmonic generation. CdS thin film preparation and characterization is also described. Polarization dependent studies of CdS thin film are carried out using sub-picosecond pulsed laser system. The relative values of tensor components of the second-order susceptibility are also determined.

Chapter 5 covers the preparation and spectral properties of CdS: Au and CdS:TiO₂ nanocomposites. In this chapter linear and nonlinear optical studies of these nanocomposites in PVA thin films are carried out. The enhancement of nonlinear optical properties of these materials is also discussed.

Chapter 6 explains the optical properties of nanocomposite materials like CdSe-CdS and CdSe-ZnS core-shell quantum dots. Optical limiting analysis of these samples also form the subject matter of this chapter.

Chapter 7 deals with the summary of the findings of the present investigations and future prospects

List of Publications

International Journals

1. **S. Mathew**, Amit kumar Prasad, Thomas Benoy, P. P. Rakesh, Misha Hari, T. M Libish, P. Radhakrishnan, V. P. N. Nampoori, C. P. G. Vallabhan, UV-Visible photoluminescence of TiO₂ nanoparticles prepared by hydrothermal method, *Journal of Fluorescence*, vol.22(6), pp. 1563-1569, 2012.
2. **S. Mathew**, Santhi Ani Joseph, P. Radhakrishnan, V. P. N. Nampoori, C. P. G. Vallabhan, Shifting of fluorescence peak in CdS nanoparticles by Excitation wavelength change, *Journal of Fluorescence*, vol. 21, Issue 4, pp.1479-1484, 2011.
3. **S. Mathew**, Amit D. Saran, Santhi Ani Joseph, Bishwajeet Singh Bhardwaj, Deep Punj, P. Radhakrishnan, V. P. N. Nampoori, C. P. G. Vallabhan, Jayesh R. Bellare, Nonlinear optical characterization and measurement of optical limiting threshold of CdSe quantum dots prepared by a microemulsion technique, *Journal of Materials Science: Materials in Electronics*, vol.23, Issue 3, pp.739-745, 2012.
4. **S. Mathew**, Bishwajeet Singh Bhardwaj, Amit D. Saran, P Radhakrishnan, V P N Nampoori, C P G Vallabhan, Jayesh R. Bellare, Effect of ZnS shell on optical properties of CdSe-ZnS core-shell quantum dots, *Optical materials*, vol.39, pp.45-51, 2015.
5. **S. Mathew**, Amit D. Saran, Bishwajeet Singh Bhardwaj, Santhi Ani Joseph, P. Radhakrishnan, V. P. N. Nampoori, C. P. G. Vallabhan, and Jayesh R. Bellare, Size dependent optical properties of the CdSe-CdS core-shell quantum dots in the strong confinement regime, *J. Appl. Phys.* vol.111, pp.074312, 2012.

Related publications with author's contribution

1. C.L. Linslal, **S. Mathew**, P. Radhakrishnan, V.P.N. Nampoori, C.P. Girijavallabhan, M. Kailasnath, Laser emission from the whispering gallery modes of a graded index fiber, *Optics Letters*, vol.38 (17), pp.3261-3263, 2013.
2. B. Nithyaja, K. Vishnu, **S. Mathew**, P. Radhakrishnan, and V. P. N. Nampoori, Studies on CdS nanoparticles prepared in DNA and bovine serum albumin based bio-templates, *J. Appl. Phys.* vol.112, pp. 064704, 2012.
3. Roseleena Thomas, Vasuja, Misha Hari, Nithyaja. B, **S. Mathew.**, Rejeena. I, Sheenu Thomas, Nampoori. V. P. N and Radhakrishnan. P, Optical limiting in TeO₂-ZnO glass from Z-scan technique, , *Journal of Nonlinear Optical Physics and Materials (JNOPM)*, vol. 20, Issue 3, pp. 351-356, 2011.
4. Pradeep. C, **S. Mathew**, Nithyaja, B., Radhakrishnan, P., & Nampoori, V. P. N. Effect of marine derived deoxyribonucleic acid on nonlinear optical properties of PicoGreen dye, *Applied Physics B*, vol.111(4), pp. 611-615, 2013.
5. Joseph, Santhi Ani, Misha Hari, **S. Mathew**, Gaurav Sharma, V. M. Hadiya, P. Radhakrishnan, and V. P. N. Nampoori, Thermal diffusivity of Rhodamine 6G incorporated in silver nanofluid measured using mode-matched thermal lens technique, *Optics Communications*, vol. 283, pp.313-317, 2010.

6. Santhi Ani Joseph, Misha Hari, **S. Mathew**, Gaurav Sharma; Soumya, Hadiya V M, Radhakrishnan P., Nampoore V. P. N, Laser induced Bessel beams can realize fast al-optical switching in gold nanosol prepared by pulsed laser ablation, *Journal of Optical Society of America B*, vol.27, pp. 577-581, 2010.
7. Santhi Ani Joseph, **S Mathew**, Gourav Sharma, Misha Hari, Achamma Kurian, P. Radhakrishnan, V. P. N. Nampoore, Photothermal characterization of nanogold under conditions of resonant excitation and energy transfer, *Plasmonics*, vol.5, pp.63-68, 2010.
8. M. Sheeba, M. Rajesh, **S. Mathew**, V. P. N. Nampoore, C. P. G. Vallabhan, and P. Radhakrishnan, Side illumination fluorescence emission characteristics from a dye doped polymer optical fiber under two-photon excitation, *Applied Optics*, vol. 47, Issue 11, pp.1913-1921, 2008.
9. V. Arun, **S. Mathew**, P.P. Robinson, M. Jose, V.P.N. Nampoore, K.K.M. Yusuff, The tautomerism, solvatochromism and non-linear optical properties of fluorescent 3-hydroxyquinoxaline-2-carboxalidine-4-aminoantipyrine, *Dyes and Pigments*, 87(2), pp.149–157, 2010.
10. Misha Hari, **S. Mathew**, B. Nithyaja, Santhi Ani Joseph, V.P.N. Nampoore, P. Radhakrishnan Saturable and reverse saturable absorption in aqueous silver nanoparticles at off-resonant wavelength, *Optical and Quantum Electronics*, 43, pp.49-58, 2012.
11. Misha Hari, Santhi Ani Joseph, Nithyaja Balan, **S. Mathew**, Ravi Kumar, Giridhar Mishra, R. R. Yadhav, P. Radhakrishnan, V. P. N. Nampoore, Linear And nolinear optical properties Of gold nanoparticles stabilized With polyvinyl alcohol, *Journal of Nonlinear Optical Physics & Materials*, 20, pp.467-475, (2011).

12. Misha Hari, Santhi Ani Joseph, **S. Mathew**, B Nithyaja, V. P. N. Nampoori, P. Radhakrishnan, Thermal diffusivity of nanofluids composed of rod-shaped silver nanoparticles, *International Journal of Thermal Sciences*, vol.64, pp. 188-194, 2013.
13. Misha Hari, Santhi Ani Joseph, **S. Mathew**, P. Radhakrishnan, and V. P. N. Nampoori, Band-gap tuning and nonlinear optical characterization of Ag:TiO₂ nanocomposites, *J. Appl. Phys.* vol.112, 074307, 2012.
14. Synthesis of monocrystalline zinc oxide microrods by wet chemical method for light confinement applications, Aparna Thankappan, Misha Hari, **S. Mathew**, Santhi Ani Joseph, Erni Rolf, Debajeet Bora, Artur Braun, V.P.N. Nampoori, *Physica E: Low-dimensional Systems and Nanostructures*, vol.44(10), pp. 2118–2123, 2012.
15. Glucose concentration sensor based on long period grating fabricated from hydrogen loaded photosensitive fiber , T. M. Libish, J. Linesh, M. C. Bobby, B. Nithyaja, **S. Mathew**, C. Pradeep, P. Radhakrishnan, *Sensors & Transducers Journal*, vol.129, Issue 6, pp. 142-148, 2011.
16. Narayanan, S., Raghunathan, S. P., **S. Mathew.**, Kumar, M. M., Abbas, A., Sreekumar, K., Cheranellore Sudha Kartha and Joseph, R. Synthesis and third-order nonlinear optical properties of low band gap 3, 4-ethylenedioxythiophene-quinoxaline copolymers. *European Polymer Journal*.vol.64, 157-169, 2015.
17. T.M. Libish, M.C. Bobby, J. Linesh, **S. Mathew**, C. Pradeep, V.P.N. Nampoori, P. Biswas, S. Bandyopadhyay, K. Dasgupta and P. Radhakrishnan, Detection of adulteration in virgin olive oil using a fiber optic long period grating based sensor, *Laser Physics*, vol.23 (4), pp. 045112-045116, 2013.

18. T.M. Libish, M.C. Bobby, J. Linesh, **S. Mathew**, P. Biswas, S. Bandyopadhyay, K. Dasgupta, P. Radhakrishnan, The effect of annealing and temperature on transmission spectra of long period gratings written in hydrogen loaded standard single mode fiber, *Optik-International Journal for Light and Electron Optics*, vol.124 (20), 4345-4348, 2013.
19. T. M. Libish, M. C. Bobby, J. Linesh, **S. Mathew**, C. Pradeep, V. P. N. Nampoore, P. Radhakrishnan, Refractive index and temperature dependent displacements of resonant peaks of long period grating inscribed in hydrogen loaded SMF-28 fiber, *Optoelectronics Letters*, vol.8(2), pp.101-104, 2012.
20. Pradeep, C., **S. Mathew**, Nithyaja, B., Radhakrishnan, P., & Nampoore, V. P. N, Studies of nonlinear optical properties of PicoGreen dye using Z-scan technique, *Applied Physics A*, vol.115, pp.1-5, 2013.
21. Indu Sebastian, **S. Mathew**, V. P. N. Nampoore, P. Radhakrishnan, and Sheenu Thomas, Concentration tuned bandgap and corresponding nonlinear refractive index dispersion in Ga-Ge-Se nanocolloids, *J. of Appl. Phys.*, vol.114, pp.053102, 2013.
22. Linslal, C. L., Peter, J., **S. Mathew** and Kailasnath, M., Multimode laser emission from dye-doped hollow polymer optical fibre, *Pramana*, vol.82 (2), 233-236, 2014.
23. Augustine, Anju K., **S. Mathew**, C. P. Girijavallabhan, P. Radhakrishnan, VP N. Nampoore, and M. Kailasnath, Size dependent variation of thermal diffusivity of CdSe nanoparticles based nanofluid using laser induced mode-matched thermal lens technique, *Journal of Optics*, vol. 44, pp.1-7, 2014.

24. Narayanan, Sona, Sreejesh Poikavila Raghunathan, Aby Cheruvathoor Poullose, **Sebastian Mathew**, Krishnapillai Sreekumar, Cheranellore Sudha Kartha, and Rani Joseph. "Third-order nonlinear optical properties of 3, 4-ethylenedioxythiophene copolymers with chalcogenadiazole acceptors." *New Journal of Chemistry*, vol.39 (4), pp.2795-2806, 2015.

Publications in International Conference Proceedings

1. Study of second-harmonic generation from CdS nanostructured thin film, **Mathew, S.**, Kalle Koskinen, Robert Czaplicki, M. Kailasnath, Pradeep Chandran, Vallabhan CPG, Martti Kauranen, and P. Radhakrishnan. In *International Conference on Fibre Optics and Photonics*, pp. M4A-46. Optical Society of America, 2014.
2. Effect of coating of CdS on optical properties of CdSe quantum dots, **S. Mathew**, Amit D. Saran, Santhi Ani Joseph, Bishwajeet Singh Bhardwaj, Deep Punj, P. Radhakrishnan, V. P. N. Nampoore, C. P. Girijavallabhan, Jayesh R. Bellare, Cochin Nano-2011: Third International Conference on Frontiers in Nanoscience and Technology, January 3-6, 2009, Department of Physics, Cochin University of Science and Technology, Cochin, India
3. Excitation wavelength dependent fluorescence behavior of CdS nanoparticles, **S. Mathew**, Litty Mathew Irimpan¹, John Thomas, Lyjo K Joseph, M N Muralidharan, V P N Nampoore¹ and C P G Vallabhan, PHOTONICS-2008: International Conference on Fiber Optics and Photonics December 13-17, 2008, IIT Delhi, India.
4. Nonlinear optical characterization of Silver/PMMA nanocomposite films, K J Thomas, **S. Mathew**, M N Muralidharan, V P N Nampoore and P Radhakrishnan, PHOTONICS-2008: International Conference on Fiber Optics and Photonics December 13-17, 2008, IIT Delhi, India.

5. Effect of self- assembly on the NLO characteristics of ZnO thin films. Litty Irimpan, **S. Mathew**, V.P.N Nampoori and P. Radhakrishnan, Cochin Nano-2009: Second International Conference on Frontiers in Nanoscience and Technology, January 3-6, 2009, Department of Physics, Cochin University of Science and Technology, Cochin, India.
6. Luminescence enhancement in nanocomposites of ZnO- Cu, Litty Irimpan, **S. Mathew**, V.P.N Nampoori and P. Radhakrishnan, Cochin Nano-2009: Second International Conference on Frontiers in Nanoscience and Technology, January 3-6, 2009, Department of Physics, Cochin University of Science and Technology, Cochin, India.
7. Photoluminescence Study of TiO₂ Nanocolloid Prepared from Hydrothermal Method, **S. Mathew**, Amit kumar Prasad, Thomas Benoy, Rakesh P. P, P. Radhakrishnan, V P N Nampoori, C P G Vallabhan ; PHOTONICS-2010: International Conference on Fiber Optics and Photonics December 2010
8. Investigation of optical nonlinear properties of cyanine dye , C. Pradeep, **S. Mathew**, B. Nithyaja, P. Radhakrishnan and V. P. N. Nampoori ; Photonics 2012, 11th International Conference on Fiber optics and Photonics, December 9-12, 2012, IIT Madras, Chennai, India
9. Linear and nonlinear optical characterization of gold nanoparticles in polyvinyl alcohol, Misha Hari, Santhi Ani Joseph, Nithyaja Balan, **S. Mathew**, Ravi Kumar, Giridhar Mishra, R. R. Yadhav, P. Radhakrishnan, V.P.N. Nampoori ; International Conference on Manufacturing Science and Technology (ICMST 2010), November 26-28, 2010, Kuala Lumpur, Malaysia

10. Bandgap tunability of CdS nanoparticles using biotemplates, Vishnu K, Nithyaja B, **S. Mathew** and Nampoory V P N; Photonics 2010: 10th International Conference on Fiber Optics & Photonics, December 11-15, 2010, IIT Guwahati, India
11. Effect of Cadmium sulphide nanoparticles on polymer light emitting diode, C Pradeep, **S. Mathew**, Manoj A G Namboothiry, C P G Vallabhan, P Radhakrishnan, V P N Nampoory International Conference on Optics and Photonics (ICOP), February 20-22,2015, University of Calcutta.
12. Design and development of diaphragm-based EFPI pressure sensor, P. P. Anish, J. Linesh, T. M. Libish, **S. Mathew**, P. Radhakrishnan ; Proc. SPIE 8173, Photonics 2010: Tenth International Conference on Fiber Optics and Photonics, 81731V

Publications in National Conference Proceedings

1. Effect of doping of Manganese on spectral properties of ZnS nanoparticles, **S. Mathew**, Linesh. J, Arif P. Ahamed, V P N Nampoory , C P Girijavallabhan, ; National Laser Symposium (NLS)-09, BARC, Mumbai, Jan 2010.
2. Nonlinear optical characteristics of nanocomposites of ZnO- TiO₂- SiO₂, Litty Irimpan, **S. Mathew**, V.P.N Nampoory and P. Radhakrishnan, National Conference on Nanophotonic Materials (NCNM-2008) on 10-12 October 2008, Department of Physics, Cochin University of Science and Technology, Cochin, India.
3. Light amplification and lasing in fluorene based copolymer, C Pradeep, **S Mathew**, C P G Vallabhan, P Radhakrishnan, V P N Nampoory, NLS-23, December 3-6, 2014, Sri Venkateswara University, Thirupathi.

4. Luminescence tuning in nanocomposites of ZnO- CdS and ZnO- TiO₂. Litty Irimpan, **S. Mathew**, V.P.N Nampoore and P. Radhakrishnan, National Conference on Nanophotonic Materials (NCNM-2008) on 10-12 October 2008, Department of Physics, Cochin University of Science and Technology, Cochin, India
5. Optical limiting in ZnO nanocomposites. Litty Irimpan, **S. Mathew**, V.P.N Nampoore and P. Radhakrishnan, National Conference on Nanophotonic Materials (NCNM-2008) on 10-12 October 2008, Department of Physics, Cochin University of Science and Technology, Cochin, India.
6. Luminescence mechanism in nano ZnO under weak confinement regime. Litty Irimpan, **S. Mathew**, V.P.N Nampoore and P. Radhakrishnan, National Conference on Nanophotonic Materials (NCNM-2008) on 10-12 October 2008, Department of Physics, Cochin University of Science and Technology, Cochin, India.
7. Multimode laser emission from dye doped hollow polymer optical fiber, C.L. Linslal, Jaison Peter, **S. Mathew**, M. Kailasnath ; National Laser Symposium, NLS - 21, February 6-8, 2013, Bhabha Atomic Research Centre, Trombay, Mumbai, India. .
8. Nonlinear optical response of PicoGreen dye on interaction with deoxyribonucleic acid, C. Pradeep, **S. Mathew**, B. Nithyaja, P. Radhakrishnan and V. P. N. Nampoore ; Indian Association of Physics Teachers Convention and Seminar, November 2-4, 2012, International School of Photonics, CUSAT, Kochi, India. .
9. PicoGreen - A new optical nonlinear material, C. Pradeep, **S. Mathew**, B. Nithyaja, P. Radhakrishnan and V. P. N. Nampoore; IONS CHENNAI, December 7-8, 2012, IIT Madras, Chennai, India. .

10. Sol gel derived lead chloride crystals for optical limiting applications, I. Rejeena, B. Lilibai, C. Pradeep Chandran, **S. Mathew**, V. P. N. Nampoori and P. Radhakrishnan ; XXIV Kerala Science Congress, January 29-31, 2012, Rubber Research Institute of India, Kottayam, Kerala, India.
11. A Fiber optic probe to study properties of binary liquid mixtures, J Linesh, K Sudeesh, **S. Mathew**, V P N Nampoori ; National Laser Symposium (NLS)- 09, BARC ,Mumbai ,Jan 2010
12. Fiber Optic Sensor for Detection of Adulteration in Sunflower Oil, T.M.Libish, J.Linesh, P.P.Anish, **S. Mathew**, V P Nampoori and P.Radhakrishnan, DAE- BRNS National Laser Symposium (NLS)-2010, Dec 2010, RRCAT, Indore

Contents

Chapter 1 Introduction to Optical Properties of Nanomaterials	1
1.1 Introduction	2
1.2 Theory of low dimensional semiconductors	3
1.2.1 Weak confinement regime	6
1.2.2 Strong confinement regime	7
1.3 Some manifestations of quantum confinement	8
1.3.1 Size dependent linear optical properties	9
1.3.2 Nonlinear optical properties	9
1.4 CdS and its nanocomposites	11
1.5 Conclusions	15
References	15
Chapter 2 Experimental Techniques	21
2.1 Introduction	22
2.2 Preparation of CdS, TiO ₂ and Au nanoparticles	22
2.3 Thin film preparation of nanomaterials	22
2.4 Characterization of Nanoparticles	23
2.4.1 X-Ray Diffraction (XRD)	24
2.4.2 Transmission Electron Microscopy (TEM)	25
2.4.3 Scanning electron microscopy (SEM)	26
2.4.4 UV-Visible Absorption Spectroscopy	26
2.4.5 Fluorescence Spectroscopy	27

2.4.6 Z-scan technique for the analysis of nonlinear optical properties of the samples investigated.....	27
2.4.7 Second harmonic generation and polarization measurements..	32
2.5 Conclusions	32
References	33

Chapter 3 Synthesis and Study of Linear Optical Properties of CdS, TiO₂ and Au Nanoparticles35

3.1 Introduction	36
3.2 Preparation and study of linear optical properties of CdS nanoparticles.....	36
3.2.1 Experimental details	37
3.2.2 Results and Discussion	37
3.3 Preparation and optical properties of TiO ₂ nanoparticles	47
3.3.1 Experimental.....	47
3.3.2 Results and Discussions.....	48
3.4 Preparation and linear optical properties of gold nanoparticles	59
3.4.1 Experimental.....	60
3.4.2 Results and Discussion	60
3.5 Conclusions	61
References	62

Chapter 4 Second-Harmonic Generation from CdS Nanostructured Thin Films67

4.1 Introduction	68
------------------------	----

4.2	Experiment	69
4.3	Results and discussion.....	71
4.3.1	Second-harmonic generation	73
4.4	Conclusions	77
	References	78

Chapter 5 Preparation and Spectral Characteristics of CdS-Au and CdS-TiO₂ Nanocomposites.....81

5.1	Introduction	82
5.1.1	Experimental.....	83
5.2	Optical properties of CdS and CdS:Au nanocomposites.....	83
5.2.1	Preparation.....	83
5.3	Results and Discussion.....	84
5.4	Optical absorption studies on CdS and CdS:Au nanoparticles	87
5.4.1	Fluorescence studies on CdS and CdS:Au nanoparticles	88
5.5	Optical properties of CdS:Au and CdS PVA nanocomposite thin films.....	90
5.5.1	Linear optical properties of CdS:Au PVA nanocomposite films	90
5.5.2	Nonlinear optical studies on CdS PVA and CdS:Au PVA thin films	92
5.6	Optical properties of CdS and CdS:TiO ₂ nanocomposites	97
5.6.1	Results and Discussion	98
5.7	Optical properties of CdS and CdS:TiO ₂ nanocomposite films	103
5.7.1	Optical absorption studies	103

5.7.2 Nonlinear optical studies on CdS PVA and CdS:TiO ₂ PVA thin films	104
5.8 Conclusions	108
References	109
Chapter 6 Optical Properties of Nanocomposite Materials like CdSe-CdS and CdSe-ZnS Core-Shell Quantum Dots	113
6.1 Introduction	114
6.2 Optical properties of CdSe-CdS core-shell with varying shell thickness of CdS.....	115
6.2.1 Preparation of the quantum dots.....	115
6.2.2 Results and discussion.....	116
6.3 Optical properties of CdSe-ZnS core-shell QDs	120
6.3.1 Results and discussion.....	121
6.3.2 Conclusions	129
References	130
Chapter 7 Conclusion and Future prospects	133

List of Tables

Table 1-1 : Basic properties of CdS.....	12
Table 3-1: Parameters deduced from absorption of Au nanoparticles	61
Table 5-1: Nonlinear optical absorption coefficient at different laser intensities	95
Table 5-2: Nonlinear optical absorption and refraction.....	96
Table 5-3: Nonlinear optical absorption coefficients	105
Table 5-4: Nonlinear absorption coefficients at different input intensities	106

List of Figures

Figure 1.1: Density of electron states for various dimensionalities	6
Figure 2.1: Z -scan set up for the measurement of optical nonlinearity	29
Figure 2.2: (a) Reverse saturable absorption curve and (b) Saturable absorption curve of open aperture Z-scan	30
Figure 2.3: (a) Negative nonlinear refraction and (b) Positive nonlinear refraction for closed aperture Z-scan curve	31
Figure 3.1: Absorption spectra of particles obtained from precursor solution of concentration 0.01M & 0.1M	38
Figure 3.2: A typical XRD pattern of CdS nanoparticles S2.....	39
Figure 3.3: SEM of S1 particles	40
Figure 3.4: Emission spectra of S1 particles when excited with excitation wavelength of 380nm	41
Figure 3.5: Excitation spectra for emission wavelengths 423nm and 520nm of S1 particles	41
Figure 3.6: Emission spectra of S1 particles when excited with excitation peaks of 274nm, 376nm and 380nm.....	42
Figure 3.7: Emission spectra of S1 particles when excited with (a) lower wavelengths (370nm-420nm) and (b) higher wavelengths (440nm-480nm).....	42
Figure 3.8: (a) Spatial electronic state correlation diagram (b) Emissions in two wells of CdS nanoparticles	45
Figure 3.9: Emission spectra of S2 particles for excitation wavelengths (370nm-420nm).....	46
Figure 3.10: Absorption spectra of colloidal TiO ₂ particles.....	48
Figure 3.11: a) Direct optical band gap transitions $(\alpha h\nu)^2$ vs $h\nu$ plot and (b) Indirect optical band gap transitions $(\alpha h\nu)^{1/2}$ vs $h\nu$ plot	50

Figure 3.12: (a) Absorption spectra of annealed TiO ₂ nanocrystals, insets (b) $(\alpha h\nu)^2$ vs $h\nu$ plot and (c) $(\alpha h\nu)^{1/2}$ vs $h\nu$ plot	51
Figure 3.13: FTIR spectrum of TiO ₂ nanocrystals	52
Figure 3.14: XRD spectra of TiO ₂ nanoparticles and annealed TiO ₂ nanocrystals	53
Figure 3.15: HRTEM picture of colloidal (T4) TiO ₂ nanoparticles	54
Figure 3.16: (a) Excitation spectrum of TiO ₂ colloidal nanoparticles and (b) Fluorescence spectrum of colloidal nanoparticles	55
Figure 3.17: Fluorescence spectrum of annealed TiO ₂ nanocrystals.....	57
Figure 3.18: Emission mechanism for TiO ₂ nanoparticles.....	58
Figure 3.19: Intensity ratio of excitonic and dominant surface state emissions	59
Figure 3.20: Absorption spectra of gold nanoparticles.....	61
Figure 4.1: Experimental setup for SHG measurements. GP - Glan polarizer, WP - wave plate (half- or quarter-wave plate was used during experiments), VI - iris, LP - long-pass filter, L - lens , RS - rotation stage with the sample, SP - short-pass filter, IF - interference filter, PMT- photomultiplier tube	70
Figure 4.2: Optical absorption spectrum of CdS nanostructured thin film. Inset shows optical band gap	71
Figure 4.3: X-ray diffraction pattern of CdS nanostructured thin film.....	72
Figure 4.4: SEM picture of the CdS nanostructured thin film.....	73
Figure 4.5: Geometry of single beam SHG where $E(\omega)$ is the field vector of the fundamental beam incident on the sample while $E_T(2\omega)$ is the field vector of the SHG beam in the transmitted direction	74
Figure 4.6: SHG intensity in the function of angle of incidence of fundamental beam and (b) Quadratic dependence of SHG intensity on the fundamental laser power of CdS thin film.....	75

Figure 4.7: (a) The p- and (b) s-polarized SHG signals as a function of the linear input polarization (the initial state of polarization, at 0 degree, is p). The black squares are the experimental data and the solid lines represent the fits to the data.....	75
Figure 4.8: Measured intensities of SHG from CdS nanostructured thin film as a function of rotation angle of the quarter-wave plate. The first label (P+S; P-S) indicates the linear polarization of the initial fundamental beam and the second one (P; P-S) that of the detected SHG signal. The symbols represent the raw experimental data, and the solid lines are simultaneous fit to all data to obtain the f, g, and h coefficients.....	77
Figure 5.1: CdS: Au and CdS nanoparticles are embedded in PVA matrix	84
Figure 5.2: (a) TEM images of CdS: Au nanoparticles (b) CdS nanoparticles	85
Figure 5.3: Energy dispersive X-ray spectrum of CdS: Au nanocomposite particles	85
Figure 5.4: (a) TEM image showing where the elemental maps were obtained (b) TEM/ Cd La1 map (c) TEM/ S Ka1 map and TEM/ Au La1 map.....	86
Figure 5.5: Optical absorption spectra of CdS and CdS: Au nanoparticles in PVA solution	87
Figure 5.6: A typical optical absorption spectrum of Au nanoparticles reduced from 0.4 mM stock solution.....	88
Figure 5.7: Fluorescence spectrum of CdS and CdS: Au nanoparticles in PVA matrix.....	89
Figure 5.8: A typical excitation spectra of CdS nanoparticles in PVA matrix.....	89
Figure 5.9: Optical absorption spectra of CdS and CdS: Au PVA nanocomposite films.....	91

Figure 5.10: Optical band gap plot of CdS PVA and CdS:Au PVA nanocomposite films.....	91
Figure 5.11: Open aperture Z- scan traces of CdS PVA and CdS:Au PVA nanocomposite films at an input intensity of 43MW/cm ²	92
Figure 5.12: Open aperture data at different input intensities of CdS:Au PVA nanocomposite films.....	93
Figure 5.13: Open aperture traces at different intensities of CdS PVA composite film	93
Figure 5.14: Closed aperture Z-scan data of CdS and CdS:Au PVA nanocomposites	95
Figure 5.15: Optical limiting curves of CdS:Au PVA and CdS PVA nanocomposite films.....	97
Figure 5.16: Photographs of (a) CdS:TiO ₂ PVA and (b) CdS PVA nanocomposites	98
Figure 5.17: HR TEM image of CdS:TiO ₂ nanocomposite particles.....	99
Figure 5.18: Energy dispersive X-ray spectrum of CdS:TiO ₂ nanocomposite nanoparticles.....	99
Figure 5.19: TEM image showing where the elemental maps were obtained	100
Figure 5.20: (a)TEM/Cd L _{α1} (b) TEM/S K _{α1} map(c)TEM/Ti K _{α1} map and TEM/O K _{α1} map	101
Figure 5.21: Optical absorption spectra of CdS and CdS:TiO ₂ nanoparticles in aqueous PVA solution.....	102
Figure 5.22: A typical absorption spectrum of TiO ₂ colloidal nanoparticles.....	102
Figure 5.23: Fluorescence spectra of CdS and CdS:TiO ₂ nanoparticles in PVA aqueous solution	103
Figure 5.24: Absorption spectra of CdS PVA and CdS:TiO ₂ PVA nanocomposite films.....	104

Figure 5.25: Optical band gap plot of CdS PVA and CdS:TiO ₂ PVA nanocomposite films.....	104
Figure 5.26: Open aperture Z-scan traces of CdS PVA and CdS:TiO ₂ PVA nanocomposite films.....	105
Figure 5.27: Open aperture Z-scan traces of CdS:TiO ₂ PVA nanocomposite films.....	106
Figure 5.28: Optical limiting curves for CdS PVA and CdS:TiO ₂ PVA nanocomposite films.....	107
Figure 6.1: Optical absorption spectrum of CdSe and CdSe-CdS QDs with varying shell thickness	117
Figure 6.2: (a), (b), (c), (d) shows the TEM images of the CdSe -CdS core-shell QDs (CS0, CS1, CS2, and CS3).....	118
Figure 6.3: A typical HRTEM micrographs (scale bar = 5 nm) for CdSe-CdS QDs.....	119
Figure 6.4: (a) Emission peak shift of CdSe-CdS QDs with increase in shell thickness under excitation wavelength 390nm (b) Emission band of CdSe-CdS QDs with increase in thickness of CdS shell under excitation 532nm	120
Figure 6.5: Absorption spectra of the CdSe -ZnS core-shell QDs (C0, C1, C2, and C3).....	122
Figure 6.6: (a), (b), (c), (d) shows the TEM images of the CdSe -ZnS core-shell QDs (C0, C1, C2, and C3).....	123
Figure 6.7: A typical HRTEM micrographs (scale bar = 5 nm) for (a)CdSe and CdSe-ZnS QDs	123
Figure 6.8: (a) Emission peak shift of CdSe-ZnS QDs with increase in shell thickness under excitation wavelength 390nm (b) Emission band of CdSe-ZnS QDs with increase in thickness of ZnS shell under excitation 532nm.....	124
Figure 6.9: Open aperture Z-scan traces of C0, C1, C2, and C3 QDs.....	125
Figure 6.10: Optical limiting curves for C0, C1, C2, and C3 QDs	128

Chapter 1

Introduction to Optical Properties of Nanomaterials

Abstract

This chapter gives an overview of the foundation of quantum confinement effects in materials for which optical properties are size dependent. This chapter also includes details of the work done by earlier workers in this field.

1.1 Introduction

Nanophotonics deals with the study of interaction of light with materials having dimensions ranging from 1nm to 100 nm. Nanophotonics include near-field interactions, near field microscopy, photonic crystals, and nanomaterials with size dependent optical properties, nanoscale optical devices and nanolithography. This field integrates areas like lasers, photonics, photovoltaics, nanotechnology and biotechnology. Nanoscale interaction between light and matter can be possible in three ways, *viz.* (1) the interaction of light on nanometer sized matter, (2) confinement of light to a nanoscale dimensions those are much smaller than the wavelength of light and (3) the nanoscale confinement of a photoprocess when we induce photochemistry or a light induced phase change [1, 2].

Nanoscale confinement effect is the basis of near field optics where a near field geometry is utilized to confine the light on nanometer scale. For examples, light is coupled by tapered optical fibers [3] or by tip of a smoothly tapered metal nanoplasmonic waveguide [4] with dimension much smaller than the wavelength of light. Nanoscale matter confinement involves various ways of confining dimensions of matter to form diverse range of nanostructures for photonics [5, 6]. For example, nanoparticles can be utilized which are having unique electronic and optical properties such as UV absorbers in sunscreen lotions [7]. Nanoparticles can be made from either inorganic or organic materials. Nanomers are organic analogues of nanoparticles. Oligomers are π -bonded series of organic structures. As the dimensions of the oligomers reach nanometer size, these oligomers are also referred to as nanomers. These nanomers possess size dependent optical properties [8]. Metallic nanoparticles exhibit unique optical properties and enhanced electromagnetic field and tremendous results and applications of metal nanoparticles lead to an area of research 'Plasmonics'. Photonic crystal is one of the main area of research in

the field of nanophotonics. Inorganic semiconductors are the most studied nanomaterials. Quantum confined semiconductors are easy to be used for band gap engineering, which deals with the manipulation of semiconductor band gap [1]. In the present thesis, the main focus of the work is on optical properties of semiconductor materials. The basic mechanisms at low dimensional structures are described in the following section.

1.2 Theory of low dimensional semiconductors

Low dimensional semiconductor structures, usually called nanocrystals or quantum dots possess unique features having importance in the field of science and technology [9]. During the last two decades, optical properties of semiconductor nanoparticles have been extensively studied due to their unique size-dependent properties which originate mainly from quantum confinement effect [10-15]. The electronic properties of solids are determined by occupation of the bands and by the absolute values of the forbidden gap between the completely occupied and the partly unoccupied or the empty bands. If all the bands at $T=0$ are either occupied or completely free, material will show dielectric properties. The highest occupied band is called valence band and the lowest unoccupied band is called conduction band. The interval between the top of the valence band, E_v , and bottom of the conduction band, E_c , is called the band gap energy, E_g . i.e, $E_g=E_v-E_c$. Electrons in the conduction band of a crystal can be described as particles with charge $-e$, spin $1/2$, mass m_e^* and quasi-momentum $\hbar k$, where $\hbar=h/2\pi$, h is Planck's constant and k is the wave vector. In the theory of many body systems, it is conventional to consider the small vector of noninteracting quasiparticles rather than considering the large number of interacting particles as the many body system consists of large number of electrons and nuclei. These quasiparticles are described as elementary excitation of the system consisting of a number of real particles. That is, an electron in the

conduction band is the primary elementary excitation of the electron subsystem of a crystal. Excitation of electron from valence band to conduction band leads to another elementary excitation called a hole, created by the removal of electron from valence band and is characterized by charge $+e$, spin $1/2$ and effective mass m_h^* . Using the concept of elementary excitations, ground state of the crystal can be taken as vacuum state in which electron in the conduction band and hole in the valence band doesn't exist. In the case of first excited state one electron in the conduction band and a hole in the valence band form an electron-hole pair. A description based on noninteracting particles as the only elementary excitations corresponds to the so-called single-particle representation. In reality, electrons and holes as charged particles do interact with each other through Coulomb potential and form an extra quasiparticle that corresponds to the hydrogen-like bound state of an electron-hole pair called an exciton. Similar to Hydrogen atom, an exciton is characterized by the exciton Bohr radius a_B and exciton Rydberg energy. Absolute values of a_B for the common semiconductors range in the interval of 10-100Å and the exciton Rydberg energy (Ry^*) takes the values approximately 1-100meV. An exciton exhibits translational center of mass motion as a single uncharged particle with the mass $M=m_e^*+m_h^*$. The dispersion relation corresponding to exciton can be written as

$$E_n(K) = E_g - \frac{Ry^*}{n^2} + \frac{\hbar^2 K^2}{2M} \quad (1.1)$$

Where K is the exciton wave vector. Taking into account that a photon possesses very small momentum; exciton creation corresponds to the discrete set of energies described as

$$E_n = E_g - \frac{Ry^*}{n^2} \quad (1.2)$$

In bulk semiconductors, de Broglie wavelength of an electron and a hole, (λ_e, λ_h) and the Bohr radius of an exciton, a_B may be much higher than the lattice

constant, a_L . Therefore, it is possible to make structures in one, two or three dimensions comparable to or even less than λ_e, λ_h while a_B is still larger than a_L . In these structures, elementary excitations will experience quantum confinement effects in the confinement axis. In the case of confinement in one dimension, the structure is called quantum well. In the case of two dimensional confinements, the structure is termed as quantum wire. If the confinement is in all three dimensions, the structure is referred to as quantum dot (QD). Figure 1.1 shows density of states of different structures [16].

In general, confinement effects must be taken into account as the material dimension is reduced to a size approaching the exciton Bohr diameter. In a semiconductor nanoparticle, many physical properties become size dependent, when the size of the nanoparticle becomes comparable to the Bohr radius of the bulk material. The main change in the optical properties is the blue shift of the excitonic peak in the absorption spectrum as the particle size is reduced in the nano-scale regime and is due to the confinement effect occurring in the nano-regime. One of the most interesting effects of quantum confinement in semiconductor nanostructures is the size dependent band gap [11].

There is also a spectral shift in the fluorescence emission when the particle size is reduced to nano-level. As the nanoparticles are characterized by large surface to volume ratio, they exhibit certain surface state effects and corresponding changes in the emission properties [9]. Thus the optical properties of semiconductor particles like Cadmium sulfide (CdS) become strongly dependent on the effective particle size.

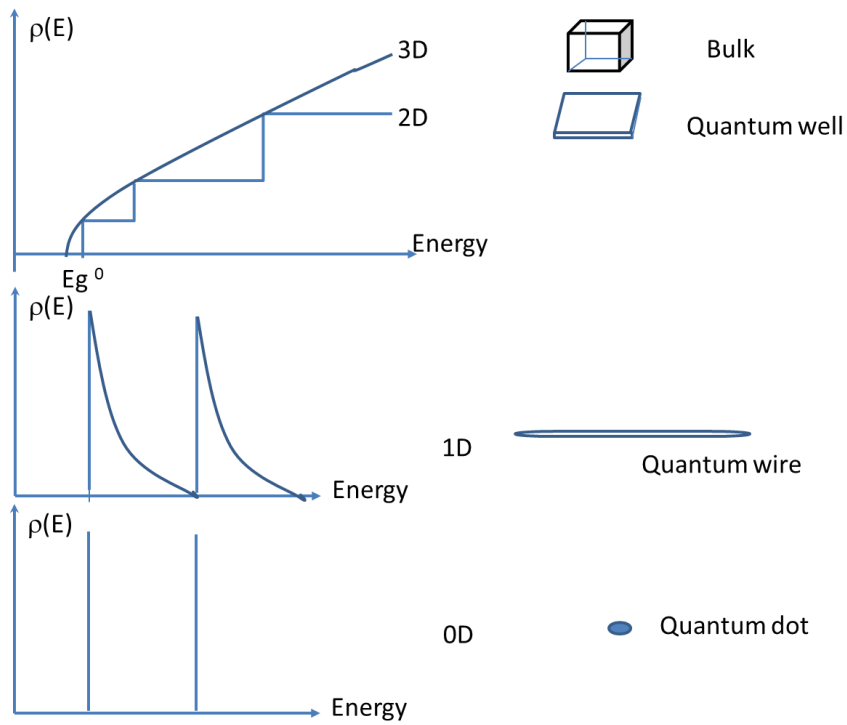


Figure 1.1: Density of electron states for various dimensionalities

Depending on the particle size, there are two confinement regimes called weak confinement and strong confinement regime, explained by A. L. Efros and Al. L. Efros [17]. Different cases of confinements are described in the following section

1.2.1 Weak confinement regime

This regime is applicable to the case where the particle size $2a$, is small but still a few times larger than the exciton Bohr diameter, $2a_B$. In this case, and Coulomb energy is much larger than the confinement energy resulting in the quantization of exciton center-of-mass motion. Thus the envelope wave function of electron-hole (e-h) pair is the product of two wave functions describing the movement of the center -of-mass motion.

In the effective mass approximation (EMA), the Hamiltonian of electron-hole system can be written as

$$H = -\frac{\hbar^2}{2m_e^*} \nabla_e^2 - \frac{\hbar^2}{2m_h^*} \nabla_h^2 + V_0^e(r_e) + V_0^h(r_h) - \frac{e^2}{\epsilon r_{eh}} \quad (1.3)$$

where m_e^* and m_h^* is the effective electron and hole mass, ϵ is the effective dielectric constant, r_{eh} is the electron-hole distance in three dimensions, and $V_0^e(r_e)$ and $V_0^h(r_h)$ is the confinement potential of the electron and hole. In the case of QDs, the potential is expected to be centrosymmetric; and hence, the potential is a constant, $V_0^e(r_e)$ [$V_0^h(r_h)$] for distances larger than the QD radius, but it is zero inside the QD.

The Bohr radius of the exciton in a QD is given by

$$a_B = \frac{\epsilon \hbar^2}{m_e e^2} \quad (1.4)$$

By solving Schrodinger equation, the possible energies corresponding to optical transitions are written as

$$E_n = E_g - E_{exc} + \frac{\hbar^2 n^2}{8MR^2} \quad (1.5)$$

where $M = m_e^* + m_h^*$ is the total mass of the e-h pair.

$R = (m_e^* r_e + m_h^* r_h) / (m_e^* + m_h^*)$ is the position of the center of mass, E_g denotes the bulk bandgap energy, E_{exc} is the exciton binding energy, and n is the quantum number.

1.2.2 Strong confinement regime

When the particle size ($2R$) is much smaller than the exciton Bohr diameter ($2a_B$), then it is considered to be in strong confinement regime. Here the Coulomb energy cannot be taken into consideration as it is negligible with respect to confinement energy. The movement of both electron and hole is independent and their confinements occur separately in the infinite spherical

potential. The confinements of electron and hole have no bound state corresponding to the hydrogen-like exciton. In this case, the uncorrelated motion of an electron and a hole may be taken as the first approximation. Confinement energies of the electron and hole depend only on n and l quantum numbers and can be written as

$$E_{nl} = E_g + \frac{\hbar^2}{2\mu R^2} \chi_{nl}^2 \quad (1.6)$$

Where χ_{nl} are the roots of Bessel function with $\chi_{1,0} = \pi, \chi_{1,1} \approx 1.43\pi, \chi_{2,1} \approx 1.83\pi, \text{ etc...}$

For this reason, when quantum dots show a discrete optical spectrum controlled by the size, quantum dots in the strong confinement is often called artificial atoms or hyper atoms. Taking into consideration of the fact that an electron and a hole are confined in space inside the quantum dot comparable with the extension of the exciton ground state in the ideal infinite crystal, Coulomb interaction cannot be neglected. Using variational approach, L.E. Brus [19] and Kayanuma [20] found that the energy of the ground electron-hole pair state (1s-1s) can be written as

$$E_{nl} = E_g + \frac{\pi^2 \hbar^2}{2\mu R^2} - 1.786 \frac{e^2}{\epsilon R} \quad (1.7)$$

Where the term proportional to $e^2/\epsilon R$ describes the effective Coulomb interaction of electron and hole.

1.3 Some manifestations of quantum confinement

Quantum confinement effect causes a number of important changes in the electronic and optical properties of semiconductors. These manifestations have been utilized in many technological applications. In the present work, we

mainly focus on those manifestations in relation to the linear and nonlinear optical properties

1.3.1 Size dependent linear optical properties

Blue shift of the band gap as well as appearance of discrete sub-bands corresponding to quantization along the direction of confinement occurs as a result of quantum confinement. As the dimensions of the confinement increases, band gap decreases resulting in the shift of interband transition to a higher wavelength and finally approach to that of the bulk value for a large dimension. This allows material scientists to have the freedom to change the properties of a material simply by controlling its particle size which leads to the fabrication of a number of devices. The size-dependence of the optical properties of quantum dots has been one of the main subjects of research work during the last decade. In many semiconductors, such size quantization has been studied. In the weak confinement regime, a translational motion of an exciton is size quantized. Quantum confinement results in squeezing of energy states in a narrow energy range. The oscillator strength of an optical an interband transition depends on the joint density of states of the levels in the valence band and levels in the conduction band between which the transition occurs. In addition to this, the oscillator strength depends on the overlap of the envelope of the wave functions of electrons and holes. Both these factors produce a large enhancement of the oscillator strength upon quantum confinement [1].

1.3.2 Nonlinear optical properties

Optical nonlinearities in bulk semiconductors have been extensively investigated for potential applications in photonics. In recent years, there has been intense research on the nonlinear optical properties of nanometer-sized semiconductors and fabrication techniques for these small particles. A large enhancement of the nonlinear coefficient in the semiconductor crystallites is

predicted by theoretical considerations that are based on the quantum size effects of the carriers in the crystallites. In the nano-regime, quantum confinement produces exciton resonances those are sharper than the corresponding ones in the bulk semiconductors, resulting in large optical nonlinearities [21]. An exciton in bulk semiconductors behaves like a harmonic oscillator which does not exhibit any nonlinear optical response. As the size of the crystallite decreases, deviation of the electronic excitation from the ideal harmonic oscillator increases. Hanamura [22] reported that very large nonlinear optical polarizability which depends on the size of the microcrystallite. He pointed out that this enhancement originated from two concepts. One is due to the size quantization of excitons i.e., exciton oscillator strength concentrate on lowest coherent state. This results in enhancement for third-order nonlinearity. The other concept is due to the deviation of the electronic excitation from an ideal harmonic oscillator.

Nonlinear optical absorption occurs at sufficiently high input intensities in which the transmittance of the material varies (increase or decrease) as a function of input intensity. This absorption can be of two types: reverse saturable absorption (RSA) and saturable absorption (SA) [23, 24]. When the absorption cross-section of the excited state is stronger than that of the ground state, the transmission of the material will decrease with increase in excitation intensity. This process is called RSA. If the excited state absorption cross-section is less than that of the ground state, the transmission of the material will increase with increase in excitation intensities. SA process is important for dyes in mode-locking. RSA is observed as a result of excited state absorption (ESA), two photon absorption (TPA) and free carrier absorption (FCA) [25-27]. TPA process involves a transition from ground state of an atom or molecule to a higher excited state of an atom or molecule through a virtual level by the simultaneous absorption of two photons. In the case of semiconductors and

polyatomic molecules, there exists a high density of states near the lower excited state of the atom and ESA is possible in this case. In ESA, electrons already in a lower excited state absorb photons and transition to higher excited state occurs. ESA can occur only after an electron is excited to a lower excited state. In semiconductors, one photon absorption or two photon absorption can generate carriers. These electron-hole pairs can be excited to higher states or lower states in conduction band under high intensities. These absorption processes are called free carrier absorption (FCA). In FCA, four possible transitions are possible: linear absorption, TPA, one photon induced FCA and two photon induced FCA.

Preeti Gupta et al [28] found that in the case of CdSe quantum dots, the intensity of photoluminescence peak is increased and the peak shifts towards blue region as the particle size is reduced. Litty et al reported the size dependent optical properties of ZnO monodispersed colloidal nanocrystals in the weak confinement regime and the enhancement in optical nonlinearity. A large nonlinear optical response is reported in semiconductor nanocrystals in the regime of strong quantum confinement where the dimension of the nanocrystal is less than the exciton Bohr diameter. Material with a high nonlinear optical absorption is of much interest in a number of applications, including frequency conversion, optical switches and optical modulation. On the other hand a completely different approach to obtain high nonlinear optical response from materials is to make nanocomposites by incorporating metal nanoparticles or different semiconductor nanoparticles etc.

1.4 CdS and its nanocomposites

Among II–VI semiconductor family, optical properties of CdS nanocrystals have been investigated exhaustively because it has a well-established relationship between the optical absorption and the size of the particle [29]. In the case of CdS, the band gap in the CdS can be tuned between

4.5eV and 2.5eV as the size is varied from molecular form to the nanocrystal form and its radiative life time for the lowest allowed optical transition ranges from tens of picosecond to several ns correspondingly [30]. Thus, the energy of exciton is expected to undergo a blue shift if the particle size is less than 6nm. The nonlinear optical properties of CdS were extensively studied. Some properties of CdS are given below [31].

Table 1-1 : Basic properties of CdS

Other names	Greenockite, Cadmium(II) sulphide
Colour	Yellow to orange
Phase	Crystalline solid
Type	n-type semiconductor II-VI group
Crystal structure	Hexagonal and cubic structure , rock salt
Bulk band gap	2.4eV
Mass of electron (m_e) and hole(m_h)	$m_e=0.19m_0$ and $m_h=0.8m_0$ where $m_0=9.1 \times 10^{-31}$ kg
Bohr radius a_B	3nm

Nanocomposites are random media consisting of domains or inclusions that are of nanometer size. Inorganic nanoparticle embedded polymer nanocomposites have attracted much attention in recent years due to their enhanced optical and electronic properties. For example, CdSe based polymer nanocomposites were used in fabrication of blue emitters [32, 33]. Silver nanoparticles embedded in PVA matrix showed improvement in its properties like transition temperature and elastic modulus than only PVA [34]. A better photoluminescence property was observed in the case of PVP- capped CdS nanoparticles embedded in PVA matrix [35].

Nanoparticles can be either capped with or coupled to different wide band gap semiconductor or metal to produce nanocomposites with novel optical properties. The role of interfacial charge transfer has been investigated in such nanocomposite systems. Boyd, Sipe and co-workers have conducted theoretical and experimental studies of local field effects on the linear and nonlinear optical properties of nanocomposites [36, 37]. Hybrid nanoparticles (HNPs) combine contrasting materials onto a single nanosystem, thus providing a powerful approach for bottom-up design of novel nanostructures. Beyond the fundamental development in synthesis, the interest in HNPs arises from their combined and often synergetic properties exceeding the functionality of the individual component such as optical nonlinearity. In the case of semiconductor nanocrystals, the quantum confinement effects determine their unique optical and electronic properties. For colloidal metal nanocrystals, plasmonic effects dictate their optical response. The achievements in synthesis of these metal and semiconductor nanocrystals provided the background for the development of semiconductor–metal HNPs. Surface plasmon resonance induced by the oscillation of the charge density of conduction electrons, and its corresponding electromagnetic field can strongly affect the optical properties of any semiconductor nanoparticles nearby.

Cadmium sulphide (CdS) is a much studied material in the form of nanocomposites. CdS-ZnS, CdS-CdSe, ZnO-CdS, CdS-TiO₂ etc composites are studied for various applications like solar cell, light emitting, nonlinear optics and photocatalysis [38-41]. Off resonant nonlinearity enhancement in Au-CdS core-shell nanocomposites, has been already reported [42]. In this reported work, Au was the core material of study. Nonlinear optical studies with CdS as core material and Au as shell have not reported widely.

TiO₂ is a very interesting UV absorbing wide band gap semiconductor not only from a scientific standpoint but also due to its technological

applications in dye sensitized solar cells, pigments, dielectric materials in capacitors, and so on [43-46]. At ambient pressure TiO_2 is known to exist in three polymorphs: rutile, anatase and brookite. Anatase and rutile are the two main crystalline phase structures of TiO_2 with band gap energies of 3.2eV and 3.0 eV respectively [47]. As an n-type semiconductor with a wide energy band gap, TiO_2 is also well-known for its potential applications in the field of photocatalysis and photo electrochemistry because of its excellent optical transmittance, high refractive index and chemical stability [48, 49]. In addition to quantum confinement effects, semiconductor nanoclusters show properties that are strongly affected by their large surface-to-volume ratios. Recently, efforts have been directed to obtain TiO_2 combined nanocomposite materials for various photonic applications such as solar cell and for optical limiting applications. Litty et.al reported optical properties of ZnO and TiO_2 nanocomposites suggesting that there is an enhancement in nonlinear optical property and it is attributed to the concentration of exciton oscillator strength [50-51]. As there are very few reports on CdS: TiO_2 nanocomposite films for the potential application as an optical limiter, this nanocomposite material has been chosen as one of the important study materials for this thesis work.

In this thesis work, we are mainly focusing on CdS nanoparticles as base materials. Preparation and characterization of nanocomposites of CdS with Au, TiO_2 , CdSe, etc. also form the subject matter of this thesis. Even though CdS and CdS based nanocomposites are much studied materials, there are some questions and problems which are still to be answered. The present thesis attempts to find solutions to some of these problems

1.5 Conclusions

In this chapter we have discussed the theory of low dimensional structures along with the manifestations of quantum confinement effects on optical properties of semiconductor nanoparticles with special reference to CdS.

References

- [1] P. N. Prasad, *Nanophotonics*. John Wiley & Sons, 2004.
- [2] H. S. Nalwa, Ed., *Nanostructured Materials and Nanotechnology*, Academic Press, 2002.
- [3] M. Achermann, K. L. Shuford, G. C. Schatz, D. Dahanayaka, L. A. Bumm and V. I. Klimov, "Near-field spectroscopy of surface plasmons in flat gold nanoparticles," *Opt. Lett.*, vol. 32, pp. 2254-2256, 2007.
- [4] M. I. Stockman, "Nanofocusing of optical energy in tapered plasmonic waveguides," *Phys. Rev. Lett.*, vol. 93, pp. 137404, 2004.
- [5] H. Gleiter, "Nanostructured materials: basic concepts and microstructure," *Acta Materialia*, vol. 48, pp. 1-29, 2000.
- [6] H. Gleiter, "Nanocrystalline materials," *Progress in Materials Science*, vol. 33, pp. 223-315, 1989.
- [7] A. Becheri, M. Dürr, P. L. Nostro and P. Baglioni, "Synthesis and characterization of zinc oxide nanoparticles: application to textiles as UV-absorbers," *Journal of Nanoparticle Research*, vol. 10, pp. 679-689, 2008.
- [8] D. Grebner, M. Helbig and S. Rentsch, "Size-dependent properties of oligothiophenes by picosecond time-resolved spectroscopy," *J. Phys. Chem.*, vol. 99, pp. 16991-16998, 1995.
- [9] L. E. Brus. "Electron–electron and electron-hole interactions in small semiconductor crystallites: The size dependence of the lowest excited electronic state". *J. Chem. Phys.* vol.80 (9), pp. 4403-4409. 1984.

- [10] S. Chang, L. Liu and S. A. Asher, "Preparation and Properties of Tailored Morphology, Monodisperse Colloidal Silica-Cadmium Sulfide Nanocomposites," *J. Am. Chem. Soc.*, vol. 116, pp. 6739-6744, 07/01; 2014/01, 1994.
- [11] S. Baskoutas and A. F. Terzis. "Size-dependent band gap of colloidal quantum dots". *J. Appl. Phys.* vol.99 (1), pp013708-1-4, 2006.
- [12] M. Nirmal and L. Brus, "Luminescence Photophysics in Semiconductor Nanocrystals," *Accounts of Chemical Research*, vol. 32, pp. 407-414, 1999.
- [13] I. Umezu, R. Koizumi, K. Mandai, T. Aoki-Matsumoto, K. Mizuno, M. Inada, A. Sugimura, Y. Sunaga, T. Ishii and Y. Nagasaki, "Optical properties of CdS nanocrystal covered by polymer chains on the surface," *Microelectronic Engineering*, vol. 66, pp. 53-58, 2003.
- [14] M. Bawendi, W. Wilson, L. Rothberg, P. Carroll, T. Jedju, M. Steigerwald and L. Brus, "Electronic structure and photoexcited-carrier dynamics in nanometer-size CdSe clusters," *Phys. Rev. Lett.*, vol. 65, pp. 1623-1626, 1990.
- [15] M. C. Klein, F. Hache, D. Ricard, and C. Flytzanis, "Size dependence of electron-phonon coupling in semiconductor nanospheres: The case of CdSe", *Phys. Rev. B*, vol.42, pp.11123-11132, 1990.
- [16] A.P. Alivisatos, "Semiconductor clusters, nanocrystals, and quantum dots," *Science*, vol. 271, pp. 933-937, 1996.
- [17] AI L. Efros and AL. Efros, "Interband Absorption of Light in a Semiconductor Sphere," *Sov. Phys. Semicond*, vol. 16, pp.772-775, 1982.
- [18] L. Brus, "Electronic wave functions in semiconductor clusters: experiment and theory," *J. Phys. Chem.*, vol. 90, pp. 2555-2560, 1986.
- [19] Y. Kayanuma, "Wannier exciton in microcrystals," *Solid State Commun.*, vol. 59, pp. 405-408, 1986.
- [20] T. Takagahara, "Excitonic optical nonlinearity and exciton dynamics in semiconductor quantum dots," *Physical Review B*, vol. 36, pp. 9293, 1987.

- [21] E. Hanamura, "Very large optical nonlinearity of semiconductor microcrystallites," *Physical Review B*, vol. 37, pp. 1273, 1988.
- [22] I. S. Lee, H. Suzuki, K. Ito and Y. Yasuda, "Surface-enhanced fluorescence and reverse saturable absorption on silver nanoparticles," *The Journal of Physical Chemistry B*, vol. 108, pp. 19368-19372, 2004.
- [23] L. De Boni, E. L. Wood, C. Toro and F. E. Hernandez, "Optical saturable absorption in gold nanoparticles," *Plasmonics*, vol. 3, pp. 171-176, 2008.
- [24] Tutt, Lee W., and S. W. McCahon. "Reverse saturable absorption in metal cluster compounds." *Optics letters* vol.15 (12) pp.700-702, 1990.
- [25] M. Balu, J. Hales, D. Hagan and E. Van Stryland, "Dispersion of nonlinear refraction and two-photon absorption using a white-light continuum Z-scan," *Optics Express*, vol. 13, pp. 3594-9, 05, 2005.
- [26] J. Staromlynska, T. J. McKay and P. Wilson, "Broadband optical limiting based on excited state absorption in Pt:ethynyl," vol. 88, pp. 1726-1732, 2000.
- [27] P. Gupta and M. Ramrakhiani, "Influence of the particle size on the optical properties of CdSe nanoparticles," *Open Nanoscience Journal*, vol. 3, pp. 15-19, 2009.
- [28] A. Eychmüller, T. Voßmeyer, A. Mews and H. Weller, "Transient photobleaching in the quantum dot quantum well CdS/HgS/CdS," *J Lumin*, vol. 58, pp. 223-226, 1994.
- [29] T. Vossmeier, L. Katsikas, M. Giersig, I. Popovic, K. Diesner, A. Chemseddine, A. Eychmüller and H. Weller, "CdS nanoclusters: synthesis, characterization, size dependent oscillator strength, temperature shift of the excitonic transition energy, and reversible absorbance shift," *J. Phys. Chem.*, vol. 98, pp. 7665-7673, 1994.
- [30] P. A. Kurian, C. Vijayan, K. Sathiyamoorthy, C. S. Sandeep and R. Philip, "Excitonic transitions and off-resonant optical limiting in CdS quantum dots stabilized in a synthetic glue matrix," *Nanoscale Research Letters*, vol. 2, pp. 561-568, 2007.
- [31] V. Colvin, M. Schlamp and A. Alivisatos, "Light-emitting diodes made from cadmium selenide nanocrystals and a semiconducting polymer," *Nature*, vol. 370, pp. 354-357, 1994.

- [32] K. Sooklal, L. H. Hanus, H. J. Ploehn and C. J. Murphy, "A Blue-Emitting CdS/Dendrimer Nanocomposite," *Adv Mater*, vol. 10, pp. 1083-1087, 1998.
- [33] Z. Mbhele, M. Salemane, C. Van Sittert, J. Nedeljkovic, V. Djokovic and A. Luyt, "Fabrication and characterization of silver-polyvinyl alcohol nanocomposites," *Chemistry of Materials*, vol. 15, pp. 5019-5024, 2003.
- [34] M. Pattabi, B. S. Amma and K. Manzoor, "Photoluminescence study of PVP capped CdS nanoparticles embedded in PVA matrix", *Materials research bulletin*, vol. 42, pp. 828-835, 2007.
- [35] R. J. Gehr and R. W. Boyd, "Optical properties of nanostructured optical materials," *Chemistry of Materials*, vol. 8, pp. 1807-1819, 1996.
- [36] J. E. Sipe and R. W. Boyd, "Nanocomposite materials for nonlinear optics based on local field effects," in *Optical Properties of Nanostructured Random Media* Anonymous. Springer Berlin Heidelberg, pp. 1-19. 2002
- [37] S. Lu, M. Wu and H. Chen, "Polymer nanocomposite containing CdS–ZnS core–shell particles: Optical properties and morphology," *J. Appl. Phys.*, vol. 93, pp. 5789-5793, 2003.
- [38] J. Zhao, J. A. Bardecker, A. M. Munro, M. S. Liu, Y. Niu, I. Ding, J. Luo, B. Chen, A. K. Jen and D. S. Ginger, "Efficient CdSe/CdS quantum dot light-emitting diodes using a thermally polymerized hole transport layer," *Nano Letters*, vol. 6, pp. 463-467, 2006.
- [39] Y. Tak, S. J. Hong, J. S. Lee and K. Yong, "Fabrication of ZnO/CdS core/shell nanowire arrays for efficient solar energy conversion," *Journal of Materials Chemistry*, vol. 19, pp. 5945-5951, 2009.
- [40] Y. Yin, Z. Jin and F. Hou, "Enhanced solar water-splitting efficiency using core/sheath heterostructure CdS/TiO₂ nanotube arrays," *Nanotechnology*, vol. 18,495608 pp.1-6, 2007.
- [41] Y. Yang, J. Shi, H. Chen, S. Dai and Y. Liu, "Enhanced off-resonance optical nonlinearities of Au-CdS core-shell nanoparticles embedded in BaTiO₃ thin films," *Chemical Physics Letters*, vol. 370, pp. 1-6, 2003.
- [42] B. O'regan and M. Grätzel, "A low-cost, high-efficiency solar cell based on dye-sensitized colloidal TiO₂ films," *Nature*, vol.353, pp. 737 – 740, 1991.

- [43] J. Wang and Z. Lin, "Dye-sensitized TiO₂ nanotube solar cells with markedly enhanced performance via rational surface engineering," *Chemistry of Materials*, vol. 22, pp. 579-584, 2009.
- [44] C. Morterra, G. Cerrato, M. Visca and D. M. Lenti, "Surface characterization of some TiO₂-based pigments. Part 3.—Coating of the pigments," *J.Mater.Chem*, vol. 2, pp. 341-355, 1992.
- [45] S. A. Campbell, D. C. Gilmer, X. Wang, M. Hsieh, H. Kim, W. L. Gladfelter and J. Yan, "MOSFET transistors fabricated with high permittivity TiO₂ dielectrics," *Electron Devices, IEEE Transactions On*, vol. 44, pp. 104-109, 1997.
- [46] Y. Liu and R. O. Claus, "Blue light emitting nanosized TiO₂ colloids," *J. Am. Chem. Soc.*, vol. 119, pp. 5273-5274, 1997.
- [47] T. L. Thompson and J. T. Yates, "Surface science studies of the photoactivation of TiO₂ new photochemical processes," *Chem. Rev.*, vol. 106, pp. 4428-4453, 2006.
- [48] M. Kalbacova, J. Macak, F. Schmidt-Stein, C. Mierke and P. Schmuki, "TiO₂ nanotubes: photocatalyst for cancer cell killing," *Physica Status Solidi (RRL)-Rapid Research Letters*, vol. 2, pp. 194-196, 2008.
- [49] L. Irimpan, B. Krishnan, V. Nampoore and P. Radhakrishnan, "Luminescence tuning and enhanced nonlinear optical properties of nanocomposites of ZnO–TiO₂", *J. Colloid Interface Sci.*, vol. 324, pp. 99-104, 2008.
- [50] L. Irimpan, B. Krishnan, V. Nampoore and P. Radhakrishnan, "Nonlinear optical characteristics of nanocomposites of ZnO–TiO₂–SiO₂", *Optical Materials*, vol. 31, pp. 361-365, 2008.
- [51] L. Irimpan, V. Nampoore and P. Radhakrishnan, "Optical limiting in ZnO nanocomposites," *Science of Advanced Materials*, vol. 2, pp. 578-582, 2010.

Chapter 2

Experimental Techniques

Abstract

This chapter is divided into two sections namely preparation of nanomaterials and experimental tools and techniques those are used in this thesis work. Methods of characterization and various experimental techniques are also included in this chapter

2.1 Introduction

Nanomaterials can normally be prepared through different chemical as well as physical processes [1-10]. The work presented in this thesis, mainly following chemical preparations for the synthesis of nanoparticles. CdS, TiO₂ and Au. The techniques used for the preparation of CdS nanoparticles, CdS thin films, CdS-Au composites and CdS-TiO₂ composites and their thin films in PVA and PMMA are described in the following sections.

2.2 Preparation of CdS, TiO₂ and Au nanoparticles

CdS nanoparticles are mainly synthesized using different chemical methods like solvo-thermal [4], chemical precipitation [5], and microemulsion techniques [6]. In the present work, mostly the precipitation technique is employed for preparation of CdS nanoparticles. The chemical mechanism of CdS precipitation technique is typically the thermal decomposition of thiourea (CS(NH₂)₂) in the presence of a cadmium salt in a basic aqueous solution containing ammonia (NH₃). Titania powders are prepared either directly from titanium-bearing minerals or by precipitation from solutions of titanium salts or alcoxides. Commonly used synthesizing techniques and based on the hydrolysis of acidic solutions of Ti (IV) salts. In the case of gold nanoparticles (Au NPs), the preparation methods generally follows a chemical reduction method, typically performed by reducing an aqueous solution of HAuCl₄ using a reducing agent such as tri-sodium citrate, sodium borohydride, or other organic compounds.

2.3 Thin film preparation of nanomaterials

Thin films can be deposited by a number of physical and chemical techniques. Chemical methods are cost effective, but their full potential for

obtaining device quality films has not been fully explored even though it is easier than the physical methods. Physical methods are more expensive but give relatively more reliable and provide more reproducible results. But there is no ideal method to prepare thin films, which will satisfy all possible requirements. Chemical bath deposition is useful method due to its low temperature and low cost nature. Chemical bath deposition (CBD), also known as chemical solution deposition, has been known for more than a hundred years. This chemical deposition process can be achieved by immersing a substrate into a beaker containing an aqueous solution of chemical precursors, placed on the top of a hot plate magnetic stirrer.

Nanoparticles can be embedded in polymer matrix and can be dip coated or drop casted to make thin films. Poly vinyl alcohol (PVA) is the main polymer used for making thin films of nanoparticles [8-9]. PVA is prepared by the partial hydrolysis of polymerized vinyl acetate monomer. The prepared nanoparticles of different materials and the polymer are mixed together. After mixing, it either drop casted or dip coated to obtain the nanoparticle embedded PVA thin films.

2.4 Characterization of Nanoparticles

The optical properties and improved performance possessed by nanomaterials are strongly dependent on their size, composition, shape, structure, and interparticle interactions. Hence characterization of these properties is of great importance in the development of nanomaterials. A range of microscopic and spectroscopic methods are needed to investigate the nanostructure. The nanoparticles (CdS and its composites) synthesized, have been characterized for their optical properties, crystallographic information and elemental composition. The characterization methods include X-ray diffraction (XRD), electron microscopy, Energy Dispersive spectroscopy, UV-VIS absorption spectroscopy, Fluorescence spectroscopy etc.

2.4.1 X-Ray Diffraction (XRD)

X-ray diffraction, often abbreviated as XRD, is widely used to characterize the crystalline form of nanoparticle and to estimate crystalline sizes. It often utilizes X-ray diffraction from powder of nanoparticles, often referred as powder diffraction [11]. X-ray diffraction of a crystalline material is based on the principle of elastic scattering of X-rays by a periodic lattice and it gives information about the types of periodicity in the material, and it gives ensemble average information on the structure of the crystal and an approximate value of particle size. When a monochromatic beam of X-rays incident on a material, the ray penetrates the sample and diffraction by the periodic lattice of the crystalline sample occurs as by Bragg's equation, $n\lambda = 2d \sin \theta$, where n is an integer, λ is the wavelength of X-ray, d is the spacing between crystallographic planes, and θ is the incidence angle.

Nanoparticles of size less than approximately 100nm show broadening of X-ray diffraction lines. The observed broadened line can be used to estimate the approximate particle size. In the case of stress-free particles, the size can be estimated from a single diffraction peak. The approximate particle size/ grain size, D , is related to the X-ray line broadening by Scherrer's formula, $D = 0.9\lambda / \beta \cos \theta$, where λ is the X-ray wavelength, β is the full width (in radian) at half-maximum intensity, θ is the diffraction angle. However, Scherrer's formula can be used for a rough estimation of particle size [1].

The sample for XRD is prepared from chemical bath technique or the microemulsion by addition of ethanol, followed by centrifuging, removing the supernatant liquid, and finally by drying the powder. The powder is then used to get the diffraction pattern on XRD (X'Pert, PANalytical, Philips)

2.4.2 Transmission Electron Microscopy (TEM)

TEM is the electron microscopic analogue of transmission optical microscope. In TEM, a focused beam of electrons is used to analyze the structures of very thin specimens through which electrons are transmitted. In TEM, an electron beam travels through the sample and gets affected by the structure of the sample. The samples in the case of TEM are kept in high vacuum. The transmitted beam is projected on to a phosphor screen or digitally processed in a computer. Focusing of electron beam is done by electromagnetic lenses, which consists of current carrying coils surrounded by iron. For TEM, the sample should be in thin and this allows high-energy electrons to pass through. Passing electrons gets scattered due to Coulomb interactions. The degree of scattering depends on the atoms in the specimen. The heavy atoms scatters more compared to the lighter atoms leading to the lower transmission of electrons through the areas where heavy atoms present and a high transmission of electrons through the areas where lighter atoms present. The intensity distribution reaching the fluorescent screen is determined by the number of electrons transmitted. This results in a relative dark area in the image of the sample, which is rich in heavy atoms. The images of nanocrystals at high resolution have been obtained by transmission electron microscope. For preparation of specimen, a drop of nanocrystal solution is first loaded on a carbon-coated grid or Copper grid, which is allowed to dry for about 15 minutes. Then 4-5 drops of n-heptane are slowly added to the grid surface, in order to remove most of the surfactant. Then the grid is dried under IR lamp for about 2 hours, after which it can be observed under the microscope. A TEM image provides information about the size and shapes of nanoparticles.

TEM was done in a JEOL 2100 HRTEM operating at 200KeV. The anti-contamination device of the TEM is filled with liquid nitrogen for better vacuum during analysis in the column. The high vacuum system of the TEM is

started and once the required vacuum is achieved, then the lanthanum hexaboride (LaB₆) filament is switched on and alignment is performed. Samples were previously prepared on film-coated TEM grids and loaded onto the standard specimen holder. Then the specimen holder is inserted in to the system. Images were grabbed by Orius Camera controlled by Digital Micrograph software.

2.4.3 Scanning electron microscopy (SEM)

Scanning electron microscopy is a technique to obtain image of a sample, by scanning of an electron beam across the surface of specially prepared samples. In SEM, an electron beam is focused on to a small area, typically in diameter 10-20nm. This spot size determines the resolution of the image. It should be noted that it is desirable to make the sample conductive in the case of SEM. SEM provides a tremendous depth of focus compared to TEM. In the case of particles less than 10nm in size, TEM is the appropriate technique. Surface imaging of nanoparticles or chemically bath deposited films are studied using Scanning electron microscope (JEOL Model JSM - 6390LV) equipped with Energy-Dispersive Spectroscopy (EDS) (JEOL Model JED – 2300) for the qualitative elemental analysis.

2.4.4 UV-Visible Absorption Spectroscopy

Absorption spectra of nanoparticles were determined using UV-Visible JASCO V-570 UV/VIS/NIR Spectrophotometer. The specifications are Optical system: Single monochromator UV-VIS region 1200lines/mm plane grating, NIR region 300lines/nm plane grating Czerny-Turner mount double beam type. Resolution 0.1nm (UV-VIS region) and 0.5nm (NIR region). The absorption spectra of these nanoparticles are useful in two ways. Firstly, we get red-shift of the absorption peak with increasing particle size. Also, we can estimate the band

gap energy and approximate mean diameter of the nanoparticles using the theory proposed by Brus[2].

2.4.5 Fluorescence Spectroscopy

Fluorescence spectra were obtained on a Cary Eclipse Fluorescence spectrophotometer of VARIAN. It has a single cell holder for liquid sample analysis and a solid sample holder accessory to perform fluorescence measurements on solid samples. The measurements were obtained from the nanoparticles using quartz cuvettes. Convenient excitation wavelengths can be chosen in this instrument as per need.

2.4.6 Z-scan technique for the analysis of nonlinear optical properties of the samples investigated

Z-scan technique introduced by Sheik Bahae[3, 4] is a single beam method for measuring the sign and magnitude of nonlinear refractive index that has a sensitivity compared to interferometric methods. It provides direct measurement of nonlinear absorption coefficient. Previous measurements of nonlinear refraction have used a variety of techniques including nonlinear interferometry, degenerate four wave mixing, nearly degenerate three wave mixing, ellipse rotation and beam distortion measurements. The first three methods namely nonlinear interferometry and wave mixing are potentially sensitive techniques, but all require complex experimental apparatus. The propagation of laser beam inside such a material and the ensuing self-refraction can be conveniently studied using the Z-scan technique. Thus it enables one to determine the third order nonlinear properties of solids, ordinary liquids, and liquid crystals.

The experimental set up for single beam Z-scan technique is given in Figure 2.1. In the ordinary single beam configuration, the transmittance of the sample is measured, as the sample is moved along the direction of the focused

Gaussian beam. A laser beam propagating through a nonlinear medium will experience both amplitude and phase variation. If transmitted light is measured through an aperture placed in the far field with respect to focal region, the technique is called closed aperture Z-scan. In this case, the transmitted light is sensitive to both nonlinear absorption and nonlinear refraction. In a closed aperture Z-scan experiment, phase distortion suffered by the beam while propagating through the nonlinear medium is converted into corresponding amplitude variations. On the other hand, if transmitted beam is measured without an aperture, the mode of measurement is termed as open aperture z-scan. In this case, the output is a measure of nonlinear optical absorption. Closed and open aperture Z-scan graphs are always normalized to linear transmittance using transmittance at large values of $|z|$.

Closed and open aperture Z-scan methods yield the real part and imaginary part of nonlinear optical susceptibility respectively. Usually closed aperture Z-scan data contains the effect of nonlinear optical absorption and its effect is cancelled by dividing closed aperture data by open aperture data. The new graph, called divided Z-scan, contains information on nonlinear refraction alone. An important requirement in the Z-scan measurement is that, the sample thickness must be less than Rayleigh's range z_0 (diffraction length of the beam, $z_0 = \pi\omega_0^2/\lambda$, where λ is the wave length of the beam and ω_0 is the beam waist radius. The beam waist radius ω_0 is given by $\omega_0 = f\lambda/D$, where f is the focal length of the lens used and D is the beam radius at the lens). This is essential to make sure that the beam profile remains constant inside the sample because Z-scan technique is highly sensitive to the beam profile and also to the thickness of the sample. Any deviation from gaussian profile of the beam and also from thin sample approximation will give rise to erroneous results.

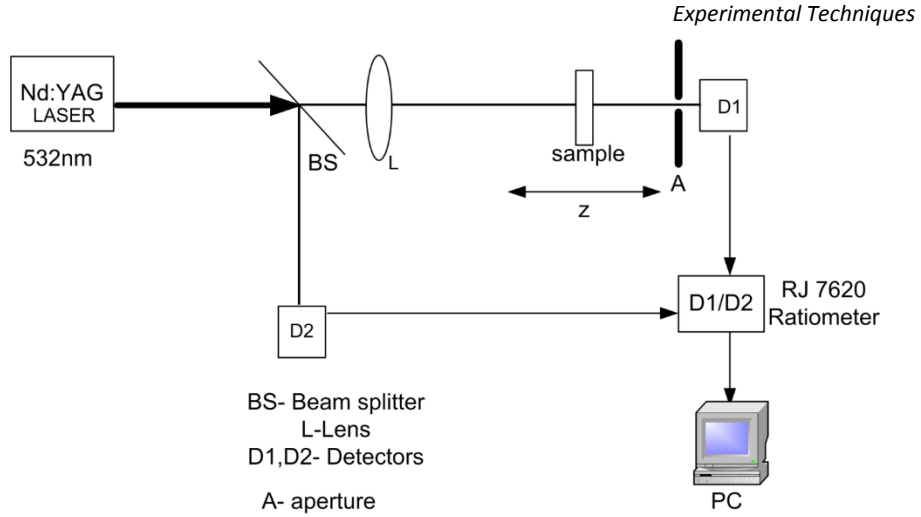


Figure 2.1: Z -scan set up for the measurement of optical nonlinearity

In Open aperture Z-scan technique, the transmitted beam through sample is measured without any aperture. In the case of an open aperture Z-scan, the transmitted light through the material is sensitive only to intensity variations. The intensity dependent nonlinear absorption coefficient, $\alpha(I)$ is given by

$$\alpha(I) = \alpha + \beta I \quad (2.1)$$

where linear absorption coefficient α and TPA coefficient β . Figure 2.2 shows a typical open aperture response for (a) reverse saturable absorption and (b) saturable absorption. The transmittance data contains a valley means reverse saturation absorption gives nonlinear optical absorption of the sample (β is positive). If the transmittance data gives a peak, which is the indication of saturable absorption (β is negative). The data are analyzed using the approach described by Sheik Bahae *et.al*[4]. The nonlinear absorption coefficient is obtained by fitting the experimental open aperture data using equation (2.2),

$$T(z, S=1) = \sum_{m=0}^{m=\infty} \frac{[-q(z,0)]^m}{(m+1)^{3/2}} \quad (2.2)$$

where $q(z,0) = \frac{\beta I_0 L_{eff}}{\left(1 + \frac{z^2}{z_0^2}\right)}$ and $L_{eff} = (1 - e^{-\alpha L})/\alpha$ is the effective

thickness with linear absorption coefficient (α), I_0 is the irradiance at the focus and L is the sample length.

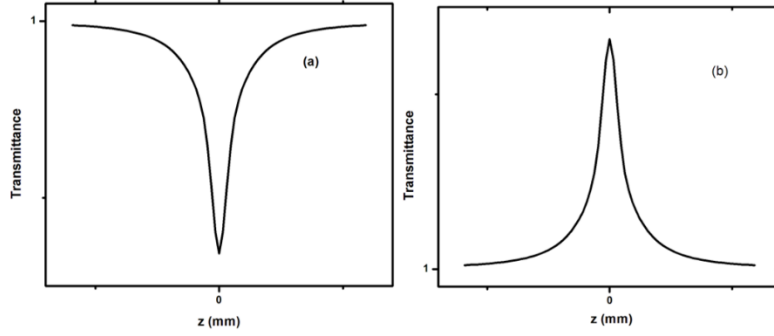


Figure 2.2: (a) Reverse saturable absorption curve and (b) Saturable absorption curve of open aperture Z-scan

For a medium having third-order optical nonlinearity, the index of refraction n can be written as [4, 5]

$$n = n_0 + n_2 |E|^2 = n_0 + n_2 I \quad (2.3)$$

where n_0 is the linear index of refraction, n_2 (m^2/W) the intensity dependent refractive index and I denotes the irradiance of the laser beam within the sample.

Figure 2.3 shows a typical closed aperture response for (a) negative nonlinear refraction and (b) positive nonlinear refraction.

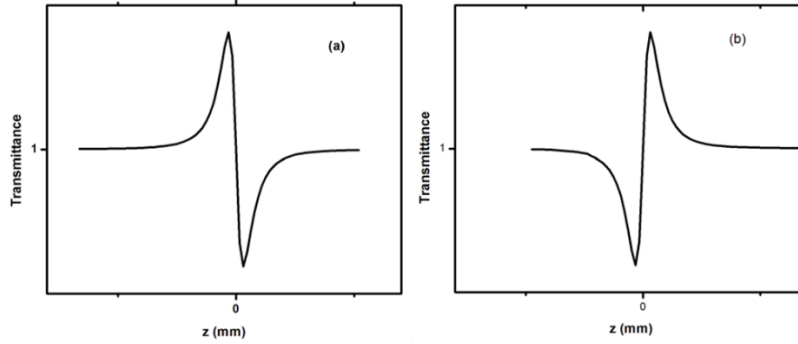


Figure 2.3: (a) Negative nonlinear refraction and (b) Positive nonlinear refraction for closed aperture Z-scan curve

A pre-focal transmittance valley and a post-focal transmittance peak is the Z-scan signature of positive refraction nonlinearity. A pre-focal transmittance peak and a post-focal transmittance valley is the z-scan signature of negative nonlinear refraction. For a positive n_2 , self-focusing occurs. For negative n_2 , self-defocusing occurs. This is the case of nonlinear refraction (symmetric peak and valley) curve in the absence of nonlinear absorption

The nonlinear phase change ($\Delta\phi$), can be obtained by the best theoretical fit of experimental data using the equation (2.4).

$$T_{(z,\Delta\phi)} = 1 - \frac{4 \Delta\phi x}{(x^2+9)(x^2+1)} \quad (2.4)$$

Where nonlinear phase change, $\Delta\phi = 2\pi \frac{\Delta n L_{\text{eff}}}{\lambda}$ and $x = z/z_0$, Δn is related to the nonlinear refraction coefficient, n_2 through the relation, $\Delta n = n_2 I$

One of the important applications of the optical nonlinearity is optical limiting [6]. To study the optical limiting property of the samples, by varying the input fluence, the nonlinear transmission of the sample is measured. The optical limiting property mainly arises from nonlinear absorption, which corresponds to the imaginary part of third-order optical susceptibility [7]. Using the standard equations for Gaussian beam waist, the fluence at each point inside the scan can be calculated from the value of fluence at the focus. Such plots of fluence vs transmittance obtained from Z-scan trace give a much better

demonstration of intensity dependent transmission of the light in the sample. Optical limiters based on nonlinear optical property have been designed for the protection from high power pulsed laser sources.

2.4.7 Second harmonic generation and polarization measurements

Second harmonic generation was the first experimentally observed nonlinear optical phenomenon [8]. With electric –dipole approximation, second order polarization density can be written as [9]

$$P_i^{(2)} = \sum_{jk} \chi_{ijk}^{(2)}(2\omega; \omega, \omega) E_j(\omega) E_k(\omega) \quad (2.5)$$

Where superscript 2 corresponds to the second order polarization density and i, j, k refer to the components along the chosen coordinate axes x, y or z. Equation (2.5) leads to the quadratic dependence of the second harmonic response on the fundamental field. Assuming everything else remains constant, the dependence can thus be described as

$$I(2\omega) \propto I^2(\omega) \quad (2.6)$$

Where $I(\omega)$ and $I(2\omega)$ are the intensities of fundamental and second harmonic light respectively. The second order susceptibility tensor is of rank three and therefore having 27 components in principle. But various symmetry conditions significantly reduce the number of non-zero and independent tensor components. A detailed experimental set up and procedure of analysis are provided in Chapter 4.

2.5 Conclusions

An overview of nanoparticle preparation were illustrated in this chapter. Various characterization techniques those were used to characterize the prepared nanomaterials were described.

References

- [1] B. Cullity, Ed., Elements of X-Ray Diffraction. Addison-Wesley, Menlo Park, CA, 1978.
- [2] L. E. Brus, "Electronic wave functions in semiconductor clusters: experiment and theory," J. Phys. Chem., vol. 90, pp. 2555-2560, 1986.
- [3] M. Sheik-Bahae, A. A. Said and Van Stryland E.W., "High-sensitivity, single-beam n_2 measurements," Opt. Lett., vol. 14, pp. 955-7, 09, 1989.
- [4] M. Sheik-Bahae, Ali. A. Said, T. H. Wei, D. J. Hagan and E. W. Van Stryland, "Sensitive measurement of optical nonlinearities using a single beam," IEEE J. Quant. Electron., vol. 26, pp. 760-769, 04, 1990.
- [5] E. Reynoso Lara, Z. Navarrete Meza, M. D. Iturbe Castillo, C. G. Treviño Palacios, E. Martí Panameño and M. L. Arroyo Carrasco, "Influence of the photoinduced focal length of a thin nonlinear material in the Z-scan technique," Optics Express, vol. 15, pp. 2517-2529, 2007.
- [6] L. W. Tutt and A. Kost, "Optical limiting performance of C60 and C70 solutions," Nature, vol. 356, pp. 225 - 226, 1992.
- [7] S. Shi, W. Ji, S. Tang, J.P. Lang and X.Q. Xin, "Synthesis and optical limiting capability of cubane-like mixed metal clusters $(n\text{-Bu}_4\text{N})_3[\text{MoAg}_3\text{BrX}_3\text{S}_4]$ ($X = \text{Cl}$ and I)" J. Am. Chem. Soc., vol. 116, pp. 3615-3616, 1994.
- [8] P. Franken, A. Hill, C. Peters and G. Weinreich, "Generation of optical harmonics" Phys. Rev. Lett., vol. 7, pp. 118-119, 1961.
- [9] R.W. Boyd, Nonlinear Optics. Academic press, 2003.

Chapter 3

Synthesis and Study of Linear Optical Properties of CdS, TiO₂ and Au Nanoparticles

Abstract

This chapter deals with preparation of CdS, TiO₂ and Au nanoparticles. It is mainly divided into three sections. Section 1 deals with preparation and optical properties of CdS nanoparticles. Excitation wavelength dependent fluorescence behavior of CdS nanoparticles is studied. Section 2 deals with preparation of TiO₂ colloidal nanoparticles and their linear optical properties. Fluorescence studies of TiO₂ colloidal nanoparticles showed four bands in the emission. Section 3 deals with the preparation and optical properties of Au nanoparticles.

3.1 Introduction

Nanometer-sized semiconductors and metals have drawn considerable attention in recent years because of their size-dependent optical properties. While conduction and valence bands of semiconductors are separated by a well-defined band gap, metal nanoclusters have close lying bands and electrons move quite freely in these materials [1-4].

Among semiconductors, CdS and TiO₂ are very well studied materials. CdS is a mid-band gap material and TiO₂ is wide-band gap material. Gold nanoparticles are vastly studied metal nanoparticles. Before investigating the optical properties of nanocomposites, it is desirable to study the optical characteristics of individual nanoparticles. Preparation and study of linear optical properties of CdS, TiO₂ and Au nanoparticles are described in the following sections.

3.2 Preparation and study of linear optical properties of CdS nanoparticles

Among II-VI semiconductor family, the CdS nanoparticles are materials which are intensively studied. Optical properties of CdS nanocrystals have been investigated exhaustively; however, there are only few experimental studies related to the excitation wavelength dependent fluorescence emission in CdS nanocrystal. In the nano-regime, of the order of 6nm in CdS, electronic and optical properties strongly depend on size, shape, and surface properties. In general only a few measurements are carried out to study the excitation wavelength dependent fluorescence in the nanoparticles [5, 6]. In the case of CdS/dendrimer nano-composites, J. R Lakowicz et.al [5, 6] reported peak emission wavelength shift around 40nm. In this chapter, it has been observed that there is much larger shift for the emission peak through a range of 120nm, when excited through 370nm-480nm for CdS nanoparticles. Further by varying

the excitation wavelength, the emission peak can be tuned through this fairly wide range of wavelengths.

3.2.1 Experimental details

CdS nanoparticles are prepared by precipitation technique from Cadmium sulphate (CdSO₄)/Cadmium acetate (Cd(CH₃-COO)₂), using thiourea and Ammonium hydroxide(NH₄OH) [7, 8]. All the chemicals are of GR grade from Merck Ltd. In this work, particles of different size are prepared by mixing aqueous solution of CdSO₄ of different concentrations range from 0.1M to 0.01M with aqueous solution of thiourea (0.2M to 0.002M concentrations). The pH of the mixture solution is kept at 10.5 by adding NH₄OH. The mixture is heated at 70°C and stirred for 1 ½ hour. The colour of the solution changed to yellow and precipitation occurs. The precipitated CdS particles are filtered, washed and dried. Dimethyl formamide (DMF) is selected as the dispersive medium for the study. The collected particles are dispersed in DMF by ultra sonification and measurement of their light absorption at room temperature is carried out using a spectrophotometer (JascoV-570 UV/VIS/IR). The fluorescence emission from the same is recorded using a Cary Eclipse fluorescence spectrophotometer (Varian). The structural properties of the samples are investigated by X-ray diffraction (XRD) on a Bruker AXS D8 Advance x-ray diffractometer with Ni-filtered Cu K α (1.5406Å) source.

3.2.2 Results and Discussion

The UV-VIS absorption spectrum of the CdS nanoparticles dispersed in DMF is shown in Figure 3.1.

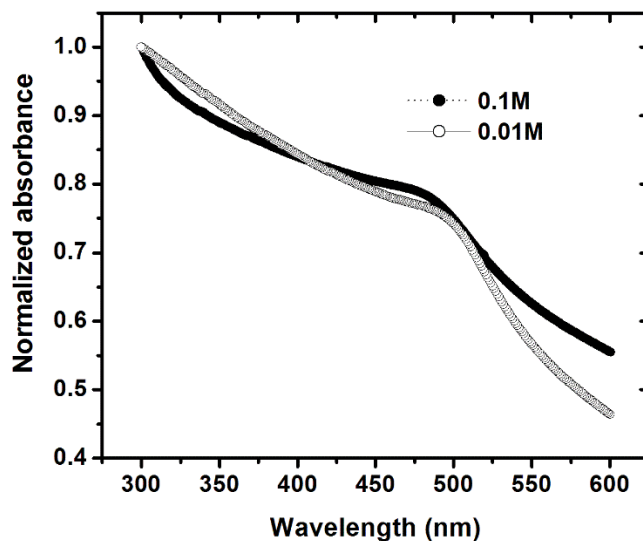


Figure 3.1: Absorption spectra of particles obtained from precursor solution of concentration 0.01M & 0.1M

The reported absorption edge for the bulk hexagonal CdS is at 512 nm (2.42eV). Comparing with the bulk CdS, it is observed that there is blue shift of absorption edge and it is well-known that the blue shift in the absorption peak is obviously caused by the quantum confinement effect [9]. From Figure.3.1, it is clear that there is a slight blue shift in absorption edge of the CdS nanoparticles when the concentration of precursor solution in the preparation changed from 0.01M to 0.1M. These results are the manifestations of quantum confinement occurring at nanolevel. The absorption spectra observed here for these particles are the same as those in the literature [10, 11].

The particle size of the CdS particles can be calculated using Brus formula based on the band gap value obtained from the absorption spectra [9]. The calculated bandgap values of these CdS nanoparticles are 2.5eV and 2.56eV. The approximate calculated sizes of the particles prepared from different concentrations (0.01M and 0.1M) of precursor solution are 9nm (S1 particles) and 6nm (S2 particles).

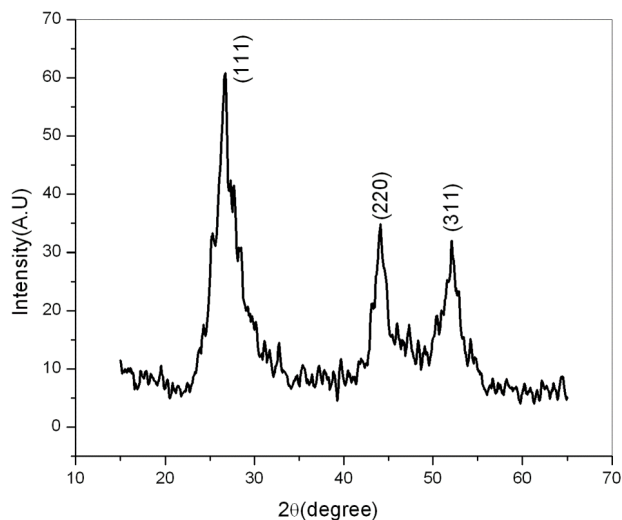


Figure 3.2: A typical XRD pattern of CdS nanoparticles S2

A typical XRD pattern of the CdS nanoparticles prepared as above is as shown in Figure 3.2. Three broad peaks at $2\theta = 26.7^\circ$, 44° and 52° belonging to (1 1 1), (2 2 0) and (3 1 1) respectively, which are in agreement with Miller indices of a cubic zinc-blende-type structure (JCPDS file no. 10454). Mixture of hexagonal and cubic phases is routinely observed in nanoparticles of CdS, as the two phases have similar energy and, hence, the transformation from one to another is most feasible [12]. It is reported that the particle size plays an important role in deciding the crystal structure. With reduction in the size, the material goes from the hexagonal wurtzite-type structure to the cubic zinc blende-type structure if the particle size is below 5 nm, above this value, the material will have a mixture of both phases. In the present pattern, the peak located at 26.7° is more symmetric and (1 0 3) peak at 48° of hexagonal phase is absent. This shows that the present nanoparticles exhibit cubic phase due to their small particle size. Using Debye–Scherrer’s formula $D = 0.89\lambda/\beta \cos(\theta)$, (where D is the particle diameter, λ is the wavelength of X-ray used, β is the full width half maximum and θ is the scattering angle), the estimated particle

size is in the range of 5nm, which is quite close to the size estimated from optical absorption measurements

Scanning electron microscopy (SEM) of CdS powder was performed on JEOL Model JSM - 6390LV. A gold film was evaporated on the samples before loading on the instrument. SEM of the powder indicated the formation of fine spherical particles of cadmium sulphide and the majority of the particles appeared in the range of below 100 nm (Figure 3.3).

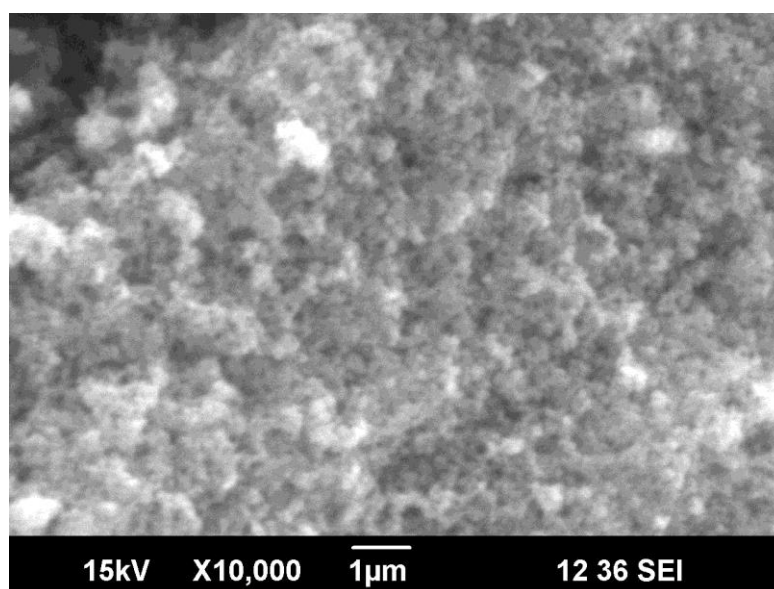


Figure 3.3: SEM of S1 particles

Figure 3.4 shows the fluorescence spectrum of S1 particles when excited with wavelengths 380nm. It shows two bands of emissions one around 423nm and other around 520nm when excited with 380 nm wavelength. There is a small emission peak at 486nm. 423nm and 486nm emissions are assigned to the excitonic emissions

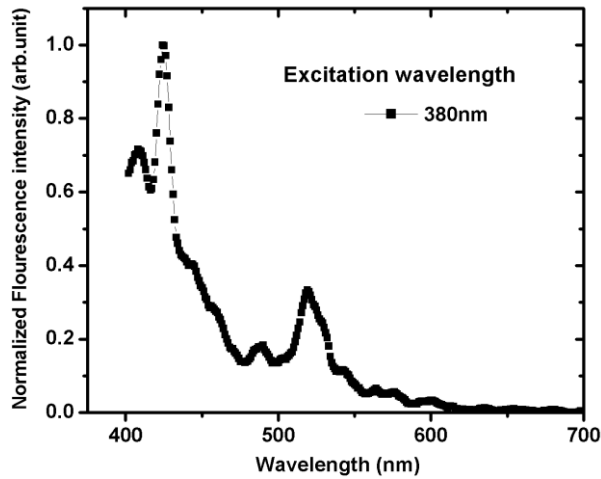


Figure 3.4: Emission spectra of S1 particles when excited with excitation wavelength of 380nm

As CdS has a broadband absorption, excitation spectrum is very significant in finding the optimum excitation wavelengths at which it has maximum emission intensity

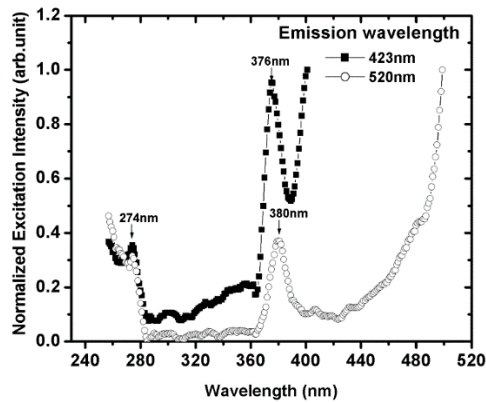


Figure 3.5: Excitation spectra for emission wavelengths 423nm and 520nm of S1 particles

Figure 3.5 shows the excitation spectrum for an emission peak of 423 nm and 520nm. For 423nm emission, the excitation spectrum shows peaks at 274nm and 376 nm. Also for 520nm emission wavelength, there exists a peak

at 274nm and another peak at 380nm that is a shift of 4nm to the later peak with respect to the 423nm emission.

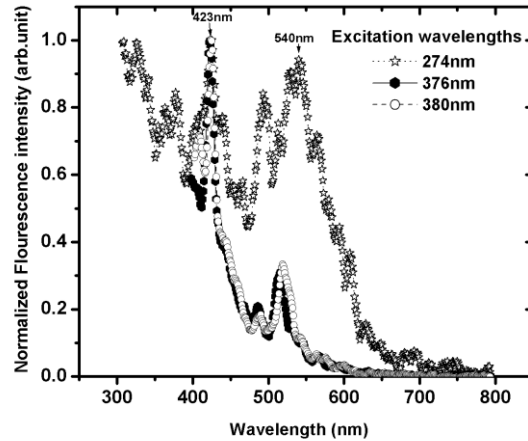


Figure 3.6: Emission spectra of S1 particles when excited with excitation peaks of 274nm, 376nm and 380nm

The fluorescence spectra of CdS nanoparticles under different excitation wavelengths of 274nm, 376 nm and 380nm are shown in Figure 3.6.

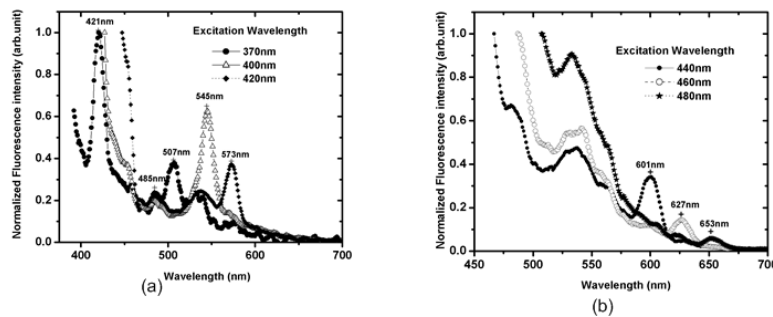


Figure 3.7: Emission spectra of S1 particles when excited with (a) lower wavelengths (370nm-420nm) and (b) higher wavelengths (440nm-480nm)

Results show that at the excitation of 274nm, there is an emission at 492nm and a broad emission band around 540nm. Also at excitation of 376nm and 380nm, the emission peaks at 516nm and 520nm occur. That is, when excitation wavelength is changed from 376nm to 380nm, the emission peak at 516nm is shifted to 520nm, i.e., a shift of 4nm, which indicates an excitation

wavelength dependent shift. This observation indicates the effect on this emission peak under different excitation wavelengths. Hence the fluorescence spectra for different excitation wavelengths could lead to interesting results. The fluorescence spectrum of S1 particles for different excitation wavelengths is shown in Figure 3.7.

It is observed that the emission peak wavelength for these S1 particles differ with the variation in the excitation wavelengths from 370nm-480nm. Figure 3.7a shows the variation of peak shift for shorter range of excitation wavelengths (370nm-420nm). When S1 particles are excited with 370nm, there are three peaks at 421nm, 485nm, 507nm and a shoulder at 454nm in the fluorescence spectrum. 507nm peak is shifted to 545nm, when excitation wavelength is changed to 400nm. This peak at 545nm is again shifted to 575nm when the excitation wavelength is changed to 420nm. For all excitation wavelengths from 380nm to 420nm, there is a weak peak present at 486nm. In Figure 3.7b, the emission peak at 575nm is shifted to 601nm for the excitation wavelength of 440nm. The above trend in the emission peak shift is continued up to the excitation wavelength of 480nm, at which the emission peak occurs at 654nm. For excitation wavelengths longer than 480nm, the emission peak intensity is very weak and further peak shift cannot be verified. Thus it is found that among four spectral peaks (421nm, 454nm, 486nm, 507nm), the shift occurs only for 507nm peak, when excited with different wavelengths. The emissions at 421nm, 454nm and 486nm are from the excitonic levels [13-15]. The emissions at 421nm, 450nm and 486nm are not shifted for these particles, which indicates that the change in the particle size does not affect the emission band associated with the nanocrystallite core [16, 17].

In the present case, the emission peaks at 423nm, 450nm and 486nm are assigned to the excitonic emissions. The emission peak at 507nm is shifted with the change in excitation wavelengths. These shifting emission peaks occurring

at larger wavelengths with respect to the band edge emission are attributed to the quasi-free recombination at the absorption band edge, the shallow- trap state near the absorption band edge, the deep-trap band far below the band edge, and a combination of these effects, are called the surface state emissions. Surface state is generally localized within the band gap of the semiconductor and they can trap the excited state electrons and lead to red-shifted emissions. The quasi free recombination and shallow trap emission could be overlapping due to broad size distribution. In this experiment, the possible trapped states may come from the anion (S^{2-}) or cation (Cd^{2+}) vacancy defects. If the trapped states were generated by the cation vacancy, such trapped states would have located at 1.5eV above the valance band [18]. Recombination from conduction band to such trapped states would have resulted in a weak emission with a wavelength of 700-760nm, in both samples which was not observed. So these emissions can be assigned to the shallow trapped states recombination formed by sulphur vacancy defects. It is reported that S^{2-} vacancy defect in CdS nanoparticles are located at about 0.6eV-0.7eV below the conduction band. That is, if an electron is trapped by this anion vacancy defect, one can expect a photoluminescence blue shift with respect to the E_g as the band gap in the CdS nanocrystals are size-dependent [18, 19]. A typical spatial electronic state for CdS nanoparticles is shown in Figure 3.8(a). From Figure 3.8(a), it is clear that when dimension of the CdS nanoparticles approach the shallow trap diameter, the shallow trap wave function overlaps strongly with the corresponding valence or conduction band wave function [19].

The peak emission shift is manifested above the emission wavelength of 507nm which is found to be the band edge emission of these nanoparticles and it is blue-shifted from bulk emission of 520nm due to the quantum confinement effect. This emission peak shift can be explained on the basis of a double well model which incorporates the surface states to account for the excited electronic

Synthesis and Study of Linear Optical Properties of CdS, TiO₂ and Au Nanoparticles

states [20] in the CdS nanoparticles as shown in Figure 3.8(b). Here one of the wells accounts for the excitonic or intrinsic core state emission and the second well is for the surface state emission. These two wells overlap when the dimensions of CdS nanoparticles become close to the shallow trap diameter. This peak emission wavelength shift is due to the selective excitation of vibronic levels in the surface state of the CdS nanoparticles. The trapping process is reported to be fast (hundreds of femtosecond) and consequently the spontaneous fluorescence cannot compete with it [20]. So the energy transfer between the upper vibrational level and lower vibrational level of the excited state of the particle becomes inefficient due to this shortening of life time, which leads to the excitation wavelength dependent emission characteristics of these nanoparticles

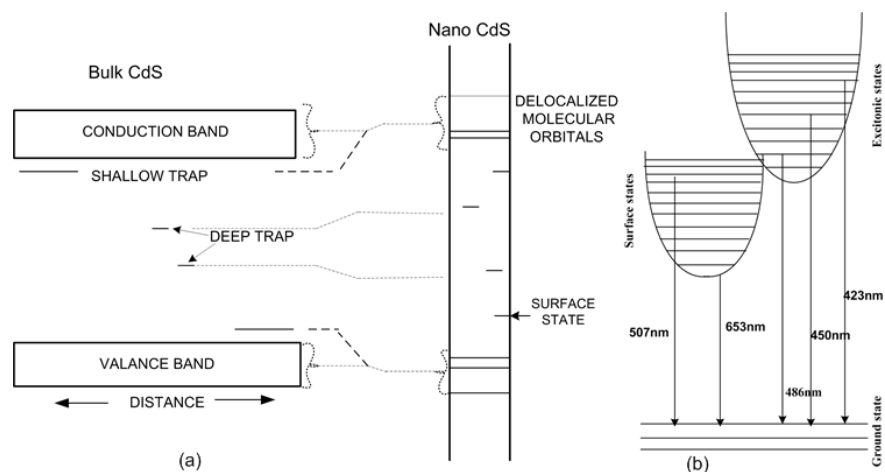


Figure 3.8: (a) Spatial electronic state correlation diagram (b) Emissions in two wells of CdS nanoparticles

There is a band structure around 532nm, which ranges from 517nm to 572nm, for the excitations from 440nm to 480nm. This broad band luminescence can be attributed to the mid-gap states and this occurs normally with low intensity [14].

The fluorescence spectrum of S2 particles also shows a similar shift of emission peaks as shown in Figure 3.9.

From Figure 3.9, it is clear that the main peak observed for S2 particles is at 421nm which is same as that of the S1 particles, when excited with 370nm. The second prominent emission peak is at 506nm which is 1nm blue shifted when compared to that of S1 particles.

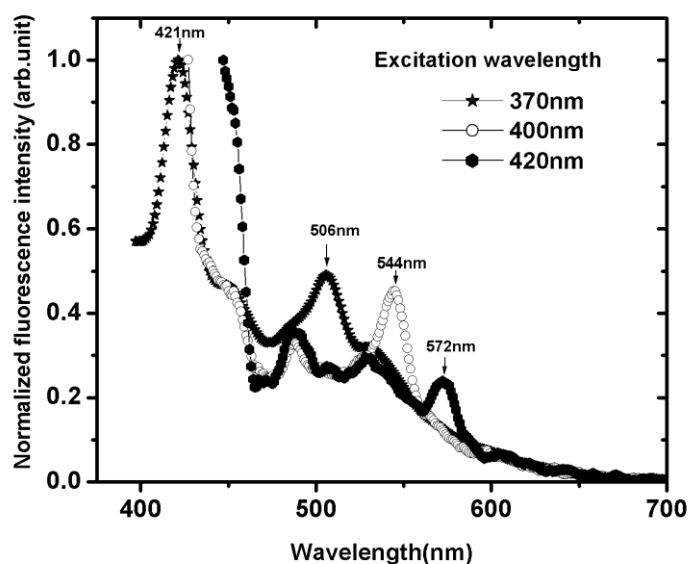


Figure 3.9: Emission spectra of S2 particles for excitation wavelengths (370nm-420nm)

This peak emission wavelength is shifted from 506nm to 572nm when the excitation wavelength is changed from 370nm to 420nm. For 440nm excitation wavelength, the emission peak is very weak. Thus, it can be stated that the peak emission wavelength shift is not observed from excitation wavelength of 440nm onwards.

The size dependence of photoluminescence (emission around 520nm) with respect to S1 and S2 particles reveals that trapped carriers at the surface states are also confined by the spatial-confinement effect. The energy of surface state can also be modified through quantum size effect, which is similar to the case of the exciton confinement.

3.3 Preparation and optical properties of TiO₂ nanoparticles

Although TiO₂ nanoparticles are considered to be one of the most important quantum semiconductor particles, there are only a few reports that describe the preparation of crystalline TiO₂ nanoparticles monodispersed in a stable suspension. The preparation of TiO₂ nanoparticles in solution phase would be one of the best synthetic routes, both for controlling the size of individual particles and for obtaining the stabilized colloidal suspensions. The suspended crystalline nanoparticles not only serve as ideal precursors for further material development but also offer some other unique opportunities, such as enabling studies of their optical, photocatalytic and other fundamental properties under solution-like conditions. The optical properties of these suspended nanoparticles have not been studied in great detail [21]. In the present study, we report the optical properties of TiO₂ colloidal nanoparticles and nanocrystallites with emphasis to fluorescence spectra.

3.3.1 Experimental

TiO₂ colloidal nanoparticles were prepared by hydrolyzing titanium isopropoxide. The materials used for the preparation of colloidal TiO₂ are: titanium (IV) isopropoxide (TIP, Ti(C₃H₇O)₄) used as titanium precursor, nitric acid (HNO₃) as peptizing agent, deionized water and isopropanol (C₃H₇OH) as solvent. Titanium (IV) isopropoxide of synthesis grade purchased from Lancaster. All the other chemicals are of GR grade from Merck Ltd

In this work, we stabilized titanium isopropoxide in acidic isopropanol / water solution prior to hydrothermal reaction. The precursor solutions is made by mixing varying volume percent of titanium isopropoxide (TIP (97%)) as 0.5%, 0.9%, 1.1%, 1.4% and 2.9%, 15ml of Isopropanol and 250ml solution of distilled water with varied pH obtained by adding HNO₃. These solutions are vigorously stirred and annealed at 60°C for 8 hours and this gives white bluish

stable TiO₂ colloidal nanoparticles as a result of the thermal decomposition of TIP are termed as T1(0.5%), T2(0.9%), T3(1.1%), T4 (1.4%) and T5(2.9%) samples. These colloidal nanoparticles are optically characterized by measurement of their light absorption at room temperature which is carried out using a spectrophotometer (JascoV-570 UV/VIS/IR). The fluorescence emission from the same sample was recorded using a Cary Eclipse fluorescence spectrophotometer (Varian). TiO₂ colloidal nanoparticles (T4) are dried and annealed at 400°C to get yellowish white nanocrystallite. These nanocrystals were also optically characterized as mentioned in the case of TiO₂ colloidal nanoparticles. The Fourier transform infrared (FT-IR) spectra of the samples were collected using Thermo Nicolet, Avatar 370 infrared spectrometer. The structural properties of this sample are investigated by X-ray diffraction (XRD) on a Bruker AXS D8 Advance x-ray diffractometer with Ni-filtered Cu K α (1.5406Å) source II. Transmission electron microscopy (TEM) of TiO₂ colloidal nanoparticles were performed on JOEL HRTEM machine for size measurement

3.3.2 Results and Discussions

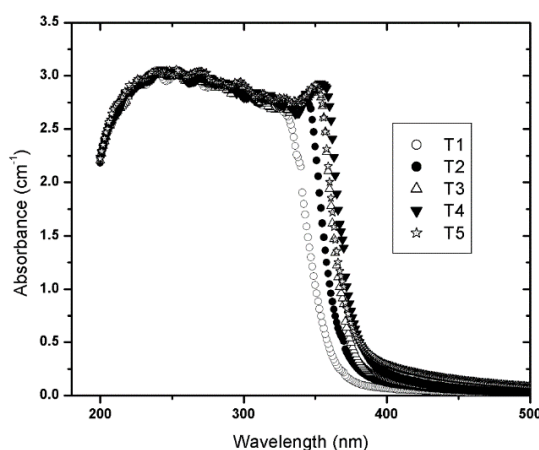


Figure 3.10: Absorption spectra of colloidal TiO₂ particles

Figure 3.10 shows the UV-VIS absorption spectra recorded for TiO₂ colloidal nanoparticles. Absorption edge is blue shifted as the concentration of the precursor is reduced. Similar observations have been made during the case of ZnO nanoparticles in colloidal solution and were interpreted in terms of quantum confinement effects [22, 23]. This is termed as Q size effects. i.e., the particle size is reduced when the concentration is reduced. Titania possesses a highly ionic lattice with the valence band composed principally of oxygen 2p orbitals, with the corresponding wave functions considerably localized on the O²⁻ lattice sites. The conduction band consists mostly of excited states of Ti⁴⁺.

In order to determine the nature of the optical band gap as either indirect or direct, one has to consider the variation of the absorption coefficient with energy. Bulk TiO₂ is an indirect band gap semiconductor. In this case a two-step process is necessary for the optical transition because a photon cannot provide the required change in momentum and the lowest-energy inter-band transition and must then be accompanied by phonon excitation. When phonon energy can be neglected, the absorption coefficient α near the absorption edge for indirect inter-band transitions is given by equation (3.1) [24]. Indirect inter-band transitions are characterized by the stronger energy dependence of the optical absorption coefficient nearer the absorption edge than is otherwise as in the case for direct transition,

$$\alpha = B_i \frac{(\hbar\nu - E_g)^2}{\hbar\nu} \quad (3.1)$$

where B_i is the absorption constant for an indirect transition, ν is the frequency. E_g -bulk bandgap. Serpone et al.[21] have established that both indirect and direct transition mechanisms are operative in nanophase TiO₂. In the case of direct band gap semiconductor, the optical absorption coefficient near the absorption edge for inter-band transitions is given by equation (3.2)

$$\alpha = B_d (\hbar\nu - E_g)^{1/2} / \hbar\nu \quad (3.2)$$

where B_d is the absorption constant for a direct transition

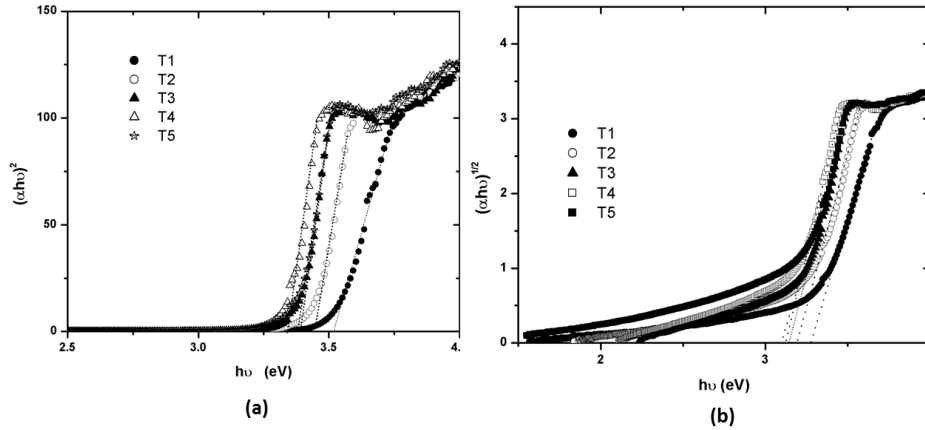


Figure 3.11: a) Direct optical band gap transitions $(\alpha h\nu)^2$ vs $h\nu$ plot and (b) Indirect optical band gap transitions $(\alpha h\nu)^{1/2}$ vs $h\nu$ plot

In our case, the spectrum is characterized by a sharp band edge along with a series of exciton states. Figure 3.11(a) and Figure 3.11(b) represent direct and indirect optical band gap plots for T1, T2, T3, T4 and T5 colloidal nanoparticles. The direct band gap of these colloidal nanoparticles are obtained by plotting $(\alpha h\nu)^2$ versus $h\nu$ graph, shown in Figure.3.11(b). The band gap of colloidal nanoparticles gets decreased, when the precursor concentration is increased. From Fig 3.11(b), the estimated direct band gap of T1, T2, T3, T4 and T5 are 3.52eV, 3.45eV, 3.39eV, 3.34eV and 3.38eV. Thus a direct band gap variation of 0.18eV can be obtained by varying the precursor concentrations and these could be attributed to the $X_1 \rightarrow X_1$ transitions. In the case of indirect direct transitions, Figure 3.12(b) shows intercepts at 3.28eV, 3.2eV, 3.15eV, 3.12eV and 3.12eV which are the indirect band gaps those are somewhat red-shifted as the concentration of the precursor is increased (a band gap tuning of around 0.16eV) and it is assigned to $\Gamma_1 \rightarrow X_1$ transitions, where X denotes the edge and Γ the centre of the Brillouin zone [25].

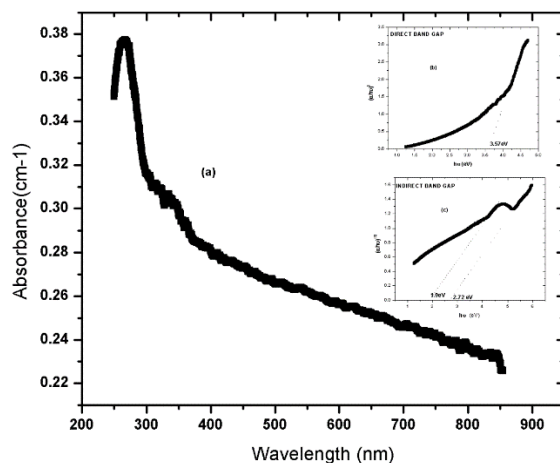


Figure 3.12: (a) Absorption spectra of annealed TiO₂ nanocrystals, insets (b) $(\alpha h\nu)^2$ vs $h\nu$ plot and (c) $(\alpha h\nu)^{1/2}$ vs $h\nu$ plot

It is observed that the absorption of colloidal nanoparticles is higher than that of annealed sample. The absorption spectrum of the annealed TiO₂ nanoparticles is shown in Figure 3.12(a). Figure 3.12(b) and (c) represents the direct and indirect band gaps for the annealed sample. The extrapolated intercept occurs at 2.72 eV which can be assigned to the indirect transition (Fig. (3.12c)) for the annealed sample. The inset in Figure 3.12 (b) represents the direct band gap plot and it is found that the value of band gap is 3.57 eV ($X_2 \rightarrow X_1$ transition) [26]. This can be explained due to the reduced ionicity of the TiO₂ phase synthesized, which results from mixing of the O²⁻ p-orbitals and Ti³⁺ d- orbitals. Similar absorption features have been seen in the work of Serpone *et al.* [21].

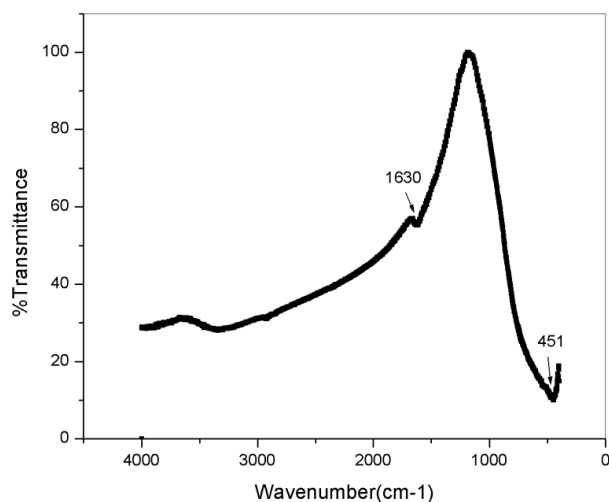


Figure 3.13: FTIR spectrum of TiO₂ nanocrystals

Figure 3.13 shows the FTIR spectrum of the TiO₂ samples prepared as described earlier. From this spectrum, it can be observed that strong band in the range of 880cm⁻¹ and 450 cm⁻¹ is apparently associated with the characteristic vibrational modes of TiO₂. The absorption at 3391 cm⁻¹ indicates the presence of hydroxyl group, which is probably due to the fact that the spectra were not recorded in situ and some re-adsorption of water from the ambient atmosphere has occurred [26]. In this figure, strong bands at 3,400 and 1,630 cm⁻¹, which are attributable to the stretching mode of the –OH group and the deformation mode of molecular water respectively, can be seen.

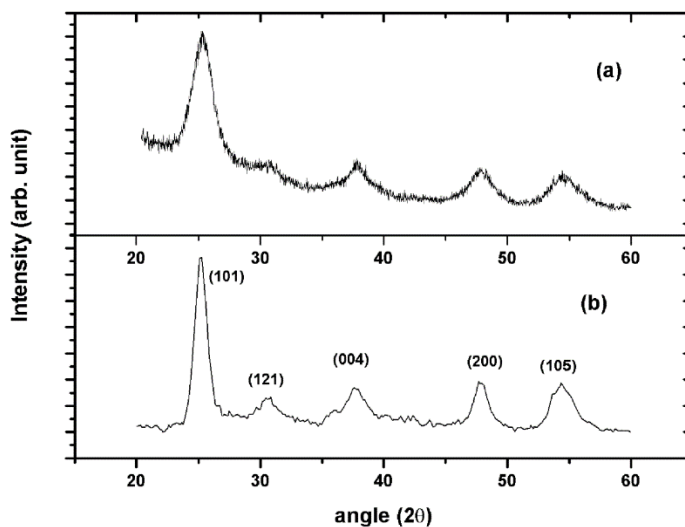


Figure 3.14: XRD spectra of TiO₂ nanoparticles and annealed TiO₂ nanocrystals

Figure 3.14 shows the XRD pattern of (a) colloidal nanoparticles and (b) annealed particles. The XRD pattern of colloidal particles shows broad peaks compared to that of annealed particles. The broadness of peaks indicates that the colloidal particles are much lower in size compared to annealed particles. All the diffraction lines are assigned well to anatase crystalline phase of titanium dioxide except a small peak at 30.65°. The separate peak at 30.65° indicates the presence of brookite phase of TiO₂. The diffraction peaks of (101), (004), (200), (105) correspond to the anatase TiO₂ phase. The separate peak at (121) assigned to the XRD pattern is in excellent agreement with a reference pattern (JCPDS 21-1272) of titanium dioxide. It should be noted that only anatase TiO₂ can be detected and no rutile phase can be found in this sample, which can be attributed to the contribution of the low concentration of oxygen vacancies due to the high concentration of gaseous oxygen during particle growth, hindering the transformation from anatase to rutile phase. It is noted that the particle size plays an important role in deciding the crystal structure. Using Debye–Scherrer’s

formula ($[D = 0.89\lambda/\beta \cos(\theta)]$, where D is the particle diameter, λ is the wavelength of X-ray used, β is the full width half maximum and θ is the scattering angle), the estimated particle size for the colloidal particles is in the range of 4nm and for the annealed particles, the estimated size is found to be around 8nm. i.e., sample while annealed at 400°C yields much larger particles compared to the non-annealed sample. This is due to the aggregation of particles while annealing the colloidal nanoparticles.

The high resolution transmission electron micrographs (HRTEM) of T₄ colloidal particles are shown in Figure 3.15. It shows that the particles are having spherical shape and the size of the particles is found out to be around 2.5nm and also shows the d-spacing of the colloidal particles around 3.62°A which is in agreement with the literature value. This is slightly less than the size of particle from X-ray diffraction analysis.

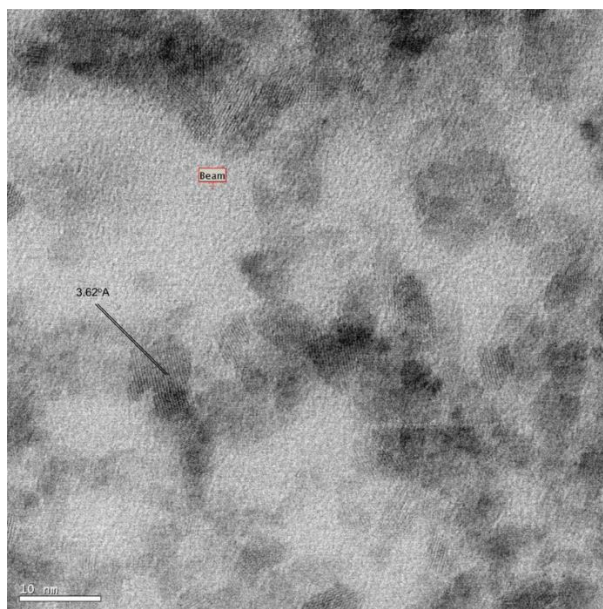


Figure 3.15: HRTEM picture of colloidal (T4) TiO₂ nanoparticles

The optical properties of a semiconductor are mainly determined by its electronic structure, so the essence of light absorption will be found by studying

the relationship between electronic structure and optical properties of TiO₂. After excitation by photon, the electron-hole pairs might recombine in the process of migration from inside to the surface of the crystal. The recombination rate is closely related to the electronic structure and crystal structure. As TiO₂ has a broadband absorption, excitation spectrum is very significant in finding the excitation wavelengths at which it has maximum emissions.

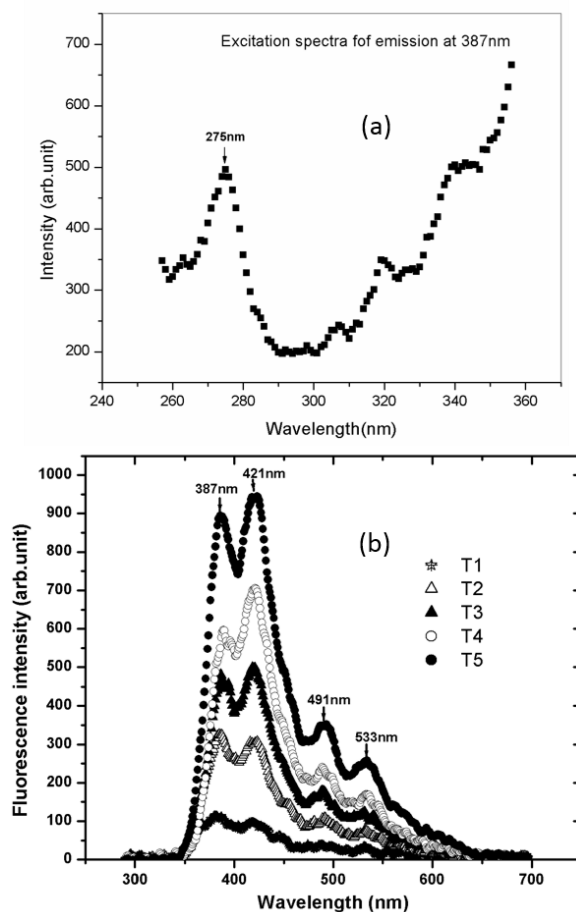


Figure 3.16: (a) Excitation spectrum of TiO₂ colloidal nanoparticles and (b) Fluorescence spectrum of colloidal nanoparticles

Figure 3.16(a) shows the excitation spectrum for emission peak of 387nm. From the absorption spectrum, it is clear that the peak wavelength 274nm of excitation spectrum is coming in the high absorption range. Figure 3.16 (b)

shows the fluorescence spectrum of the TiO₂ colloidal nanoparticles (T1, T2, T3, T4 and T5) for the excitation wavelength of 274 nm.

From the fluorescence spectrum, emissions at 387nm, 421nm, 491nm and 533 nm are observed. These emission peaks occurring at larger wavelengths with respect to the band edge emission (387nm) are attributed to the quasi-free recombination at the absorption band edge, the shallow trap state near the absorption band edge, the deep-trap band far below the band edge, and a combination of these effects, which are called the surface state emissions. Surface state is generally localized within the band gap of the semiconductor and they can trap the excited state electrons and lead to higher wavelength emissions. The quasi free recombination and shallow trap emission could be overlapping due to broad size distribution as there is no capping agent is used in this preparation. The oxygen vacancies and surface hydroxyl groups are dominant sites for trapped electrons and holes. These trapped carriers which are captured by oxygen vacancies and surface hydroxyl groups, contribute to the visible luminescence in these nanoparticles. Emission at 387nm is found to be excitonic emission. 421nm, 491nm, 533nm emissions are assigned to the surface state emissions and are due to the recombination of trapped electron-hole arising from dangling bonds in the TiO₂ nanoparticles.

Figure 3.17 shows the fluorescence spectrum of the annealed sample, the intensity of emission peak at 422nm is higher than that of 387nm which indicates that the nanoparticle having more surface states dominate the excitonic emission. Other emissions around 493nm, 534nm and 573nm are having less intensity compared to the peaks at 421nm and 387nm. The emission at 534nm is found to be due to O²⁻ vacancies. In this case, the photoluminescence is mostly a surface phenomenon, and a change in the surface environment would have a significant effect on the photoluminescence process.

Therefore, it is concluded that the visible luminescence band originates from the oxygen vacancies associated with Ti^{3+} in anatase TiO_2 . Similar description of the visible luminescence band was reported earlier [27, 28].

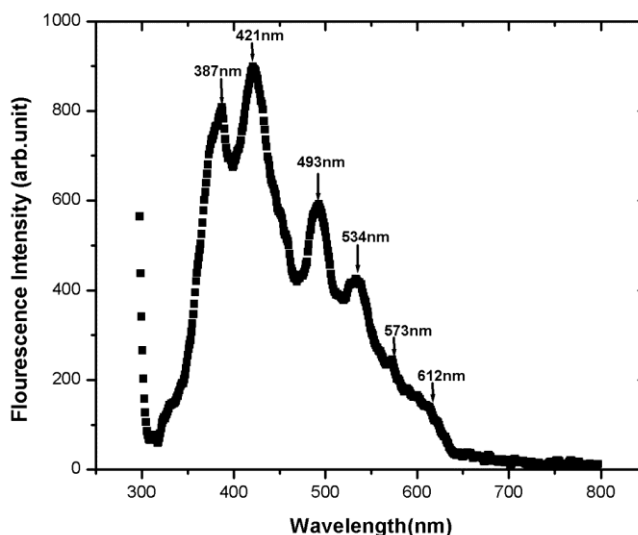


Figure 3.17: Fluorescence spectrum of annealed TiO₂ nanocrystals.

The whole emission mechanism is depicted in the Figure 3.18. It is observed that the surface state emission basically consists of two categories of emission. One set occurs as series giving emissions at 421nm, 491nm and 573nm with almost a difference of nearly 80nm. This set of emissions is from the deexcitation from lower vibronic levels in Ti^{3+} 3d states of TiO_2 lattice to the deep trap levels (acceptor) created by (OH^-) . And other set is having emission wavelengths 533nm and 612nm, which are also separated by nearly 80nm. These emissions are due to deexcitation from lower vibronic levels in the oxygen vacancies of TiO_2 lattice to the ground state.

In order to find out dependence of the increase in particle size of colloidal TiO_2 nanoparticles on the excitonic and surface state emission, ratio of the emission intensity of 387nm to that of 421nm is plotted against volume

percentage of precursor in Figure 3.19. As the volume percentage increases, the excitonic emission at 387nm, gets decreased compared to the surface state emission at 421nm.

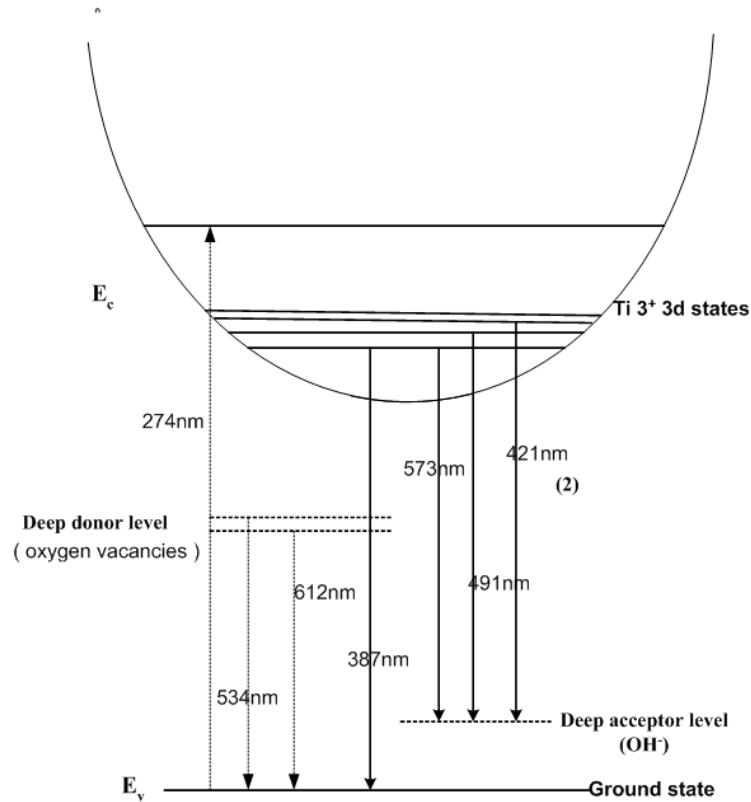


Figure 3.18: Emission mechanism for TiO₂ nanoparticles

Normally we expect the relative intensity of surface states to increase as the particle size decreases. However E. Hanamura [28] showed that there will be increase in oscillator strength with the decrease in particle size, so that there is an overall decrease in relative intensity of surface state emission. In the present case, beyond 1.4% volume concentration, we infer the oscillator strength gets stabilized so that the relative intensity shows a reverse trend. However at this concentration the particle size distribution also gets affected as seen from the broader nature of the emission spectrum.

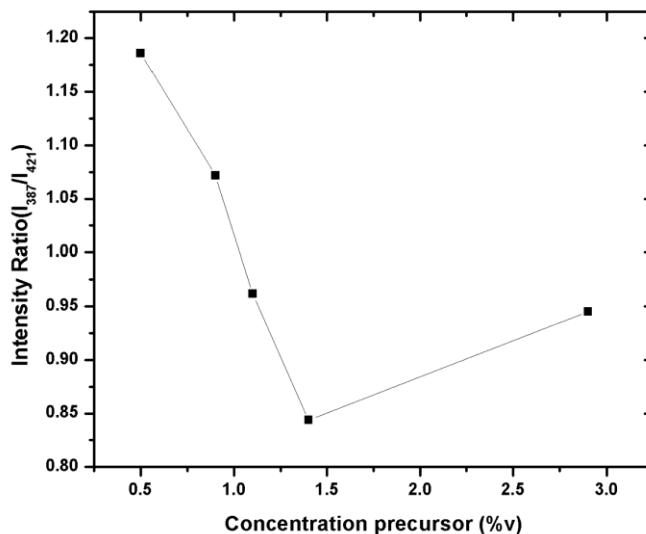


Figure 3.19: Intensity ratio of excitonic and dominant surface state emissions

Comparing the emissions of colloidal TiO₂ nanoparticles, it is clear that the size reduction of particles actually makes an impact on the fluorescence emission. Annealing the colloidal nanoparticles can cause aggregation and hence defect densities from grain boundaries. Thus confinement effects and also the increased surface states at nano regime play a vital role in the fluorescence emission of colloidal and annealed TiO₂ nanoparticles.

3.4 Preparation and linear optical properties of gold nanoparticles

Noble metal nanoparticles such as gold or silver exhibit plasmon bands depending on their shape and size and have a wide variety of potential applications such as sensors, nonlinear optical applications etc [29,30]. Numerical physical methods or chemical methods have been employed to prepare Au nanoparticles such laser ablation, chemical reduction etc [31, 32]. In the present work, chemical reduction technique have been employed.

3.4.1 Experimental

The colloidal gold nanoparticles are prepared following a method introduced by Turkevich [33]. Initially 1mM trisodium citrate solution prepared in 50ml deionized water. 1ml of 10mM HAuCl₄ is added is dissolved in 50 ml of deionized water. Both solutions are mixed and thus obtained solution is vigorously stirred for 1 hr and a red colour Au nanocolloidal solution is formed. Different nanocolloids are prepared by varying the volume of precursor stock solution (10mM HAuCl₄) from 1ml, 1.5ml and 2ml. These colloids are termed as Au1 Au2 and Au3. The measurement of their light absorption at room temperature is carried out using a spectrophotometer (JascoV-570 UV/VIS/IR).

3.4.2 Results and Discussion

Figure 3.20 shows the UV-VIS absorption spectra recorded for Au colloidal nanoparticles. Absorption edge is slightly red shifted as the concentration of the precursor is increased. Absorption peak is found to be 523nm, 525nm and 524nm for Au1, Au2 and Au3 nanoparticles respectively. And these absorption peaks are characteristics of relatively small particles [30, 34]. The surface scattering is related to Fermi velocity (V_f 1.4×10^8 cm/s for gold) and particle radius by equation [35],

$$\omega_s = \frac{AV_f}{r} \quad (3.3)$$

This expression can be interpreted as a limitation of the mean free path of the free electrons by the particle dimensions. The proportionality factor, A, is on the order of unity assuming the scattering to be isotropic. The sizes of the nanoparticles calculated by the above relation are 4.88nm, 4.9nm and 4.89nm for Au1, Au2 and Au3 nanoparticles.

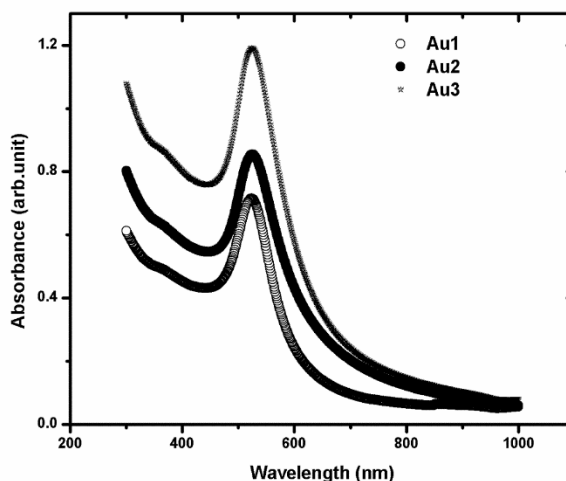


Figure 3.20: Absorption spectra of gold nanoparticles

There was no fluorescence emission found for these nanoparticles. The parameters deduced from optical absorption are shown below in table 3.1.

Table 3-1: Parameters deduced from absorption of Au nanoparticles

Sample	FWHM (nm)	Size (nm)
Au1	52.4	4.9
Au2	58.9	4.9
Au3	58.7	4.9

From the above values it is clear that the size of the nanoparticles are not much dependent on the concentration of the precursor solution.

3.5 Conclusions

In conclusion, we prepared CdS, TiO₂ and Au nanoparticles. We observed that the fluorescence behaviour of the CdS nanoparticles, prepared by precipitation technique, depends on excitation wavelength. It is found that the peak emission wavelength can be shifted by as much as 147nm by varying the excitation wavelengths and the reason for this phenomenon is the selective

excitation of the surface states in the nanoparticles. This provides certain amount of tunability for the emission which results from surface states. TiO_2 nanoparticle colloids were prepared by hydrothermal method. The optical absorption study shows a blue shift of absorption edge, indicating quantum confinement effect. The large spectral range investigated allows observing simultaneously direct and indirect band gap optical recombination. The emission studies carried out show four peaks, which are found to be generated from excitonic as well as surface state transitions. It is found that the emission wavelengths of these colloidal nanoparticles and annealed nanoparticles show two category of surface state emission in addition to the excitonic emission. Au nanoparticles are prepared by Turkevich method shows nanoparticles of size below 5nm using plasmonic absorption calculation. It is also found that there is almost no variation in size as the concentration of precursor is changed from 0.2mM to 0.4mM.

References

- [1] B. Palpant, B. Prével, J. Lermé, E. Cottancin, M. Pellarin, M. Treilleux, A. Perez, J. Vialle and M. Broyer, "Optical properties of gold clusters in the size range 2–4 nm," *Physical Review B*, vol. 57, pp.1963-1970, 1998.
- [2] J. Z. Zhang, Z. Wang, J. Liu, S. Chen and G. Liu, "Optical, Electronic, and Dynamic Properties of Semiconductor Nanomaterials," *Self-Assembled Nanostructures*, pp. 201-255, 2004.
- [3] J. Tittel, W. Göhde, F. Koberling, T. Basché, A. Kornowski, H. Weller and A. Eychmüller, "Fluorescence spectroscopy on single CdS nanocrystals," *The Journal of Physical Chemistry B*, vol. 101, pp. 3013-3016, 1997.
- [4] H. Weller, "Quantum size colloids: From size-dependent properties of discrete particles to self-organized superstructures," *Current Opinion in Colloid & Interface Science*, vol. 3, pp. 194-199, 1998.

- [5] J. R. Lakowicz, I. Gryczynski, Z. Gryczynski and C. J. Murphy, "Luminescence spectral properties of CdS nanoparticles," *The Journal of Physical Chemistry B*, vol. 103, pp. 7613-7620, 1999.
- [6] L. Irimpan, B. Krishnan, A. Deepthy, V. Nampoori and P. Radhakrishnan, "Excitation wavelength dependent fluorescence behaviour of nano colloids of ZnO," *J. Phys. D*, vol. 40, pp. 5670-5674, 2007.
- [7] D. Lincot, R. Ortega-Borges and M. Froment, "Epitaxial growth of cadmium sulfide layers on indium phosphide from aqueous ammonia solutions," *Appl. Phys. Lett.*, vol. 64, pp. 569-571, 1994.
- [8] P. Raji, C. Sanjeeviraja and K. Ramachandran, "Thermal properties of nano crystalline CdS," *Crystal Research and Technology*, vol. 39, pp. 617-622, 2004.
- [9] L. Brus, "Electronic wave functions in semiconductor clusters: experiment and theory," *J. Phys. Chem.*, vol. 90, pp. 2555-2560, 1986.
- [10] Y. Jian-Xi, Z. Gao-Ling and H. Gao-Rong, "The effect of the ratio of thiourea to Cd²⁺ on the properties of CdS nanoparticles," *Microelectronic Engineering*, vol. 66, pp. 115-120, 2003.
- [11] M. Pattabi, B. S. Amma and K. Manzoor, "Photoluminescence study of PVP capped CdS nanoparticles embedded in PVA matrix," *Mater. Res. Bull.*, vol. 42, pp. 828-835, 2007.
- [12] S. Takeuchi and K. Suzuki, "Stacking fault energies of tetrahedrally coordinated crystals," *Physica Status Solidi (a)*, vol. 171, pp. 99-103, 1999.
- [13] [13] J. Fernandez, M. de Souza-Parise and P. Morais, "Optical investigation of the red band emission of CdS nanoparticles," *Surf. Sci.*, vol. 601, pp. 3805-3808, 2007.
- [14] Y. Li, F. Huang, Q. Zhang and Z. Gu, "Solvothermal synthesis of nanocrystalline cadmium sulfide," *J. Mater. Sci.*, vol. 35, pp. 5933-5937, 2000.
- [15] J. Yao, G. Zhao and G. Han, "Synthesis and characterization of the thiourea-capped CdS nanoparticles," *J. Mater. Sci. Lett.*, vol. 22, pp. 1491-1493, 2003.

- [16] R. Rossetti, S. Nakahara and L. E. Brus, "Quantum size effects in the redox potentials, resonance Raman spectra, and electronic spectra of CdS crystallites in aqueous solution," *J. Chem. Phys.*, vol. 79, pp. 1086-1086, 1983.
- [17] J. He, W. Ji, G. Ma, S. Tang, H. Elim, W. Sun, Z. Zhang and W. Chin, "Excitonic nonlinear absorption in CdS nanocrystals studied using Z-scan technique," *J. Appl. Phys.*, vol. 95, pp. 6381-6386, 2004.
- [18] G. Ma, S. Tang, W. Sun, Z. Shen, W. Huang and J. Shi, "Size-dependent excited state properties of CdS nanocrystals," *Physics Letters A*, vol. 299, pp. 581-585, 2002.
- [19] N. Chestnoy, T. Harris, R. Hull and L. Brus, "Luminescence and photophysics of cadmium sulfide semiconductor clusters: the nature of the emitting electronic state," *J. Phys. Chem.*, vol. 90, pp. 3393-3399, 1986.
- [20] Z. Bing-Suo, W. Zhen-Yu, C. Li, D. Jian-Hua, Z. Ze-Bo, N. Yu-Xin and X. Si-Shen, "Core-shell Structure and photoluminescence of CdS quantum dots," *Chinese Physics Letters*, vol. 18, pp.1275, 2001.
- [21] N. Serpone, D. Lawless and R. Khairutdinov, "Size effects on the photophysical properties of colloidal anatase TiO₂ particles: size quantization versus direct transitions in this indirect semiconductor?" *J. Phys. Chem.*, vol. 99, pp. 16646-16654, 1995.
- [22] L. Irimpan, V. Nampoore, P. Radhakrishnan, A. Deepthy and B. Krishnan, "Size dependent fluorescence spectroscopy of nanocolloids of ZnO," *J. Appl. Phys.*, vol. 102, pp. 063524-1-6, 2007.
- [23] U. Koch, A. Fojtik, H. Weller and A. Henglein, "Photochemistry of semiconductor colloids. Preparation of extremely small ZnO particles, fluorescence phenomena and size quantization effects," *Chemical Physics Letters*, vol. 122, pp. 507-510, 1985.
- [24] J. I. Pankove, *Optical Processes in Semiconductors*. Courier Corporation, 2012.
- [25] N. Daude, C. Gout and C. Jouanin, "Electronic band structure of titanium dioxide," *Physical Review B*, vol. 15, pp. 3229, 1977.

- [26] P. M. Kumar, S. Badrinarayanan and M. Sastry, "Nanocrystalline TiO₂ studied by optical, FTIR and X-ray photoelectron spectroscopy: correlation to presence of surface states," *Thin Solid Films*, vol. 358, pp. 122-130, 2000.
- [27] S. Mochizuki, "Intense white luminescence of Sm₂O₃ irradiated with ultraviolet laser light under vacuum," *Physica B: Condensed Matter*, vol. 340, pp. 944-948, 2003.
- [28] D. Pan, N. Zhao, Q. Wang, S. Jiang, X. Ji and L. An, "Facile synthesis and characterization of luminescent TiO₂ nanocrystals," *Adv Mater*, vol. 17, pp. 1991-1995, 2005.
- [29] B. Karthikeyan, M. Anija and R. Philip, "In situ synthesis and nonlinear optical properties of Au:Ag nanocomposite polymer films," *Appl. Phys. Lett.*, vol. 88, pp. 053104-053104, 2006.
- [30] S. Link and M. A. El-Sayed, "Size and temperature dependence of the plasmon absorption of colloidal gold nanoparticles", *The Journal of Physical Chemistry B*, vol. 103, pp. 4212-4217, 1999.
- [31] C. Vargas-Hernandez, M. M. Mariscal, R. Esparza and M. J. Yacaman, "A synthesis route of gold nanoparticles without using a reducing agent," *Appl. Phys. Lett.*, vol. 96, pp. 213115-213115, 2010.
- [32] A. Kabashin and M. Meunier, "Synthesis of colloidal nanoparticles during femtosecond laser ablation of gold in water," *J. Appl. Phys.*, vol. 94, pp. 7941-7943, 2003.
- [33] J. Kimling, M. Maier, B. Okenve, V. Kotaidis, H. Ballot and A. Plech, "Turkevich method for gold nanoparticle synthesis revisited", *The Journal of Physical Chemistry B*, vol. 110, pp. 15700-15707, 2006.
- [34] P. K. Jain, X. Huang, I. H. El-Sayed and M. A. El-Sayed, "Review of some interesting surface plasmon resonance-enhanced properties of noble metal nanoparticles and their applications to biosystems," *Plasmonics*, vol. 2, pp. 107-118, 2007.
- [35] S. K. Ghosh and T. Pal, "Interparticle coupling effect on the surface plasmon resonance of gold nanoparticles: from theory to applications," *Chem. Rev.*, vol. 107, pp. 4797-4862, 2007.

Chapter 4

Second-Harmonic Generation from CdS Nanostructured Thin Films

Abstract

In this chapter, the second-order nonlinear optical properties of a nanostructured cadmium sulfide thin films by optical second-harmonic generation are investigated. Preparation of CdS thin films are described in experimental section. Optical Polarization dependent measurements are included in results and discussion section. These measurements reveal that the studied thin film has in-plane isotropy. The relative values of the components of the second-order susceptibility tensor are found out in this section

4.1 Introduction

Second-harmonic generation (SHG) is one of the most common nonlinear optical processes, in which the conversion of two photons at the fundamental frequency (ω) to one photon at the second-harmonic frequency (2ω) takes place. Within the electric dipole approximation, SHG is forbidden in centrosymmetric materials and in order to be observed, a non-centrosymmetric medium is needed [1]. This requirement is satisfied at the surfaces or interfaces of materials where the symmetry is broken. Therefore, SHG is a useful tool to probe molecular orientation and surface symmetry in absorbates or thin films [2, 3].

Second harmonic generation in a thin film, described by the susceptibility tensor ($\chi^{(2)}$), is strongly symmetry dependent. The symmetry of the material determines which components of the susceptibility tensor are allowed to have unique and non-zero values [4]. In general, lower the symmetry; the more complex will be the second harmonic tensor. For example, C_2 symmetry possesses only symmetry operation of 180° rotation about the surface normal allowing eight components of the susceptibility tensor independent and non-zero. A higher symmetry D_2 adds another symmetry operation that is 180° rotation about an in-plane axis limiting the number of independent tensor components to three.

Recently, inorganic semiconductor nanocrystalline structures have received a lot of attention [5, 6]. The high nonlinearity in such materials can be used in applications in integrated optics [7, 8]. Among II-VI semiconductor family, optical properties of CdS nanocrystals have been previously investigated [9-15] including experimental studies related to the SHG emission in CdS nanocrystals [16]. The electronic and optical properties of nanocrystalline CdS depend strongly on the size and shape of the nanocrystals. The CdS nanocrystals embedded in glass or suspended in a solution have been studied by Hyper-

Rayleigh scattering which, contrary to coherent SHG, is an incoherent process. However, only a few reports are available about the real nature of SHG from CdS nanocrystals.

In this chapter, we investigate second-harmonic generation from a nanostructured CdS thin film. The studied 340 nm thin film was fabricated by chemical bath deposition and contains nanocrystals of around 20 nm size. The polarization dependent SHG was studied by modulating the polarization state of the fundamental beam and indicates that CdS thin film possesses in-plane isotropy. The tensorial properties of observed SHG radiation were also addressed.

4.2 Experiment

Nanostructured CdS films were prepared by chemical bath technique from $\text{Cd}(\text{CH}_3\text{COO})_2$, using thiourea and NH_4OH [17-19]. All the chemicals were of GR (Guaranteed reagent) grade from Merck Ltd. Particles of different size were prepared by mixing aqueous solutions of cadmium acetate (concentration 0.1 M) and thiourea (0.15 M). The pH of the mixture was kept at 10.5 by adding NH_4OH . The mixture was heated to 70 °C and stirred for 1.5 hours. The color of the solution changed to yellow and precipitation occurred. Thin films of CdS were fabricated by dipping glass slides in the solution for two days. During the dipping, one side of the glass substrate was protected against film deposition. Moreover, in order to remove any CdS from the back side of the substrate, this side was additionally cleaned.

The linear optical absorption spectra were measured at room temperature using a spectrophotometer (JascoV-570 UV/VIS/IR) and the structural properties of the samples were investigated by X-ray diffraction (XRD) using a Bruker AXS D8 X-ray diffractometer (PANalytical X'Pert Pro) with $\text{Cu K}\alpha$ ($\lambda = 1.5418 \text{ \AA}$) radiation for recording the diffraction pattern.

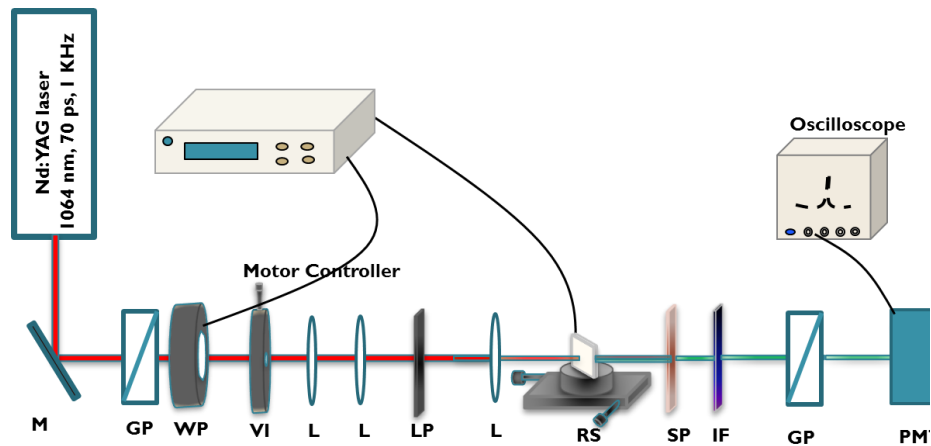


Figure 4.1: Experimental setup for SHG measurements. GP - Glan polarizer, WP - wave plate (half- or quarter-wave plate was used during experiments), VI - iris, LP - long-pass filter, L - lens , RS - rotation stage with the sample, SP - short-pass filter, IF - interference filter, PMT- photomultiplier tube

The SHG measurements were done using the setup shown in Figure 4.1. Light from a Q-switched Nd:YAG laser (1064 nm, 70 ps, 1 kHz) was used as the source of excitation. The resulting second harmonic wavelength is 532nm. The polarizers and waveplates by various manufacturers were carefully tested prior to measurements to ensure their high quality and the reliability to our results. Two photon fluorescence can easily disturb the second harmonic measurements. But fluorescent light is not coherent leading to rapid attenuation of the signal with increasing distance unless imaging optics is used, while the second harmonic signal propagates as a well collimated beam. We used both distance and bandpass filtering to make sure only second harmonic generation was measured. The laser beam was collimated to a diameter of 1-2 mm and then nearly focused on the CdS film. The polarization state of the beam was controlled by the combination of a calcite Glan polarizer and a continuously rotating zero-order quarter-wave plate (QWP) or half-wave plate (HWP), allowing for polarization-dependent measurements. A filter blocking visible light blocks any second harmonic generated in the optical components before the sample. The transmitted fundamental beam is filtered out behind the sample

with a filter blocking infrared light and the remaining second harmonic beam is passed through another Glan-Taylor polarizer that is rotated to detect the chosen polarization. An interference filter whose passband is centered on 532nm is placed before the photomultiplier tube. In order to perform SHG measurements for various angles of incidence, the sample was fixed on a high precision rotation stage with 0.001° angular resolution. The SHG signal transmitted through the sample was detected with a photomultiplier tube (PMT).

4.3 Results and discussion

The UV-VIS absorption spectrum of the CdS thin film is shown in Figure 4.2.

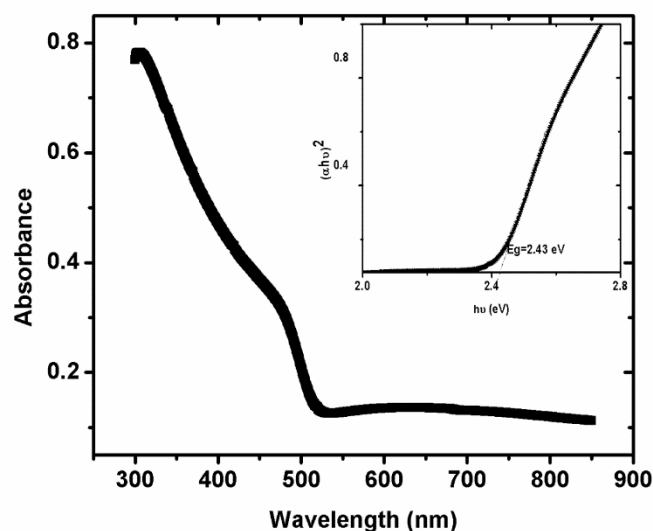


Figure 4.2: Optical absorption spectrum of CdS nanostructured thin film. Inset shows optical band gap

The reported absorption edge for the bulk hexagonal CdS is at 520 nm (2.38 eV) [20]. From Figure 4.2, it is observed that there is a blue shift for the absorption edge compared with the bulk CdS; resulting in a band gap of 2.43eV

(inset of Figure 4.2). These results are the manifestations of quantum confinement at the nano-level [21].

Figure 4.3 shows the X-ray diffraction pattern of CdS thin film deposited on a glass plate showing broadened diffraction profiles. The XRD pattern shows a peak at 26.5° could be indexed to the (002) plane of hexagonal CdS (JCPDS card no. 75-1545). The particle diameter D of the nanocrystalline films is estimated using the Scherrer formula $D = 0.89\lambda / \beta_{2\theta} \cos(\theta)$, (where λ is the wavelength of X-ray used (1.5418 \AA), $\beta_{2\theta}$ is the full-width half maximum of (002) peak and θ is the scattering angle, the Bragg angle (2θ) is around 26.5°). The estimated crystalline size is in the range of 20 nm.

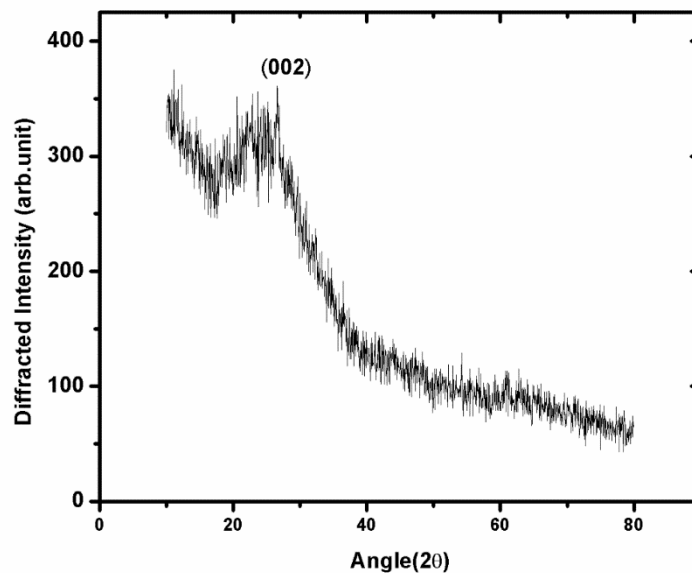


Figure 4.3: X-ray diffraction pattern of CdS nanostructured thin film.

Scanning electron microscopy (SEM) of CdS thin film was performed on JEOL Model JSM - 6390LV. A gold film was evaporated on the samples before loading on the instrument. SEM of the CdS film indicated the formation

of nanostructured cadmium sulfide and the size of nanostructures were below 100 nm (Figure 4.4). The thickness of the CdS film was measured to be 340 nm using stylus profiler (Dektak6M).

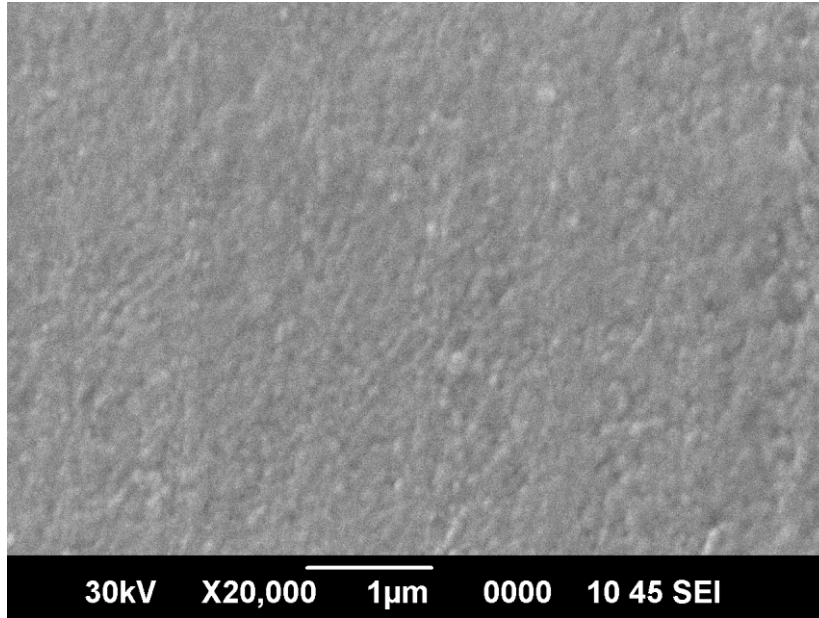


Figure 4.4: SEM picture of the CdS nanostructured thin film

4.3.1 Second-harmonic generation

The SHG measurements were performed in transmission according to the geometry shown in Figure 4.5. In order to find the maximum SHG radiation from the CdS thin film, p -polarized SHG was detected for p -polarized incident light when the angle of incidence was varied (Figure 4.6a). The quadratic dependence of the SHG signal on the incident intensity was verified at the angle of incidence of maximum signal (55°) with excellent agreement (Figure 4.6b). For the sample orientation, polarization-dependent SHG measurements were also performed. By modulating the incident polarization with the HWP, in-plane isotropy of the sample (symmetry group $C_{\infty v}$) was verified by observing that the s -polarized SHG signal vanishes for p and s -polarized incident light (Figure 4.7). The symmetry group $C_{\infty v}$ has only seven non-vanishing tensor

components, i.e. χ_{zzz} , $\chi_{zxx} = \chi_{zyy}$ and $\chi_{xxz} = \chi_{xzx} = \chi_{yyz} = \chi_{yyx}$, where z -direction is the film normal and x and y are the two orthogonal in-plane directions. Although the susceptibility tensor of the material is not directly accessible in an experiment, it can be extracted from the measurable expansion coefficients, which are linear combinations of the components of the tensor

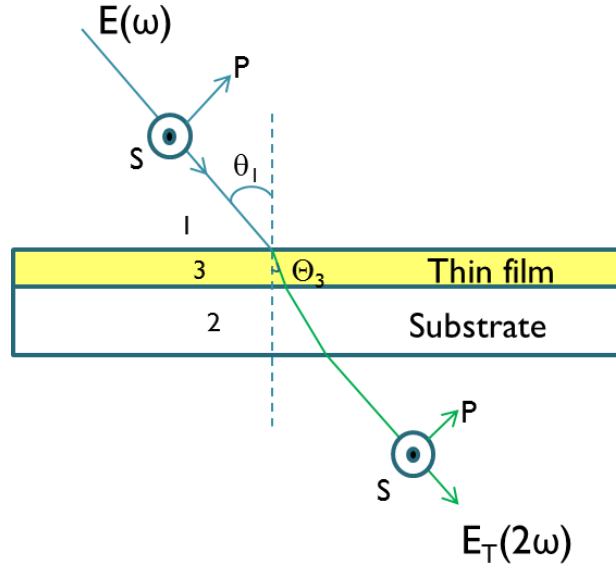


Figure 4.5: Geometry of single beam SHG where $E(\omega)$ is the field vector of the fundamental beam incident on the sample while $E_T(2\omega)$ is the field vector of the SHG beam in the transmitted direction

In order to uniquely determine the components of the tensor, the HWP was replaced by a QWP. This change allowed us to obtain a unique set of expansion coefficients which are tied with the intensity of SHG by the following expression [22, 23]

$$I^{SHG}(2\omega) = \left| fE_p^2(\omega) + gE_s^2(\omega) + hE_p(\omega)E_s(\omega) \right|^2, \quad (4.1)$$

where E_p and E_s are the p - and s -polarized components of the beam at the fundamental frequency. In general, the expansion coefficients f , g , and h are complex valued and can be found by simultaneous fitting of the SHG data obtained from several polarization dependent measurements.

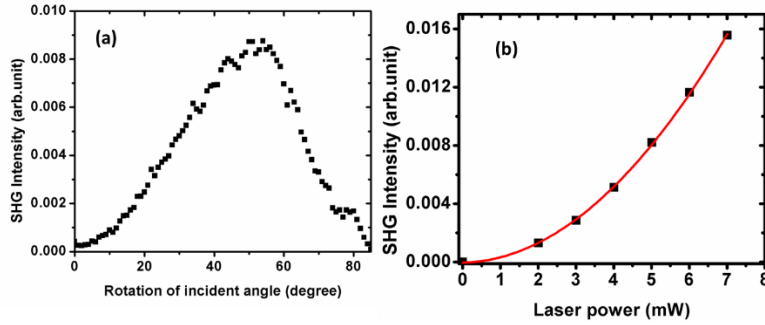


Figure 4.6: SHG intensity in the function of angle of incidence of fundamental beam and (b) Quadratic dependence of SHG intensity on the fundamental laser power of CdS thin film

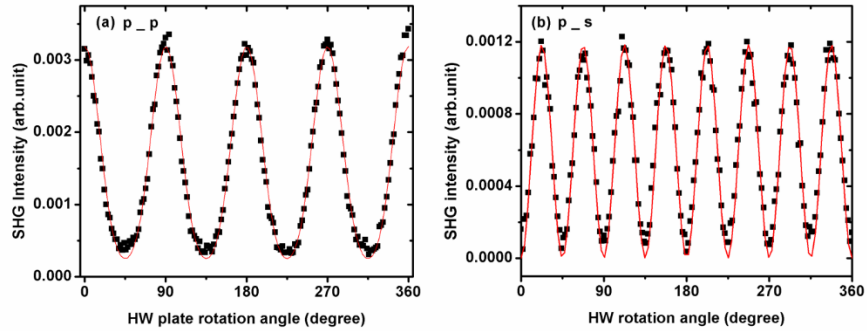


Figure 4.7: (a) The p- and (b) s-polarized SHG signals as a function of the linear input polarization (the initial state of polarization, at 0 degree, is p). The black squares are the experimental data and the solid lines represent the fits to the data

Furthermore, the coefficients are linear combinations of several components of the susceptibility tensor and they also depend on the experimental geometry and linear optical properties of the material. The results of simultaneous fitting of SHG data, obtained from measurements with incident polarization rotated by QWP, are plotted in Figure 4.8 and the expansion coefficients obtained from the fitting are $f = 1$, $g = 0.21$ and $h = 1.03$.

In order to obtain the relative values of the tensor components, we used a simplified version of the Green's function formalism [24, 25] proposed by Ning *et al.* [26]. The model neglects multiple reflections within the film. The

expansion coefficients can then be expressed by the set of following equations [26, 27]:

$$\begin{aligned} f &= At_{p13}^2 T_{p32} T_{p21} \left(\chi_{xxz} \sin 2\theta_3 + \chi_{zxx} (\cos \theta_3)^2 \tan \Theta_3 + \chi_{zzz} (\sin \theta_3)^2 \tan \Theta_3 \right), \\ g &= At_{s13}^2 T_{p32} T_{p21} \chi_{zxx} \tan \Theta_3, \\ h &= A / \cos \Theta_3 \left(2t_{p13} t_{s13} T_{s32} T_{s21} \chi_{xxz} \sin 2\theta_3 \right), \end{aligned} \quad (4.2)$$

where $A = (4\pi\omega / N_3 c) [\exp(i\Delta k L) - 1] / \Delta k$, $\Delta k = 2\omega(n_3 \cos \theta_3 - N_3 \cos \Theta_3) / c$ is the phase mismatch between the fundamental and second-harmonic beams and subscripts 1, 2 and 3 refer to air, substrate and thin film, respectively. The lower case letters describe quantities at fundamental frequency, while the upper case letters denote quantities at 2ω (n, N – refractive indices, θ, Θ – propagation angles, t, T – Fresnel transmission coefficients), c is the speed of light, ω is the angular frequency and, L is the thickness of the film and subscripts p and s refer to p - and s -polarized light respectively. The refractive indices at fundamental ($n = 2.33$) and second-harmonic ($N = 2.66$) wavelength, used in the calculations, were taken from ref. [26] and the obtained tensor components are $\chi_{zzz} = 1$, $\chi_{xxz} = 0.14$, and $\chi_{zxx} = 0.07$, where χ_{zzz} has been normalized to unity. These preliminary results suggest that the film has relatively strong orientational effects along the normal direction

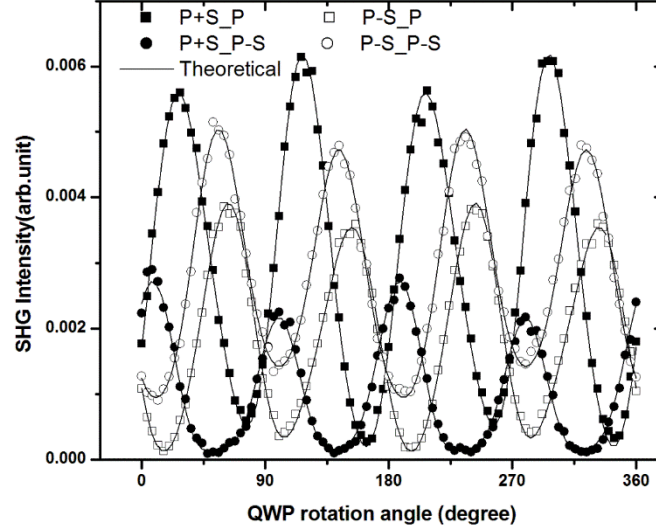


Figure 4.8: Measured intensities of SHG from CdS nanostructured thin film as a function of rotation angle of the quarter-wave plate. The first label (P+S; P-S) indicates the linear polarization of the initial fundamental beam and the second one (P; P-S) that of the detected SHG signal. The symbols represent the raw experimental data, and the solid lines are simultaneous fit to all data to obtain the f, g, and h coefficients.

4.4 Conclusions

We have observed SHG from CdS nanostructured thin film prepared on glass plate substrate by chemical bath deposition technique. The results point out that studied sample has in-plane isotropy. The relative values of tensor components of the second-order susceptibility were determined to be $\chi_{zzz} = 1$, $\chi_{xxz} = 0.14$, and $\chi_{zxx} = 0.07$. These values suggest that the nanocrystals are oriented along the normal direction. However, the origin of such orientation remains unknown at present. Thus CdS is a promising nonlinear optical material for photonic applications, particularly for integrated photonic devices. Future plans

involve the calibration of obtained values of tensor components as well as more in depth analysis of the origin of SHG signal from CdS films.

References

- [1] R. W. Boyd, *Nonlinear Optics*. Academic press, 2003.
- [2] C. T. Williams and D. A. Beattie, "Probing buried interfaces with non-linear optical spectroscopy," *Surf. Sci.*, vol. 500, pp. 545-576, 2002.
- [3] Y. Rao, Y. Tao and H. Wang, "Quantitative analysis of orientational order in the molecular monolayer by surface second harmonic generation," *J. Chem. Phys.*, vol. 119, pp. 5226, 2003.
- [4] Y. Shen, "Principles of nonlinear optics," 1984.
- [5] M. Jacobsohn and U. Banin, "Size dependence of second harmonic generation in CdSe nanocrystal quantum dots," *The Journal of Physical Chemistry B*, vol. 104, pp. 1-5, 2000.
- [6] M. Lippitz, M. A. van Dijk and M. Orrit, "Third-harmonic generation from single gold nanoparticles," *Nano Letters*, vol. 5, pp. 799-802, 2005.
- [7] C. Xiong, W. Pernice, K. K. Ryu, C. Schuck, K. Y. Fong, T. Palacios and H. X. Tang, "Integrated GaN photonic circuits on silicon (100) for second harmonic generation," *Opt. Express*, vol. 19, pp. 10462-10470, 2011.
- [8] K. Rivoire, S. Buckley, F. Hatami and J. Vuckovic, "Second harmonic generation in GaP photonic crystal waveguides," *Applied Physics Letters*, vol. 98, pp. 263113-263113-3, 2011.
- [9] Z. Rizwan, B. Azmi and M. Sabri, "Effect of annealing temperature on the optical properties of nanostructured CdS films prepared by chemical bath deposition technique," *Optoelectronics and Advanced materials – Rapid communications*, vol. 5, pp. 393-397, 2011.
- [10] S. Tiwari and S. Tiwari, "Electrical and optical properties of CdS nanocrystalline semiconductors," *Crystal Research and Technology*, vol. 41, pp. 78-82, 01, 2006.

- [11] P. Gupta and M. Ramrakhiani, "Influence of the particle size on the optical properties of CdSe nanoparticles," *Open Nanoscience Journal*, vol. 3, pp. 15-19, 2009.
- [12] R. A. Ganeev, M. Baba, M. Morita, D. Rau, H. Fujii, a. I. Ryasnyansky, N. Ishizawa, M. Suzuki and H. Kuroda, "Nonlinear optical properties of CdS and ZnS nanoparticles doped into zirconium oxide films," *Journal of Optics A: Pure and Applied Optics*, vol. 6, pp. 447-453, 04, 2004.
- [13] I. Umezu, R. Koizumi, K. Mandai, T. Aoki-Matsumoto, K. Mizuno, M. Inada, A. Sugimura, Y. Sunaga, T. Ishii and Y. Nagasaki, "Optical properties of CdS nanocrystal covered by polymer chains on the surface," *Microelectronic Engineering*, vol. 66, pp. 53-58, 2003.
- [14] K. K. Nanda, S. N. Sarangi, S. Mohanty and S. N. Sahu, "Optical properties of CdS nanocrystalline films prepared by a precipitation technique," *Thin Solid Films*, vol. 322, pp. 21-27, 06, 1998.
- [15] V. Sivasubramanian, a. K. Arora, M. Premila, C. S. Sundar and V. S. Sastry, "Optical properties of CdS nanoparticles upon annealing," *Physica E: Low-Dimensional Systems and Nanostructures*, vol. 31, pp. 93-98, 01, 2006.
- [16] B. S. Santos, G. A. L. Pereira, D. V. Petrov and C. D. Donega, "First hyperpolarizability of CdS nanoparticles studied by hyper-Rayleigh scattering", *Optics communications*, vol.178 pp.187-192, 2000.
- [17] H. Hu and P. K. Nair, "Chemical deposition of photosensitive CdS thin films on polyester foils," *J. Cryst. Growth*, vol. 152, pp. 150-157, 1995.
- [18] R. S. Mane and C. D. Lokhande, "Chemical deposition method for metal chalcogenide thin films," *Mater. Chem. Phys.*, vol. 65, pp. 1-31, 2000.
- [19] T. Chu, S. S. Chu, N. Schultz, C. Wang and C. Wu, "Solution-Grown Cadmium Sulfide Films for Photovoltaic Devices," *J. Electrochem. Soc.*, vol. 139, pp. 2443-2446, 1992.
- [20] P. A. Kurian, C. Vijayan, K. Sathiyamoorthy, C. S. Sandeep and R. Philip, "Excitonic transitions and off-resonant optical limiting in CdS quantum dots stabilized in a synthetic glue matrix," *Nanoscale Research Letters*, vol. 2, pp. 561-568, 2007.

- [21] S.Arora and S. Sundar Manoharan, "Size-dependent photoluminescent properties of uncapped CdS particles prepared by acoustic wave and microwave method", *Journal of Physics and Chemistry of Solids*, vol.68 (10) pp. 1897-1901, 2007
- [22] F. X. Wang, M. Siltanen and M. Kauranen, "Uniqueness of determination of second-order nonlinear optical expansion coefficients of thin films" *Physical Review B*, vol. 76, pp.085428-1-6, 2007.
- [23] M. Kauranen, T. Verbiest, J. J. Maki and A. Persoons. Second-harmonic generation from chiral surfaces. *J. Chem. Phys.* vol.101 (9), pp. 8193-8199. 1994
- [24] J. E. Sipe, "New Green-function formalism for surface optics," *JOSA B*, vol. 4, pp. 481-489, 1987.
- [25] J. J. Maki, M. Kauranen, T. Verbiest and A. Persoons, "Uniqueness of wave-plate measurements in determining the tensor components of second-order surface nonlinearities," *Physical Review B*, vol. 55, pp. 5021, 1997.
- [26] T. Ning, H. Pietarinen, O. Hyvärinen, J. Simonen, G. Genty and M. Kauranen, "Strong second-harmonic generation in silicon nitride films," *Appl. Phys. Lett.*, vol. 100, pp. 161902, 2012.

Chapter 5

Preparation and Spectral Characteristics of CdS- Au and CdS-TiO₂ Nanocomposites

Abstract

In this chapter, CdS based nanocomposites are studied in the context of nonlinear optical applications. In the first section of this chapter, optical properties of CdS: Au nanocomposite particles and films are investigated. Properties of CdS:TiO₂ nanocomposite particles are optically studied in the second section.

5.1 Introduction

In recent years, fabrication of nanoscale composites comprising surface modified metals semiconductors and metal–semiconductor is a thrust area of research to obtain tailored materials with tunable electronic and photonic properties [1-4]. In the case of semiconductors, conduction and valence bands are separated by a well-defined bandgap, but metal nanoclusters possess close lying bands and electrons are free to move. The surface plasmon absorption band of a metal cluster is dependent on both the cluster size and chemical environment [5, 6]. Nano particles embedded in polymer matrices have got much importance in the area of nanophotonics due to their photonic applications such as luminescence tuning [7], band gap engineering [8], optical nonlinearity [9]etc. Nonlinear optical properties of nanocomposites can be very important in high speed communication network as all optical switching, wavelength manipulation and signal processing [10-12]. A large enhancement of the nonlinear optical property in the semiconductor nanoparticles is predicted by theoretical considerations that are based on the quantum confinement effects of the carriers in those materials [13, 14].

Among II-VI semiconductors, CdS is a mostly studied material. Large third-order nonlinearities of CdS nanocrystallites embedded in polymer films have been reported [15-19]. There are a number of reports on optical properties of nanocomposite consisting of CdS and other materials. Enhanced optical nonlinearities of Au/CdS core/shell QDs have also been reported [20]. But the optical properties of nanocomposites in which CdS as base material is not well-studied. It is well-known that noble metal nanoparticles possess absorption called surface plasmon resonance in the visible region. Out of various metal nanoparticles, gold and silver are well studied materials. In this work, Au is selected for the preparation of nanocomposites with CdS. With the view of

combining plasmonic and excitonic effect, clubbing of CdS and Au nanoparticles is the main objective of this study.

TiO₂ is recently getting much attention due to its nanocomposites are exhibiting high optical nonlinearity [21-23]. Litty *et.al* reported that enhanced nonlinearity of ZnO due to the doping of TiO₂ [24]. So influence of TiO₂ on nonlinear optical property of CdS was taken up in the present study. The first section of this chapter, the preparation of CdS:Au nanoparticles is discussed. Thus prepared Au coated CdS nanoparticles are dispersed in a polymer matrix and cast into homogeneous transparent film. Subsequently we characterized the linear absorption and fluorescence properties of the composites. The nonlinear optical properties of the composite films were also measured through Z-scan technique. In the second section, optical properties of CdS:TiO₂ PVA nanocomposite structures have been reported.

5.1.1 Experimental

The linear optical absorption spectrum was measured at room temperature using a spectrophotometer (JascoV-570 UV/VIS/IR). Transmission electron microscopy (TEM) of CdS and CdS: Au nanoparticles were performed on a JOEL 2100 HRTEM machine for size measurement. The fluorescence emission from the same is recorded using a Cary Eclipse fluorescence spectrophotometer (Varian). Nonlinear optical measurement was carried out by Z-scan measurement

5.2 Optical properties of CdS and CdS:Au nanocomposites

5.2.1 Preparation

CdS nanoparticles were prepared by chemical bath technique from Cd(CH₃COO)₂, using thiourea and NH₄OH [25, 26]. All the chemicals were of GR (Guaranteed reagent) grade from Merck Ltd. CdS nanoparticles were

prepared by mixing aqueous solutions of cadmium acetate (concentration 0.1 M) and thiourea (0.15 M). The pH of the mixture was kept at 10.5 by adding NH_4OH . The mixture was heated to 70°C and stirred for 1.5 hours. The color of the solution changed to yellow and precipitation occurred.

0.1 g of CdS nanoparticles were added to the Au Stock solution (0.4mM). After stirring around 11/2 hour, the resultant CdS nanoparticles are filtered and washed. Thus formed CdS:Au nanoparticles are then dried and used for further optical studies.

5.3 Results and Discussion

Figure 5.1 shows photographs of (a) CdS:Au and (b) CdS nanoparticles dispersed in the PVA matrix.

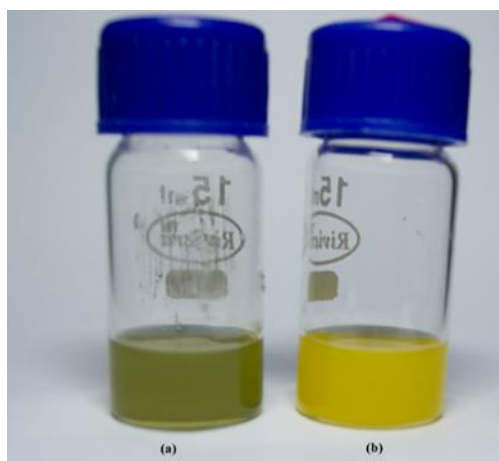


Figure 5.1: CdS:Au and CdS nanoparticles are embedded in PVA matrix

Figure 5.2 (a) and Figure 5.2(b) presents TEM images for CdS:Au and CdS nanoparticles. From TEM images, it is clear that CdS:Au nanoparticles are of the order of 5nm. Average size of CdS nanoparticles are of 4nm. This increase in size of CdS:Au nanocomposite particles indicates the narrow coating of Au.

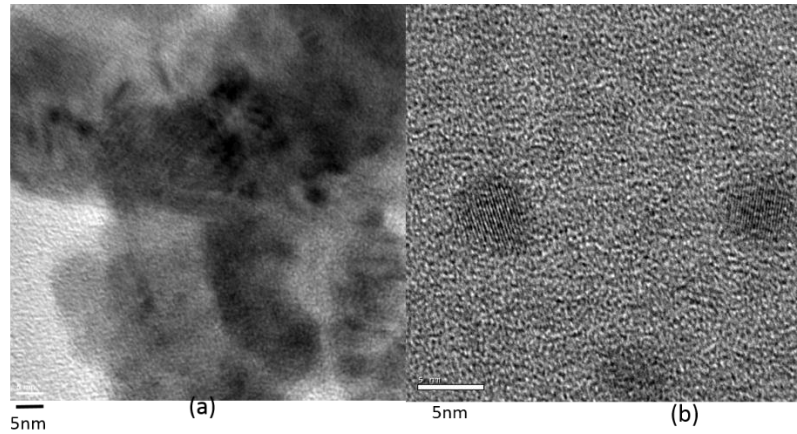


Figure 5.2: (a) TEM images of CdS:Au nanoparticles (b) CdS nanoparticles

Figure 5.3 shows represents the energy dispersive X-ray (EDS) spectrum of CdS:Au nanocomposite particles.

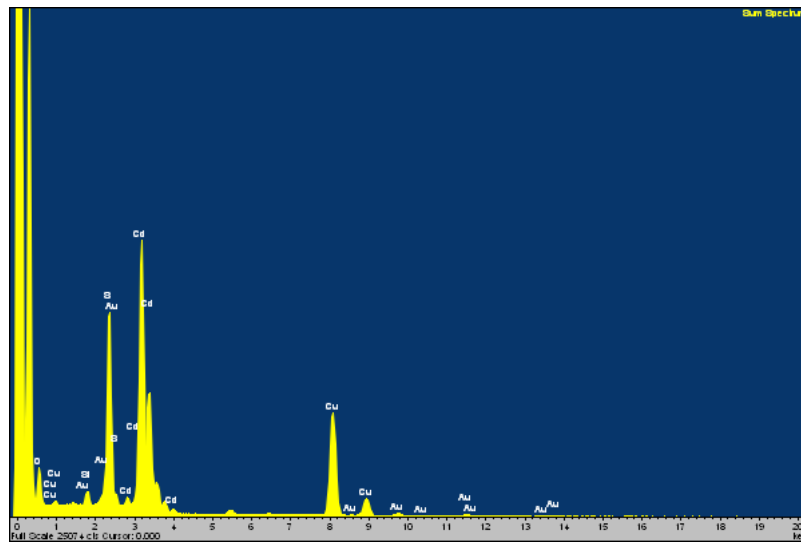


Figure 5.3: Energy dispersive X-ray spectrum of CdS:Au nanocomposite particles

It shows the atomic percentage of elements involved in formation. The EDS analysis shows that the percentage of atoms of Cd and S elements are roughly of the same percentage (34% and 27%). This indicates that the material

retain the stoichiometry without much change. The percentage of Au is only 0.55%. So it is indicative of the fact that gold forms only a coating on the CdS nanoparticles. Cu and Si percentage may be ignored as their presence are expected due to the method of preparation and characterization. The part of O comes from surface oxides.

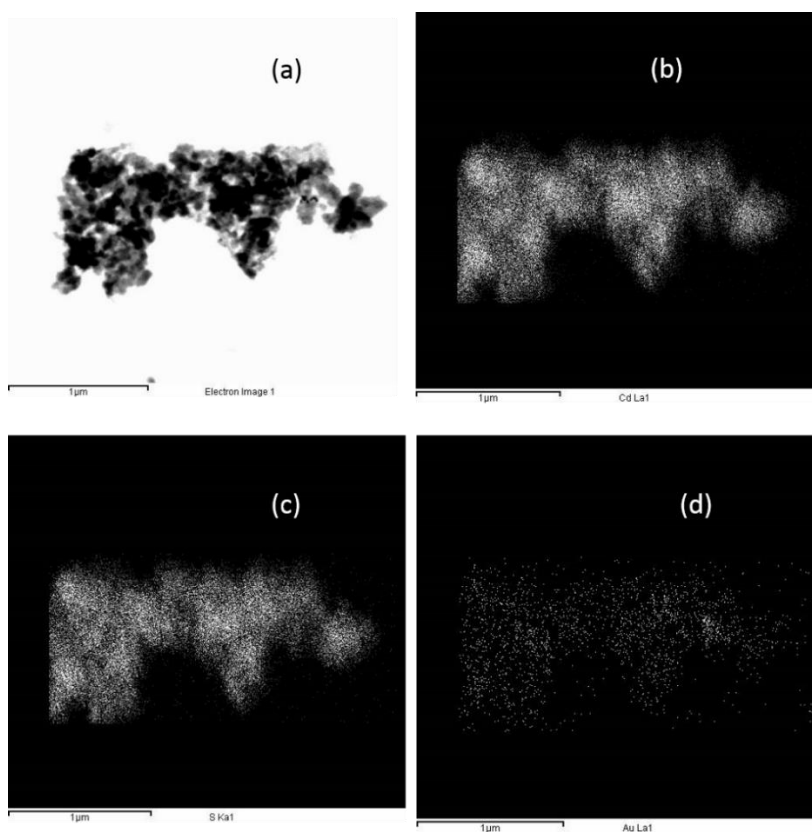


Figure 5.4: (a)TEM image showing where the elemental maps were obtained (b) TEM/Cd La1 map(c)TEM/S Ka1 map and TEM/Au La1 map

Figure 5.4 shows the transmission electron microscopy (TEM) elemental maps of CdS:Au nanocomposite particles. In addition to aggregation/agglomeration of the nanocomposite particles [27], the elemental maps clearly illustrate the binding of CdS nanoparticles to gold nanoparticles to

form CdS:Au nanocomposite particles. This clearly indicates the presence of Au on CdS nanoparticles.

5.4 Optical absorption studies on CdS and CdS:Au nanoparticles

0.001g of CdS nanoparticles and CdS:Au nanoparticles are dispersed in 10ml of 4wt%PVA solution. Figure 5.5 shows the absorption spectra of the nanoparticles. The absorption spectra show the onset absorption edges of CdS:Au nanoparticles and CdS nanoparticles and are almost at 485nm and 479nm. But the tail of the absorption edge of CdS:Au is red-shifted compared to that of CdS nanoparticles. The absorption spectrum of gold nanoparticles prepared at 0.4mM is shown in Figure 5.6.

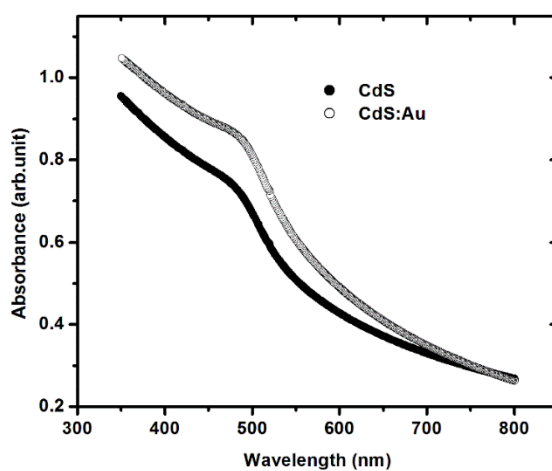


Figure 5.5: Optical absorption spectra of CdS and CdS:Au nanoparticles in PVA solution

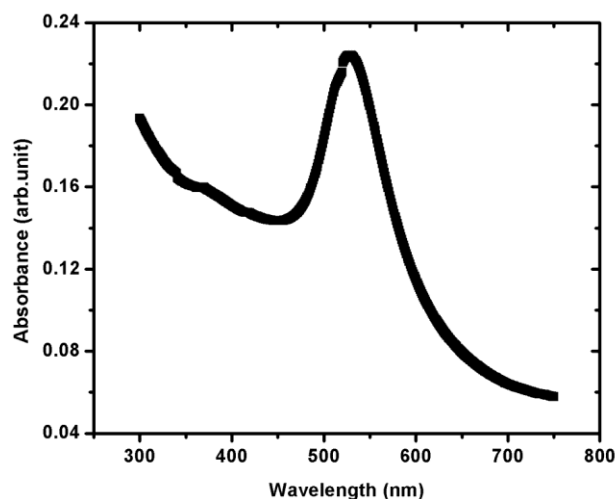


Figure 5.6: A typical optical absorption spectrum of Au nanoparticles reduced from 0.4 mM stock solution

5.4.1 Fluorescence studies on CdS and CdS:Au nanoparticles

0.001g of CdS and CdS:Au nanoparticles are dispersed in 10ml of 4wt% PVA solution and emission spectra are taken. Figure 5.7 shows the fluorescence spectrum of CdS and CdS:Au nanoparticles in PVA aqueous solution under the excitation of 386nm. Figure 5.8 shows the excitation spectrum of CdS nanoparticles. It shows a maximum at 386nm and this wavelength is used for fluorescence excitation. From the emission spectra it is clear that emission intensity of CdS:Au nanoparticles is almost the same as that of CdS nanoparticles. This indicates that the plasmonic absorption of Au does not play any part due to the small amount of Au nanoparticles present in the CdS:Au nanoparticles. So the expected change in the emission intensity of CdS nanoparticles in the CdS:Au nanocomposite particles is not observed.

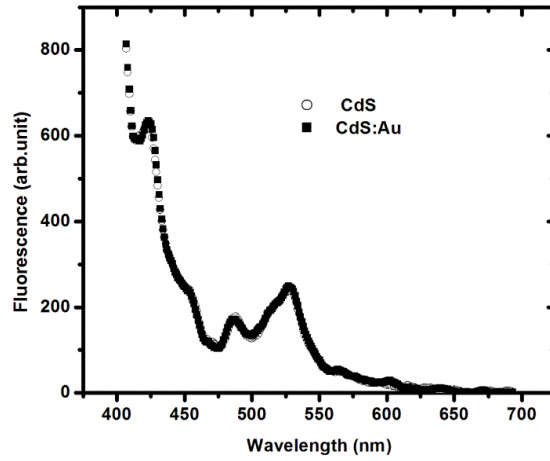


Figure 5.7: Fluorescence spectrum of CdS and CdS:Au nanoparticles in PVA matrix

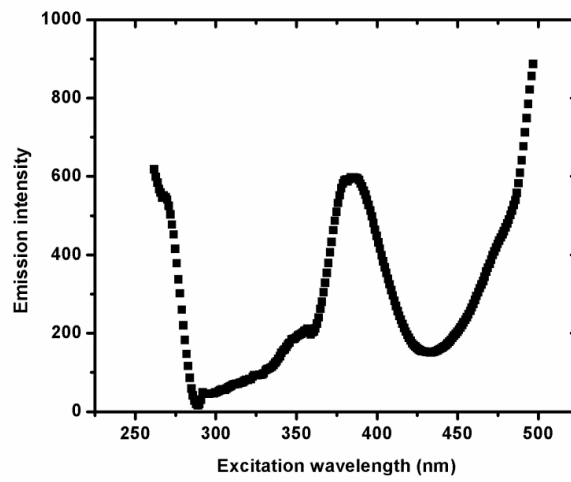


Figure 5.8: A typical excitation spectra of CdS nanoparticles in PVA matrix

5.5 Optical properties of CdS: Au and CdS PVA nanocomposite thin films

5.5.1 Linear optical properties of CdS: Au PVA nanocomposite films

For studying the nonlinear optical properties of the nanocomposites in optical limiting application, CdS and CdS: Au nanoparticles have to be embedded in film form. Firstly these nanoparticles are embedded in PVA matrix. The procedure is described as follows. 0.006 g of CdS and CdS: Au nanoparticles are added to 10ml of 10 wt % PVA aqueous solution by stirring and followed by ultra-sonication for 6hrs until uniform dispersion is achieved. The resultant viscous solution is drop casted and kept for a day to dry out to form thin films. Thus formed CdS and CdS: Au PVA composite films are optically characterized using Spectrophotometer. The optical absorption spectra of these films are shown in Figure 5.9. From the absorption spectra it is clear that Au coated CdS leads to a red shift in the onset of absorption edge. Considering the absorption spectrum of CdS: Au PVA nanocomposite films, it is observed that there is no distinct plasmonic absorption peak of Au but it's merged with the absorption spectrum of CdS nanoparticles leading to a red-shift of absorption tail for the CdS: Au PVA nanocomposite compared to the CdS PVA nanocomposite. Band gap is measured to be 2.40 eV and 2.35eV for CdS and CdS: Au PVA nanocomposite films respectively. The thickness of the films is measured to be 55micrometer.

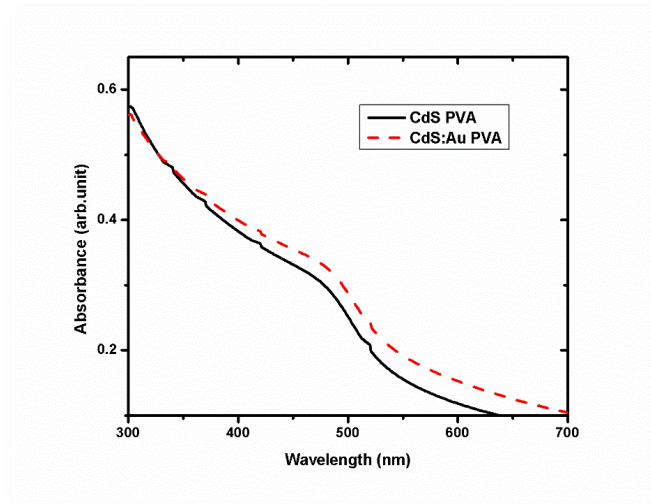


Figure 5.9: Optical absorption spectra of CdS and CdS:Au PVA nanocomposite films

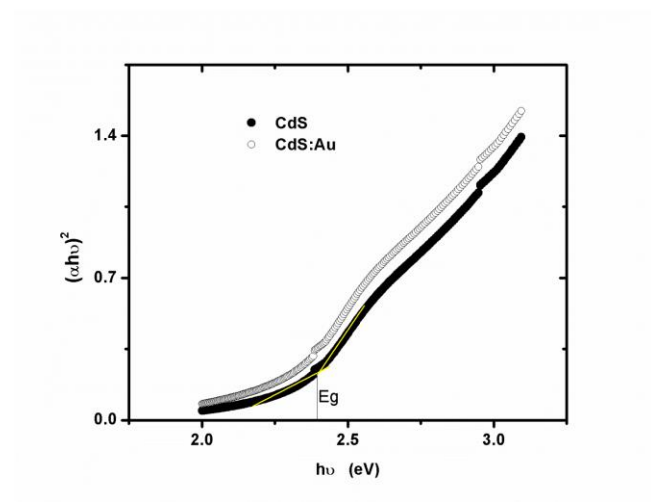


Figure 5.10: Optical band gap plot of CdS PVA and CdS:Au PVA nanocomposite films

Band gap of CdS:Au PVA film is reduced compared to the band gap of CdS PVA thin film. This is due to the influence of plasmonic peak of Au which extends the tail to higher wavelength resulting in a red-shift for absorption tail of CdS:Au PVA nanocomposite film.

5.5.2 Nonlinear optical studies on CdS PVA and CdS:Au PVA thin films

Nonlinear optical studies of CdS:Au PVA and CdS PVA thin films were carried out using Z-scan experiment. Figure 5.11 gives open aperture Z-scan traces of CdS PVA and CdS:Au PVA nanocomposite films at a typical fluence of 43MW/cm². Figure.5.12-5.13 yield the open aperture Z-scan traces of CdS:Au PVA and CdS PVA nanocomposite films for different input intensities

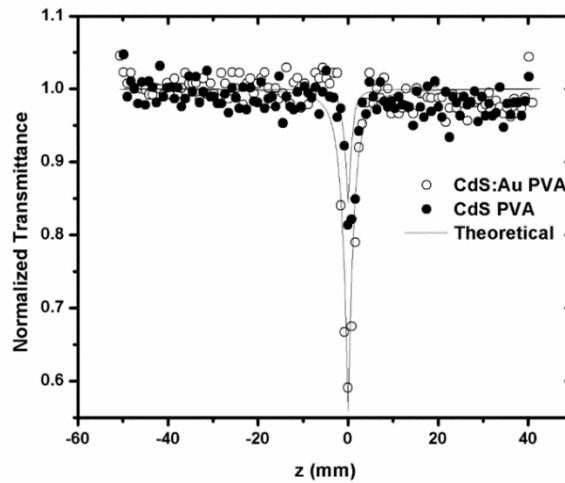


Figure 5.11: Open aperture Z- scan traces of CdS PVA and CdS:Au PVA nanocomposite films at an input intensity of 43MW/cm²

The open-aperture curve exhibits a normalized transmittance valley, indicating the presence of reverse saturable absorption in these nanoparticles. The nonlinear absorption coefficient is obtained by fitting the experimental open aperture data using equation (2.2),

$$T(z, S = 1) = \sum_{m=0}^{m=\infty} \frac{[-q(z,0)]^m}{(m+1)^{3/2}} \dots\dots(2.2)$$

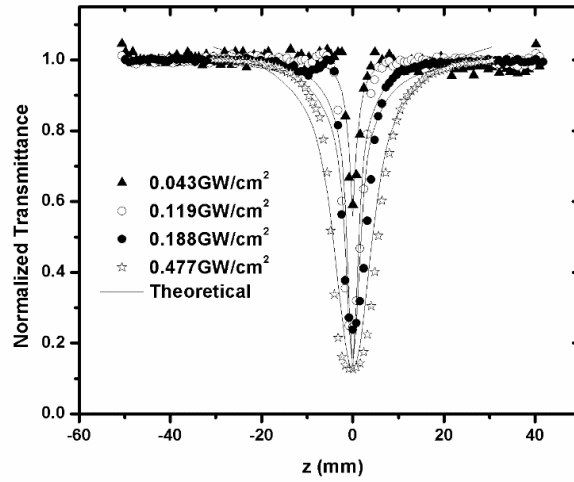


Figure 5.12: Open aperture data at different input intensities of CdS:Au PVA nanocomposite films

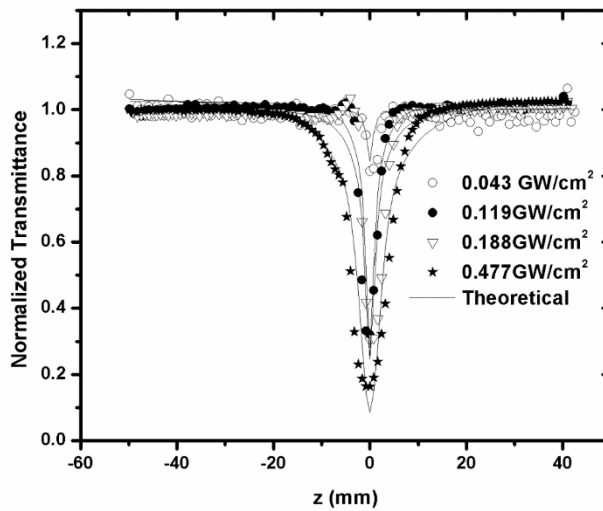


Figure 5.13: Open aperture traces at different intensities of CdS PVA composite film

The solid curves in Figure 5.11-5.13 are the theoretical fit to the experimental data. The open-aperture Z-scan scheme was used to measure β .

Generally, optical response of nanoparticles consists of absorption, refraction and scattering. In this case, scattering does not play any significant role as the size of these nanoparticles is much less and can be neglected. In order to explain the optical nonlinearity of these nanocomposite films, the system can be considered as a two band system. As the excitation wavelength is 532nm, which is in the range of the band gap of these nanoparticles, we can consider that the nonlinear absorption is mainly contributed by an excited-state absorption or free carrier absorption process, in which electrons in the valence band are excited to intermediate energy states because of the linear absorption tail. Thus a large number of free carriers are generated by one-photon excitation under a 532nm laser pulse. Subsequently, the free carriers thus formed could further absorb another photon and get excited to a higher conduction-band level, resulting in a transient absorption. In this process, we suggest that the lower level of conduction band may act as an intermediate state to generate the reverse saturable absorption. CdS:Au nanocomposite film is having high nonlinear absorption compared to CdS PVA film. This is due to the overall effect of plasmonic and excitonic contribution in the case of CdS:Au PVA nanocomposite films.

From Table 5.1, it is clear that the nonlinear optical absorption coefficient is decreased with the increase in input intensity.

The decrease in the nonlinear optical absorption coefficient is due to the saturation behavior which is typical of two photon absorption, excited state absorption etc. due to the third order optical nonlinearity.

Table 5-1: Nonlinear optical absorption coefficient at different laser intensities

Input intensity (GW/cm ²)	Nonlinear optical absorption coefficient (β) x10 ⁻⁶ (cm/W)	
	CdS PVA film	CdS:Au PVA film
0.043	2.71	6.28
0.119	2.73	2.87
0.188	1.74	1.82
0.477	0.724	0.741

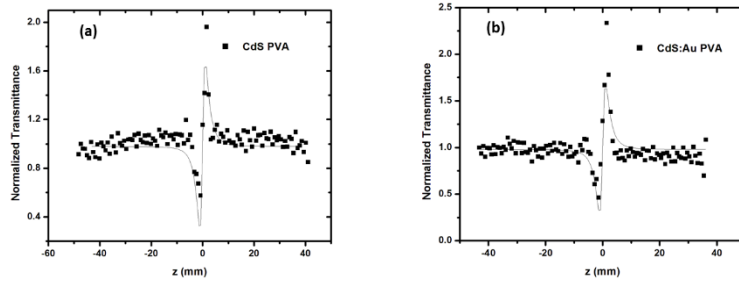


Figure 5.14: Closed aperture Z-scan data of CdS and CdS:Au PVA nanocomposites

Figure 5.14(a) and (b) shows the closed aperture Z-scan plot of CdS PVA and CdS:Au PVA thin films at input fluence of 119MW/cm². The closed-aperture curves have shape corresponding to a positive value of the nonlinear refractive index n_2 and it is the self-focusing nonlinearity. By dividing the normalized closed-aperture transmittance by the corresponding normalized open aperture data, we can retrieve the phase distortion created due to the change in refractive index. It is observed that the valley–peak of the closed-aperture Z-scan distance comes within the range of $\Delta z = 1.7 z_0$, and thus confirming the third-

order optical nonlinearity. The nonlinear phase change ($\Delta\varphi$), can be obtained by the best theoretical fit of experimental data using the equation (2.4).

$$T_{(z,\Delta\varphi)} = 1 - \frac{4 \Delta\varphi x}{(x^2+9)(x^2+1)} \quad (2.4)$$

where $\Delta\varphi = 2\pi \frac{\Delta n_{eff} L}{\lambda}$ and $x = z/z_0$, Δn is related to the nonlinear refraction coefficient γ through the relation, $\Delta n = \gamma I_0(t)$. The calculated values of nonlinear optical parameters are shown in the table.5.2.

It is clear from table 5.2 that the formation CdS: Au PVA nanocomposites causes an increase in nonlinear absorption as well as nonlinear refraction property compared to CdS PVA nanocomposites.

Table 5-2: Nonlinear optical absorption and refraction

sample	β (cm/W) $\times 10^{-6}$	γ (cm ² /W) $\times 10^{-11}$
CdS: Au PVA film	6.28	4.86
CdS PVA film	2.71	3.72

Yin et.al [28] reported the value of nonlinear refractive index for bulk CdS to be $-5.3 \times 10^{-13} \text{cm}^2/\text{W}$ at 532nm. Even though the weight percentage (0.03% wt) of CdS and CdS: Au nanoparticles in the composite films is small, the magnitude of nonlinear refraction is much higher than (100 times) that of the reported value of bulk CdS material. Recently Du et.al [29] measured optical nonlinearity of 2-17% wt CdS\PS nanocomposite particles and observed a maximum nonlinear refraction coefficient of $-3 \times 10^{-13} \text{cm}^2/\text{W}$ at 532nm. Very recently Jing et.al [30] investigated third-order nonlinear optical properties of 18.2% wt of CdS/PVP nanocomposite films using Z-scan technique and obtained large nonlinear optical refraction and nonlinear absorption coefficient values of $-1.65 \times 10^{-11} \text{cm}^2/\text{W}$ and $-4.25 \times 10^{-7} \text{cm}/\text{W}$ respectively at 532nm. This result confirms our values on

nonlinear optical coefficients of CdS:Au PVA and CdS PVA nanocomposite films. Hence these samples can show promising applications for optical devices in photonics.

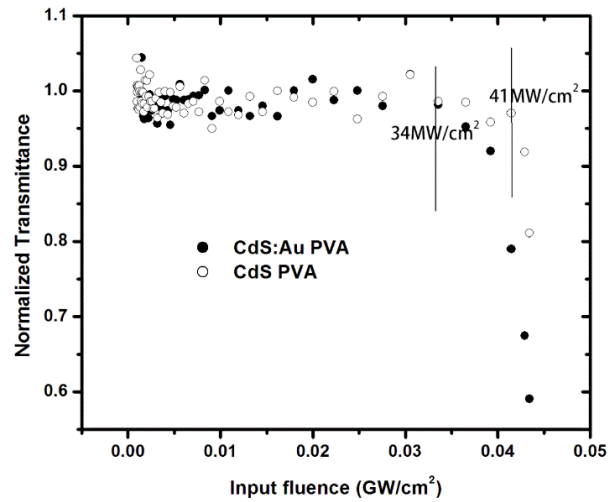


Figure 5.15: Optical limiting curves of CdS:Au PVA and CdS PVA nanocomposite films

From Figure 5.15, it is clear that for CdS:Au PVA nanocomposite films are having low limiting threshold ($34\text{MW}/\text{cm}^2$) compared to CdS PVA thin films ($41\text{MW}/\text{cm}^2$).

5.6 Optical properties of CdS and CdS:TiO₂ nanocomposites

CdS:TiO₂ nanoparticles are prepared by chemical bath technique from Cd(CH₃COO)₂, using thiourea and NH₄OH and TiO₂ colloidal nanoparticle solution [15-17]. All the chemicals were of GR (Guaranteed reagent) grade from Merck Ltd. TiO₂ colloidal nanoparticles are prepared by hydrolyzing titanium isopropoxide (1.4% volume) TiO₂ nanoparticle and then thermally decomposed to TiO₂ colloidal nanoparticles as described in section 3 of chapter 3. CdS:TiO₂ nanoparticles are prepared by mixing aqueous solutions of cadmium acetate

(concentration 0.1 M) and thiourea (0.15 M). Then 2ml of TiO₂ colloidal nanoparticles is added to the mixture. The pH of the mixture was kept at 10.5 by adding NH₄OH. The mixture was heated to 70 °C and stirred for 1.5 hours. The color of the solution changed to bright yellow and precipitation occurred indicating the formation of CdS:TiO₂ nanoparticles. The particles are filtered, washed and then dried in vacuum oven and used for further studies. Figure 5.16 shows the photographs of CdS:TiO₂ and CdS nanoparticles. It clearly indicates that the colour of CdS:TiO₂ is brighter yellowish compared to the colour of CdS nanoparticles.

5.6.1 Results and Discussion

0.001g of CdS and CdS:TiO₂ nanoparticles are dispersed in 10ml of 4%wt PVA aqueous solution. Figure 5.16 photographs of CdS:TiO₂ and CdS PVA nanocomposites. Brighter yellow for CdS:TiO₂ nanocomposite compared to the yellowish CdS nanoparticles indicate the influence of TiO₂ nanoparticles in the CdS:TiO₂ PVA nanocomposite particles.



Figure 5.16: Photographs of (a) CdS:TiO₂ PVA and (b) CdS PVA nanocomposites

Figure 5.17 presents HRTEM images for CdS:TiO₂ and CdS nanoparticles. From HR TEM image (fringes), CdS:TiO₂ nanoparticles are of the order of 4nm. Average size of CdS nanoparticles are of 4nm. It is not able to identify d-spacing of CdS and TiO₂ from this image. So EDS analysis was carried out to find out the presence of TiO₂

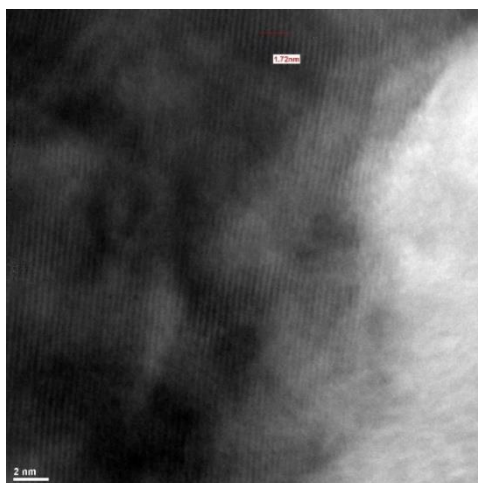


Figure 5.17: HR TEM image of CdS:TiO₂ nanocomposite particles

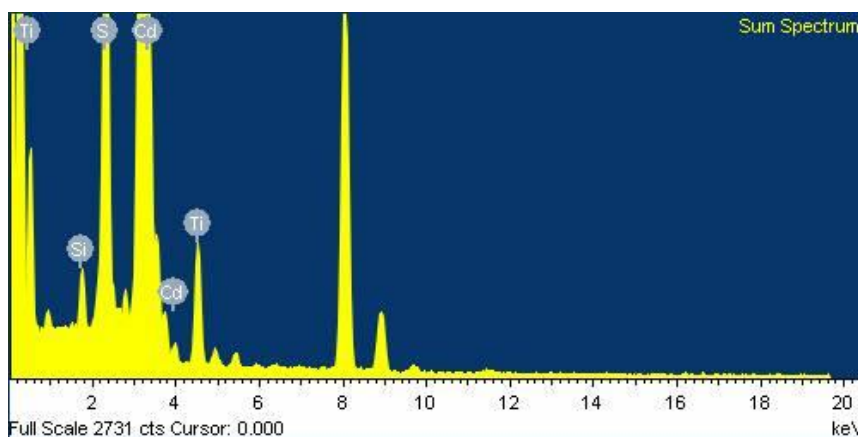


Figure 5.18: Energy dispersive X-ray spectrum of CdS:TiO₂ nanocomposite nanoparticles

Figure 5.18 shows represents the energy dispersive X-ray (EDS) spectrum of CdS:TiO₂ nanocomposite particles.

It shows the atomic percentage of elements involved in formation. The EDS analysis shows that the percentage of atoms of Cd and S elements are roughly of the same percentage (50% and 42%). This indicates that the material retain the stoichiometry without much change. The percentage of Ti is only 5%. So it is indicative of the fact that TiO₂ is doped into the CdS nanoparticles. Cu and Si percentage may be ignored as their presence are expected due to the method of preparation and characterization. .

Figure 5.19 is the TEM image where elemental maps are observable. Figure 5.20 shows the transmission electron microscopy (TEM) elemental maps of CdS:TiO₂ nanocomposite particles. In addition to aggregation/agglomeration of the nanocomposite particles [16], the elemental maps clearly illustrate the binding of CdS nanoparticles to TiO₂ nanoparticles to form CdS:TiO₂ nanocomposite particles. This clearly indicates the presence of TiO₂ on CdS nanoparticles.

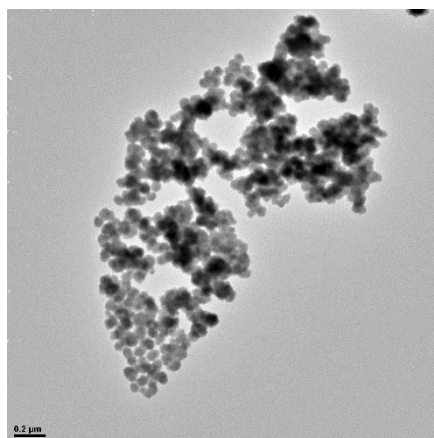


Figure 5.19: TEM image showing where the elemental maps were obtained

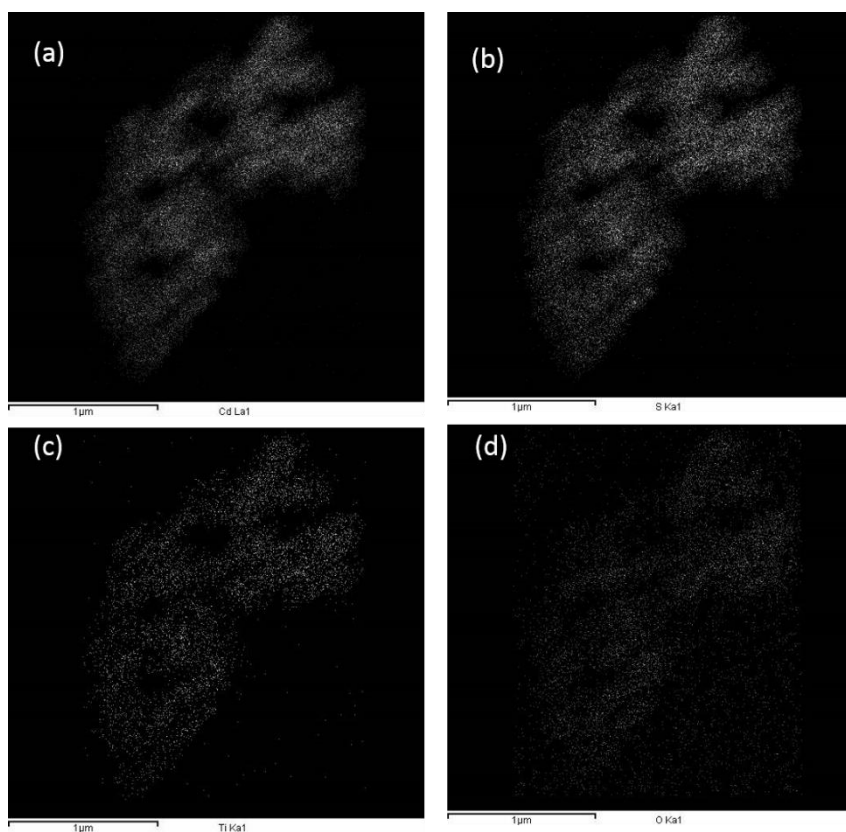


Figure 5.20: (a)TEM/Cd La1(b) TEM/S Ka1 map(c)TEM/Ti Ka1 map and TEM/O Ka1 map

Figure 5.21 is the absorption spectra of these nanocomposite particles in PVA solution. The absorption spectra show the onset absorption edges of CdS:TiO₂ nanoparticles and CdS nanoparticles at 479nm and 475nm indicating a red-shift. It is clear from spectra that the tail of the absorption edge of CdS:TiO₂ red-shifted compared to that of CdS nanoparticles.

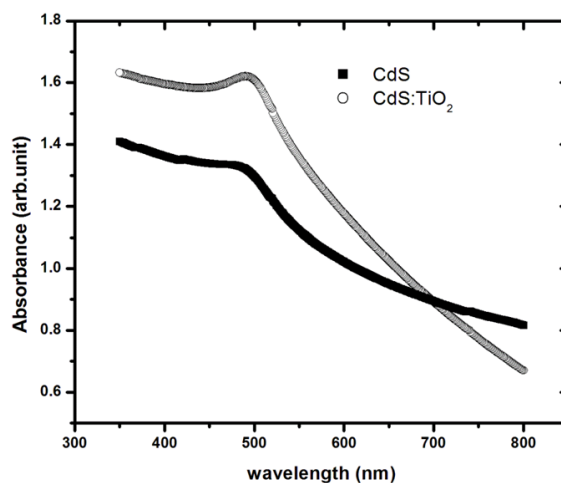


Figure 5.21: Optical absorption spectra of CdS and CdS:TiO₂ nanoparticles in aqueous PVA solution

A typical absorption spectrum of TiO₂ colloidal nanoparticles prepared is shown in Figure 5.22.

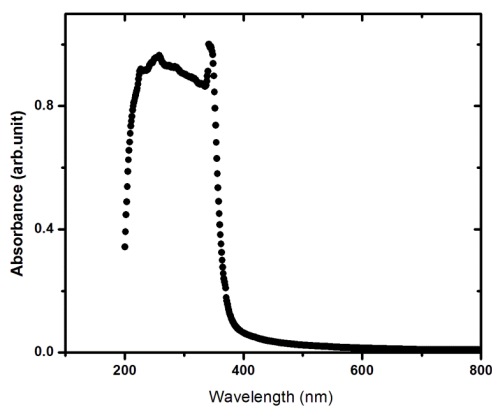


Figure 5.22: A typical absorption spectrum of TiO₂ colloidal nanoparticles

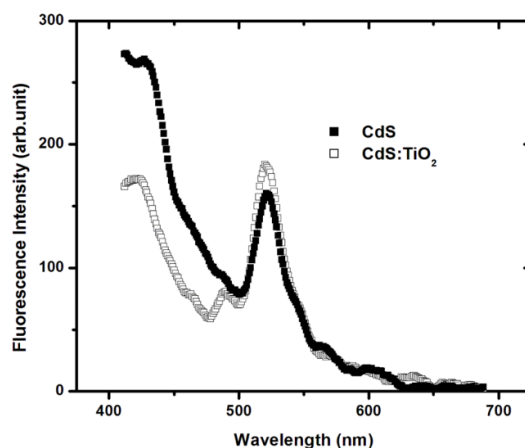


Figure 5.23: Fluorescence spectra of CdS and CdS:TiO₂ nanoparticles in PVA aqueous solution

Fluorescence spectra of CdS and CdS:TiO₂ nanocomposite particles are shown in Figure 5.23. There is an increase in emission intensity around 530nm for CdS:TiO₂ nanocomposite particles compared to CdS nanoparticles

5.7 Optical properties of CdS and CdS:TiO₂ nanocomposite films

5.7.1 Optical absorption studies

For studying the nonlinear optical properties for optical limiting application, CdS and CdS:TiO₂ nanoparticles have to be embedded in film form. Firstly these nanoparticles are embedded in PVA matrix. The procedure is described as follows. 0.006 g of CdS and CdS:TiO₂ nanoparticles are added to 10ml of 10 wt % PVA aqueous solution by stirring and followed by ultrasonication for 6hrs until uniformly dispersed. The resultant viscous solution is drop casted and kept for a day to dry out to form thin films. Thus formed CdS and CdS:TiO₂ PVA composite films are optically characterized by a Spectrophotometer JASCO570 UV\VIS\IR. The optical absorption spectra of these films are shown in Figure 5.24. From the absorption spectra it is clear that

in the case of CdS:TiO₂, there is a red shift for the onset absorption edge. Band gap is measured to be 2.40 eV and 2.24eV for CdS and CdS:TiO₂ respectively from Figure. 5.25.

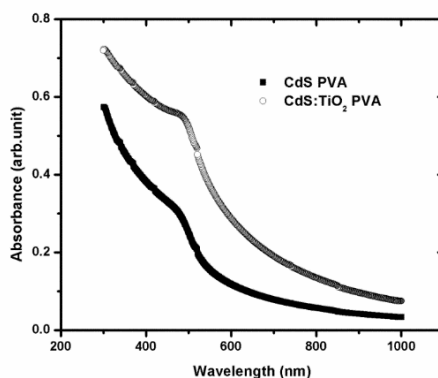


Figure 5.24: Absorption spectra of CdS PVA and CdS:TiO₂ PVA nanocomposite films

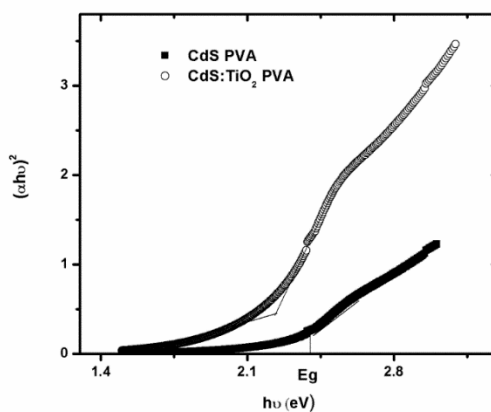


Figure 5.25: Optical band gap plot of CdS PVA and CdS:TiO₂ PVA nanocomposite films

5.7.2 Nonlinear optical studies on CdS PVA and CdS:TiO₂ PVA thin films

Figure.5.26 gives open aperture Z-scan traces of CdS PVA and CdS:TiO₂ PVA nanocomposite films at a typical fluence of 43MW/cm².

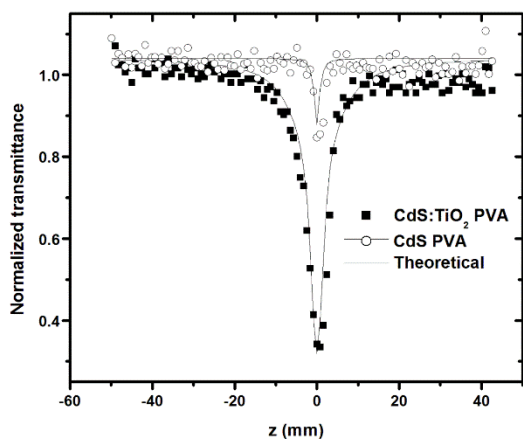


Figure 5.26: Open aperture Z-scan traces of CdS PVA and CdS:TiO₂ PVA nanocomposite films

Figure 5.27 yields the open aperture Z-scan traces of the CdS:TiO₂ PVA nanocomposite films at different input intensities.

Table 5-3: Nonlinear optical absorption coefficients

sample	$\beta \times 10^{-6}(\text{cm/W})$
CdS:TiO ₂ PVA film	8.23
CdS PVA film	2.71

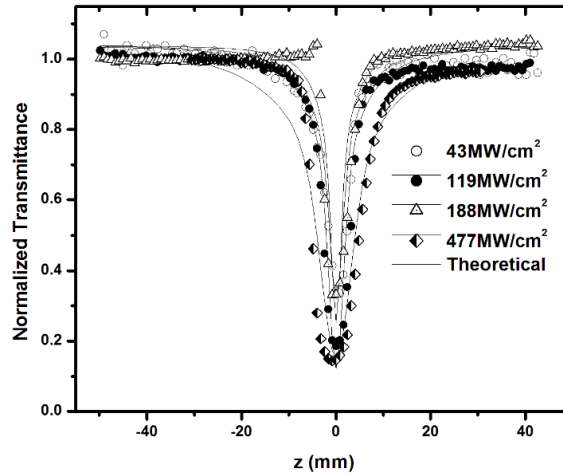


Figure 5.27: Open aperture Z-scan traces of CdS:TiO₂ PVA nanocomposite films

Table 5-4: Nonlinear absorption coefficients at different input intensities

Input intensities (MW/cm ²)	β (cm/W) ($\times 10^{-6}$)
43	8.23
119	3.20
188	1.95
477	0.8

Very recently Jing et.al investigated third-order nonlinear optical properties of 18.2%wt of CdS/PVP nanocomposite films using Z-scan technique and obtained large nonlinear absorption coefficient value of -4.25×10^{-7} cm/W at 532nm[30]. This result confirms our values on nonlinear optical coefficients of CdS: Au PVA and CdS PVA nanocomposite films. Hence these samples can show promising application for optical devices in photonics. These increased values can be attributed to contribution from excitonic and defect states and this is confirmed from the fluorescence studies. From fluorescence spectra

(Figure.5.23), it is clear that the emission peak at 530nm is increased in respect of CdS:TiO₂ nanocomposite particles compared to CdS nanoparticles. This increase of emission intensity is due to the increase in the population of defect states which is acting as luminescent centers. So this will sensitively influence the nonlinear optical property of the material as well. The nonlinear absorption of CdS:TiO₂ PVA thin films is found to be more than three times that of CdS PVA thin films.

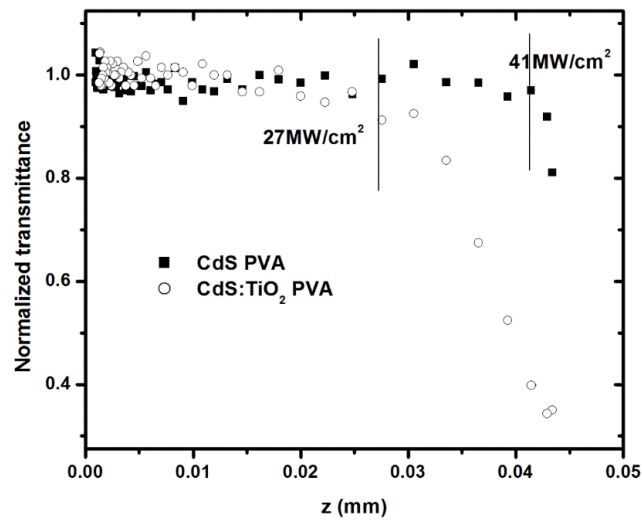


Figure 5.28: Optical limiting curves for CdS PVA and CdS:TiO₂ PVA nanocomposite films

Figure 5.28 shows the optical limiting curves for CdS:TiO₂ PVA and CdS PVA nanocomposite films. The limiting threshold is reduced to a low value of 27MW/cm² in the case of CdS:TiO₂ PVA nanocomposite compared to the limiting threshold of CdS PVA nanocomposite (41MW/cm²).

5.8 Conclusions

CdS:Au nanocomposite particles were prepared by mixing CdS nanoparticles with Au colloidal nanoparticles. Optical absorption study of these nanoparticles in PVA solution suggests that absorption tail was red shifted compared to CdS nanoparticles. TEM and EDS analysis suggested that the amount of Au nanoparticles present on CdS nanoparticles is very small. Fluorescence emission is unaffected indicating the presence of low level of Au nanoparticles. CdS:Au PVA and CdS PVA nanocomposite films were fabricated and optically characterized. The results showed a red-shift for CdS:Au PVA film for absorption tail compared to CdS PVA film. Nonlinear optical analysis showed a huge nonlinear optical absorption for CdS:Au PVA nanocomposite and CdS:PVA films. Also an enhancement in nonlinear optical absorption is found for CdS:Au PVA thin film compared to the CdS PVA thin film. This enhancement is due to the combined effect of plasmonic as well as excitonic contribution at high input intensity. Samples of CdS doped with TiO₂ were also prepared. Linear optical absorption spectra of these nanocomposite particles clearly indicated the influence of TiO₂ nanoparticles. TEM and EDS studies have confirmed the presence of TiO₂ on CdS nanoparticles. Fluorescence studies showed that there is an increase in emission peak around 532nm for CdS nanoparticles. Nonlinear optical analysis of CdS:TiO₂ PVA nanocomposite films indicated a large nonlinear optical absorption compared to that of CdS:PVA nanocomposite film. The values of nonlinear optical absorption suggests that these nanocomposite particles can be employed for optical limiting applications.

References

- [1] R. J. Gehr and R. W. Boyd, "Optical properties of nanostructured optical materials," *Chemistry of Materials*, vol. 8, pp. 1807-1819, 1996.
- [2] R. T. Tom, A. S. Nair, N. Singh, M. Aslam, C. Nagendra, R. Philip, K. Vijayamohanan and T. Pradeep, "Freely dispersible Au-TiO₂, Au-ZrO₂, Ag-TiO₂, and Ag-ZrO₂ core-shell nanoparticles: One-step synthesis, characterization, spectroscopy, and optical limiting properties," *Langmuir*, vol. 19, pp. 3439-3445, 2003.
- [3] Y. Yin, Z. Jin and F. Hou, "Enhanced solar water-splitting efficiency using core/sheath heterostructure CdS/TiO₂ nanotube arrays," *Nanotechnology*, vol. 18, pp. 495608-1-6, 2007.
- [4] M. R. Bockstaller and E. L. Thomas, "Optical properties of polymer-based photonic nanocomposite materials," *The Journal of Physical Chemistry B*, vol. 107, pp. 10017-10024, 2003.
- [5] C. Noguez, "Surface plasmons on metal nanoparticles: the influence of shape and physical environment," *The Journal of Physical Chemistry C*, vol. 111, pp. 3806-3819, 2007.
- [6] J. Heath, "Size-dependent surface-plasmon resonances of bare silver particles," *Physical Review B*, vol. 40, pp. 9982-9985, 1989.
- [7] H. Xiong, Z. Wang, D. Liu, J. Chen, Y. Wang and Y. Xia, "Bonding polyether onto ZnO nanoparticles: an effective method for preparing polymer nanocomposites with tunable luminescence and stable conductivity," *Advanced Functional Materials*, vol. 15, pp. 1751-1756, 2005.
- [8] M. Sahana, C. Sudakar, G. Setzler, A. Dixit, J. Thakur, G. Lawes, R. Naik, V. Naik and P. Vaishnava, "Bandgap engineering by tuning particle size and crystallinity of SnO₂-Fe₂O₃ nanocrystalline composite thin films" *Appl. Phys. Lett.*, vol. 93, pp. 231909-1-3, 2008.
- [9] H. Elim, W. Ji, A. Yuwono, J. Xue and J. Wang, "Ultrafast optical nonlinearity in poly (methylmethacrylate)-TiO₂ nanocomposites," *Appl. Phys. Lett.*, vol. 82, pp. 2691-2693, 2003.

- [10] M. Asobe, H. Itoh, T. Miyazawa and T. Kanamori, "Efficient and ultrafast all-optical switching using high Δn , small core chalcogenide glass fibre", *Electron. Lett*, vol. 29, pp. 1966-1968, 1993.
- [11] D. Cotter, R. J. Manning, K. J. Blow, A. D. Ellis, A. E. Kelly, D. Nesses, I. D. Phillips, A. J. Poustie and D. C. Rogers, "Nonlinear Optics for High-Speed Digital Information Processing," *Science*, vol. 286, pp. 1523-1528, 1999.
- [12] J. Harbold, F. Ilday, F. Wise, J. Sanghera, V. Nguyen, L. Shaw and I. Aggarwal, "Highly nonlinear As-S-Se glasses for all-optical switching," *Opt. Lett.*, vol. 27, pp. 119-121, 2002.
- [13] E. Hanamura, "Very large optical nonlinearity of semiconductor microcrystallites," *Physical Review B*, vol. 37, pp. 1273-1279, 1988.
- [14] T. Takagahara, "Excitonic optical nonlinearity and exciton dynamics in semiconductor quantum dots," *Physical Review B*, vol. 36, pp. 9293-9296, 1987.
- [15] J. He, W. Ji, G. H. Ma, S. H. Tang, E. S. W. Kong, S. Y. Chow, X. H. Zhang, Z. L. Hua and J. L. Shi, "Ultrafast and large third-order nonlinear optical properties of CdS nanocrystals in polymeric film," *The Journal of Physical Chemistry.B*, vol. 109, pp. 4373-4376, 2005.
- [16] C. Chang, Q. Chang and Y. Song, "Effects of host and shape on nonlinear optical properties of CdS nanorods and nanoparticles," in *Nanoelectronics Conference (INEC), 2010 3rd International*, 2010, pp. 555.
- [17] E. F. Hilinski, P. A. Lucas and Y. Wang, "A picosecond bleaching study of quantum-confined cadmium sulfide microcrystallites in a polymer film," *J. Chem. Phys.*, vol. 89, pp. 3435-3441, 1988.
- [18] R. E. Schwerzel, K. B. Spahr, J. P. Kurmer, V. E. Wood and J. A. Jenkins, "Nanocomposite photonic polymers. 1. Third-order nonlinear optical properties of capped cadmium sulfide nanocrystals in an ordered polydiacetylene host," *The Journal of Physical Chemistry A*, vol. 102, pp. 5622-5626, 1998.
- [19] Y. Wang and W. Mahler, "Degenerate four-wave mixing of CdS/polymer composite," *Opt. Commun.*, vol. 61, pp. 233-236, 1987.

- [20] Y. Yang, J. Shi, H. Chen, S. Dai and Y. Liu, "Enhanced off-resonance optical nonlinearities of Au-CdS core-shell nanoparticles embedded in BaTiO₃ thin films," *Chemical Physics Letters*, vol. 370, pp. 1-6, 2003.
- [21] H. Elim, W. Ji, A. Yuwono, J. Xue and J. Wang, "Ultrafast optical nonlinearity in poly (methylmethacrylate)-TiO₂ nanocomposites," *Appl. Phys. Lett.*, vol. 82, pp. 2691-2693, 2003.
- [22] C. Sciancalepore, T. Cassano, M. Curri, D. Mecerreyes, A. Valentini, A. Agostiano, R. Tommasi and M. Striccoli, "TiO₂ nanorods/PMMA copolymer-based nanocomposites: highly homogeneous linear and nonlinear optical material," *Nanotechnology*, vol. 19, pp. 205705-1-8, 2008.
- [23] S. Wang, L. Zhang, H. Su, Z. Zhang, G. Li, G. Meng, J. Zhang, Y. Wang, J. Fan and T. Gao, "Two-photon absorption and optical limiting in poly (styrene maleic anhydride)/TiO₂ nanocomposites," *Physics Letters A*, vol. 281, pp. 59-63, 2001.
- [24] L. Irimpan, B. Krishnan, V. Nampoore and P. Radhakrishnan, "Luminescence tuning and enhanced nonlinear optical properties of nanocomposites of ZnO-TiO₂," *J. Colloid Interface Sci.*, vol. 324, pp. 99-104, 2008.
- [25] D. Lincot, R. Ortega-Borges and M. Froment, "Epitaxial growth of cadmium sulfide layers on indium phosphide from aqueous ammonia solutions," *Appl. Phys. Lett.*, vol. 64, pp. 569-571, 1994.
- [26] L. Zhen, L. Yanyan, F. Yaoguo, P. Liwei, L. Tiebing and W. Minghong, "A novel and facile route for the synthesis of water-soluble cadmium sulfide quantum dots," in *Nanoelectronics Conference (INEC), 2010 3rd International*, 2010, pp. 466-467.
- [27] J. Jiang, G. Oberdörster and P. Biswas, "Characterization of size, surface charge, and agglomeration state of nanoparticle dispersions for toxicological studies," *Journal of Nanoparticle Research*, vol. 11, pp. 77-89, 2009.
- [28] M. Yin, H. Li, S. Tang and W. Ji, "Determination of nonlinear absorption and refraction by single Z-scan method," *Applied Physics B*, vol. 70, pp. 587-591, 2000.

- [29] H. Du, G. Xu, W. Chin, L. Huang and W. Ji, "Synthesis, characterization, and nonlinear optical properties of hybridized CdS-polystyrene nanocomposites," *Chemistry of Materials*, vol. 14, pp. 4473-4479, 2002.
- [30] C. Jing, X. Xu, X. Zhang, Z. Liu and J. Chu, "In situ synthesis and third-order nonlinear optical properties of CdS/PVP nanocomposite films," *J. Phys. D*, vol. 42, pp. 075402, 2009.

Chapter 6

Optical Properties of Nanocomposite Materials like CdSe-CdS and CdSe-ZnS Core-Shell Quantum Dots

Abstract

In this chapter, we study the influence of CdS on CdSe quantum dots and ZnS on CdSe quantum dots. The first part of this chapter deals with the influence of shell thickness of CdS on linear optical properties of CdSe QDs. The second section deals with the influence of ZnS on optical properties of CdSe QDs. In this section, CdSe-ZnS QDs with varying shell thickness is studied as an optical limiting material.

6.1 Introduction

Quantum dots (QDs) whose diameters are smaller than the bulk exciton Bohr diameter show size dependent optical and electronic properties [1]. They possess unique optical properties, such as tunable luminescence with narrow bandwidth, high quantum yield, and large multiphoton absorption cross-section and fast-response nonlinear refractive index [2-5]. Recently, the research for the optical nonlinearity of various kinds of semiconductor QDs has gained much attention [6-9]. Among semiconductor nanocrystals from group II-VI or III-V elements, commonly termed as quantum dots (QDs), CdSe is the most studied one. CdSe quantum dots show a vast range of applications, such as light-emitting devices, non-linear optical devices, solar cells, and as fluorescent bio-labels [10-12]. In weak confinement regime, the radius (R) of the nanocrystals greater than the Bohr radius (a_B) ($R \gg a_B$), the weakly correlated exciton-pair states are responsible for the nonlinearity. In the strong-confinement regime ($R \ll a_B$), the photo-excited electron and hole are individually confined [13]. Theoretical and experimental works have revealed that the state-filling effect accounts for the optical nonlinearity in this regime. In the case of strong confinement of electrons and holes, i.e., when the quantum dot diameter is smaller in size than an exciton, large optical nonlinearities are expected [14]. Influence of other semiconductors like ZnS, CdS etc on optical properties CdSe quantum dots is vastly investigated [15-18]. In this chapter, the influence of CdS on the optical properties of CdSe quantum dots is mainly studied.

We have investigated CdSe-CdS core-shell quantum dots. As the core size is varied keeping shell thickness constant, we have seen that this size variation has effect on emission and nonlinear optical properties of the resulting material. The detailed study is in reference [19]. The optical nonlinearity is found to be decreased with increase in core size.

In another similar work, we have altered the shell size by keeping the core size fixed and analyzed the optical properties. Preparation of the core-shell particles with different shell thickness is described as below

6.2 Optical properties of CdSe-CdS core-shell with varying shell thickness of CdS.

6.2.1 Preparation of the quantum dots

The chemicals used in the preparation: The surfactant, dioctyl sulfosuccinate sodium salt (Aerosol-OT, or AOT- 99% purity), Cadmium Nitrate and Zinc Nitrate (AR grade) and n-heptane (extrapure, 99%) were bought from S.D. Fine (India) chemicals. Ammonium sulfide ((NH₄)₂S) (25% aqueous solution), and Sodium Sulfite (anhydrous) were supplied by Alfa Aesar, (U.K). Selenium powder (black, GR grade) of 99.5% purity was purchased from Kemie Labs, India. All the chemicals were used without any further purification.

The synthesis of CdSe QDs was carried as per a simplified microemulsion method reported recently by an earlier work [20]. Reverse micelle system is made by dissolving AOT in n-heptane (0.1M). The reverse micelles were then swollen with appropriate aqueous precursor solutions thus forming microemulsions. Microemulsions of Cd(NO₃)₂ (0.3M) and Na₂SeSO₃ (0.1M), were prepared at water-to-surfactant molar ratio (R) = 4. The microemulsion was stirred with vortex mixer till it became completely clear. The two microemulsions (Cd(NO₃)₂ and Na₂SeSO₃) are prepared and then vortex-mixed, thus leading to the formation of CdSe inside the reverse micelles.

For preparing core-shell nanoparticles, we start with CdSe micro emulsion. To prepare CdSe-CdS with R=4 and shell to core molar ratio S=2, we start with CdSe (R=4) and add microemulsions of (NH₄)₂S (0.2M) (R=4) and then of Cd (NO₃)₂ (0.2M) (R=4) stepwise with proper vortex-stirring at each step,

to give finally a microemulsion of CdSe-CdS with R= 4 and S= 2. For varying shell thickness, the parameter S is varied as 1, 2 and 3 at a fixed R= 4. Thus in this work, CdSe QDs (CS0) and CdSe- CdS core- shell QDs with different shell thickness are obtained by changing the value of S, so that samples are designated as CS1(S=1), CS2(S=2) and CS3(S=3). The concentration of all prepared quantum dots found in the range of 1.2 to 1.6 μM which is further diluted to give the concentration of 1.0 μM each for the experimental analysis

6.2.2 Results and discussion

Figure 6.1 shows the absorption spectra of CdSe-CdS (CS1, CS2 and CS3) quantum dots and bare CdSe (CS0) quantum dots. The excitonic peak is found to be red-shifted with increase in shell thickness of these QDs with respect to the bare CdSe QDs. The onset absorption for these quantum dots are found to be 598nm (CS3), 584nm (CS2), 558nm(CS1) and 470nm(CS0). The particle size of the QDs can be calculated from the band gap of CdSe -CdS core-shell QDs by using L E Brus equation [21].

$$E_n = E_g + \frac{h^2}{8^* r^2} \left[\frac{1}{m_e^*} + \frac{1}{m_h^*} \right] - \frac{1.8e^2}{4\pi\epsilon_0\epsilon_r r} \quad (6.1)$$

where E_n is the band gap energy of nanoparticles which is found out from Fig.1 and E_g is the bulk band gap of CdSe which is 1.7eV, h is Planks constant, ϵ is dielectric constant of semiconductor, e the charge of electron, $m_e^* = m_e m_0$ and $m_h^* = m_h m_0$. Here m_e and m_h are the effective masses of electron and hole respectively for CdSe, and m_0 is the mass of an electron. By using equation (1), we estimate the mean sizes of CdSe and CdSe-CdS core-shell QDs. The parameter values used for CdSe [22] are: $m_e = 0.12$, $m_h = 0.8$, $m_0 = 9.1 \times 10^{-31}$ kg, $\epsilon_r = 9.57$, $\epsilon_0 = 8.854 \times 10^{-12}$ F/m, $e = 1.6 \times 10^{-19}$ C, $h = 6.626 \times 10^{-34}$ J/s. In the case of CdSe-CdS core-shell, the core-shell nanoparticle band gap is used in equation(6.1), however the other parameters are kept same. The calculated

particle size of these core-shell QDs from absorption edges are 3.8nm, 4.75nm, 5.2nm and 5.5nm for CS0, CS1, CS2 and CS3 QDs.

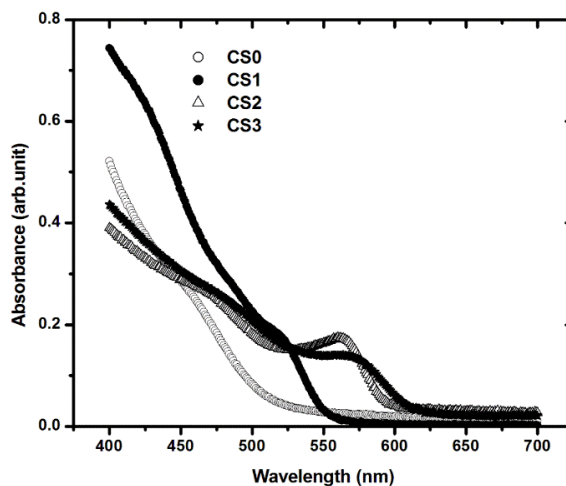


Figure 6.1: Optical absorption spectrum of CdSe and CdSe-CdS QDs with varying shell thickness

Figure. 6.2 (a), (b), (c), (d) shows the TEM images of the CdSe -CdS core-shell QDs (CS0, CS1, CS2, and CS3). Two important observations can be derived from these micrographs. We observe from these images that these QDs are well defined and nearly spherical in shape. The core-shell structure of the QDs cannot be deciphered from these micrographs. However, average diameter of these QDs is found to be 4.35 nm, 4.46nm, 5.46 and 5.74 nm for CS0, CS1, CS2 and CS3 QDs respectively. Comparing CS0 and CS1, it is clear that there is an increase of thickness 0.11nm when the shell of CdS is formed around the CdSe QDs. As the S value increases, the shell thickness of the QDs are also increased which can be proved from the TEM images of CS2 and CS3. There is a slight variation in the calculated values of the size of these QDs.

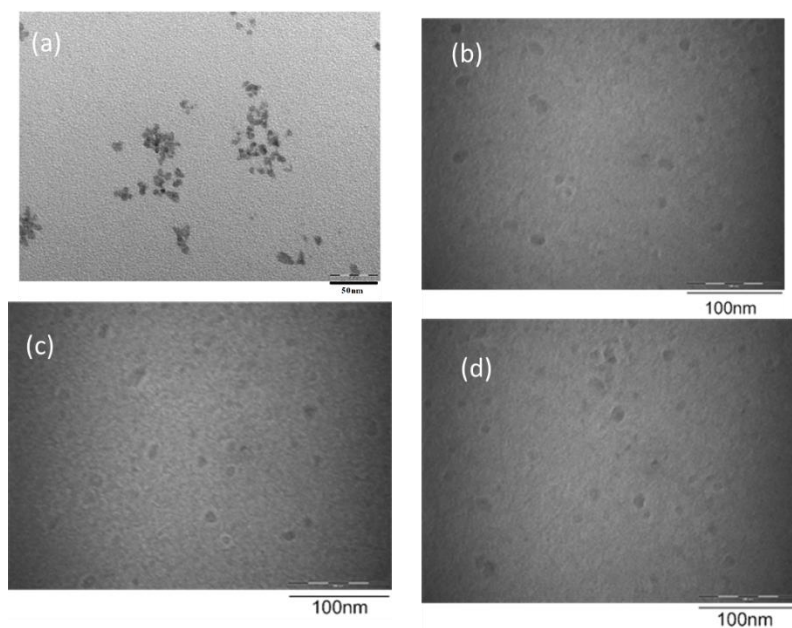


Figure 6.2: (a), (b), (c), (d) shows the TEM images of the CdSe -CdS core-shell QDs (CS0, CS1, CS2, and CS3)

Figure 6.3 presents a typical HRTEM for CdSe-CdS QDs to clearly exhibit the lattice structures for both core and shell of core-shell QDs. Figure 6.3 shows HRTEM micrographs (scale bar = 5 nm) for CdSe-CdS clearly showing the lattice fringes for the core and shell materials. From the figure, a clear core-shell structure with a denser CdSe core (a spacing of 3.48 angstroms corresponding to plane [1 1 1] of CdSe) and a lighter CdS shell (a spacing of 2.11 angstroms corresponding to plane [2 2 0] of CdS).

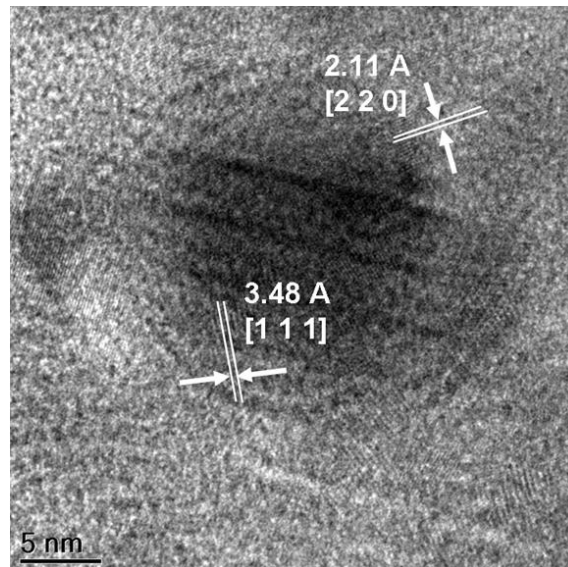


Figure 6.3: A typical HRTEM micrographs (scale bar = 5 nm) for CdSe-CdS QDs

Figure 6.4 (a) shows the fluorescence spectrum of these CdSe -CdS core-shell QDs under excitation of 390nm using Cary Eclipse fluorescence spectrophotometer. The emission peak of CS0 is at 537 nm, which is shifted to 541nm for CS1 sample and which is again shifted to 551nm in the case of CS2. Hence a shift of 4nm when the shell is introduced to the CdSe QDs. For CS2 QDs a shift of 10nm occurred in comparison with the CS1 QDs. Thus there is a red shift of emission peaks as the shell thickness of these core-shell QDs increases. For CS3 QDs, there is a peak around 572nm. The emissions of these QDs are assigned to excitonic emissions corresponding to that reported for the 1se-1sh excitonic state of the CdSe QDs. Thus the red shift of the emission wavelength with increase of particle size reveals the quantum confinement effect which is already reported in the case of CdSe-ZnS quantum dots [23].

Figure 6.4(b) shows the emission spectra of these QDs under the excitation of 532nm. It shows an emission around 745nm which is getting enhanced with the increase of shell thickness. This is a clear sign of the effect of CdS shell around CdSe QDs. This emission is asymmetric. Introduction of CdS

will enhance the defect structure of CdSe thereby increases the emission intensity. The 700-800nm region is in the water dip so that this light can be useful in the biomedical field. As the shell of CdS is increased, the defect state emission is reduced. This is due to the usual concentration quenching resulting from enhanced luminescent centers arising from defect structures. Above optimal shell thickness, non-radiative interactions between the defect structures cause such decrease in the fluorescence emission.

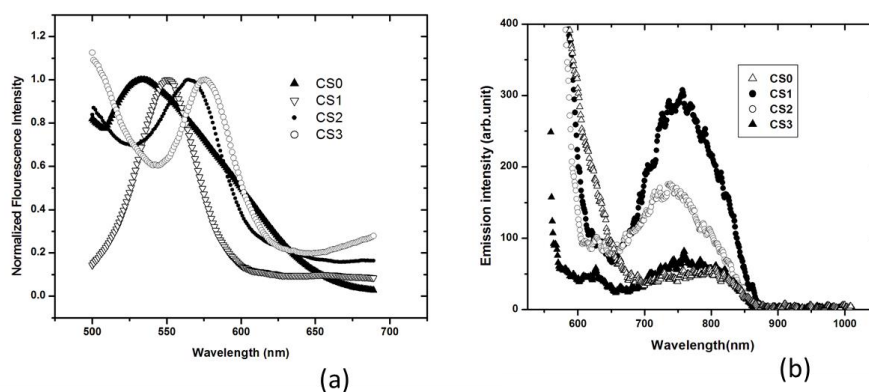


Figure 6.4: (a) Emission peak shift of CdSe-CdS QDs with increase in shell thickness under excitation wavelength 390nm (b) Emission band of CdSe-CdS QDs with increase in thickness of CdS shell under excitation 532nm

The nonlinear optical measurements were carried out, but there is reduction of optical nonlinearity. Thus a new emission band (700nm-800nm) is observed for CdSe QDs and introduction of CdS shell around CdSe QDs enhances the emission and then decreases and reaching same level of emission of bare CdSe QDs. Indication of generation of more trap states by the introduction of CdS shell and then healing of the trap states by CdS occurs.

6.3 Optical properties of CdSe-ZnS core-shell QDs

For preparing core-shell nanoparticles, we start with CdSe micro emulsion. To prepare CdSe-ZnS with $R=4$ and shell to core molar ratio $S=2$, we start with CdSe ($R=4$) and add microemulsions of $(\text{NH}_4)_2\text{S}$ (0.2M) ($R=4$)

and then of $\text{Zn}(\text{NO}_3)_2$ (0.2M) (R=4) stepwise with proper vortex-stirring at each step, to give finally a microemulsion of CdSe-ZnS with R= 4 and S= 2. For varying shell thickness, the parameter S is varied as 1, 2 and 3 at a fixed R= 4. Thus in this work, CdSe QDs (C0) and CdSe- ZnS core-shell QDs with different shell thickness are obtained by changing the value of S, so that samples are designated as C1(S=1), C2(S=2) and C3(S=3). The final concentrations of QDs in the microemulsions used in the analysis are as follows 1.3 μM , 1.3 μM , 1.3 μM and 1.6 μM for C0, C1, C2 and C3 samples respectively. The variation of concentrations is negligible.

6.3.1 Results and discussion

The absorption spectrum of the CdSe -ZnS core-shell QDs are given in Figure 6.5. The excitonic peak was found to be red-shifted with the increase in shell thickness of these QDs with respect to the bare CdSe QDs. This clearly indicated the quantum confinement in the QDs. All spectroscopic measurements were performed using spherical CdSe-ZnS core-shell QDs. The observed dependence of the absorption band gap on the size of CdSe-ZnS core-shell QDs is used to determine the particle size. Particle sizes were approximated from the “effective band gap” values E_g from the absorption edges and found out to be 2.64 eV, 2.35eV, 2.42eV and 2.44eV for C0, C1, C2, C3 QDs. The particle size of the QDs can also be calculated from the band gap of CdSe -ZnS core-shell QDs by using the well-known equation [21].

In the case of CdSe-ZnS core-shell, the core-shell nanoparticle band gap is used in equation (6.1), however the other parameters are kept the same. The calculated particle size of these core-shell QDs from absorption edges are 3.8nm, 4.4nm, 4.3nm and 4.2nm for C0, C1, C2 and C3 QDs. From these values, it is clear that the core size is almost constant.

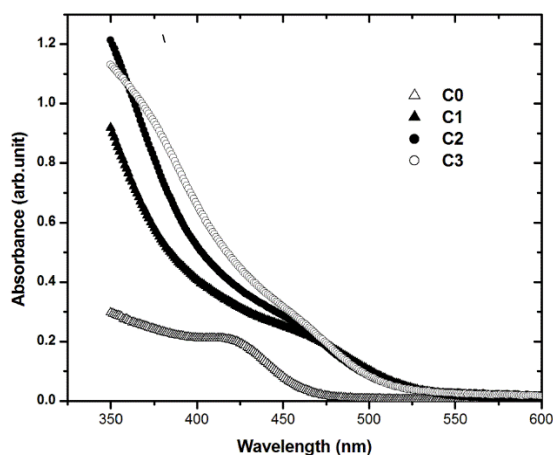


Figure 6.5: Absorption spectra of the CdSe -ZnS core-shell QDs (C0, C1, C2, and C3)

Figure 6.6 (a), (b), (c), (d) shows the TEM images of the CdSe -ZnS core-shell QDs (C0, C1, C2, and C3). Two important observations can be derived from these micrographs. We observe from these images that these QDs are well defined and nearly spherical in shape. The core-shell structure of the QDs cannot be deciphered from these micrographs. However, average diameter of these QDs is found to be 4.35 nm, 5.14nm, 5.72nm and 5.96 nm for C0, C1, C2 and C3 QDs respectively. Comparing C0 and C1, it is clear that there is an increase of thickness 0.79nm when the shell is formed around the CdSe QDs. As the S value increases, the shell thickness of the QDs are also increased which can be proved from the TEM images of C2 and C3. There is a slight variation in the calculated values of the size of these QDs. The electron diffraction pattern indicates highly crystalline structures having fcc pattern.

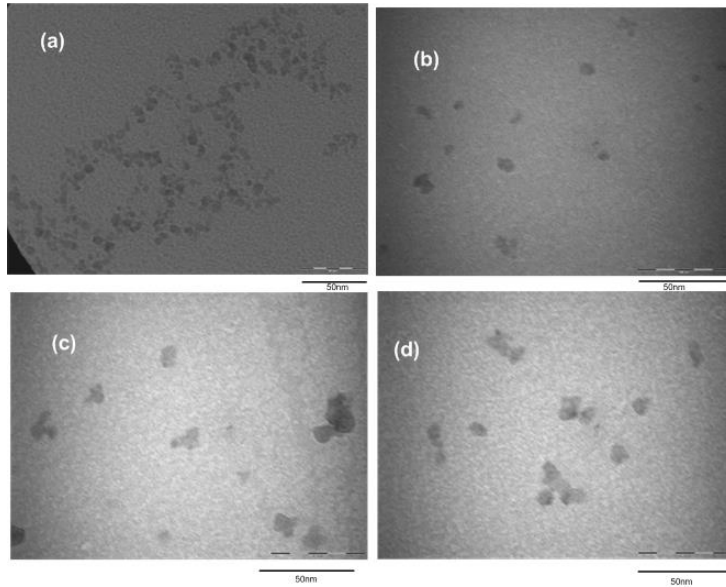


Figure 6.6: (a), (b), (c), (d) shows the TEM images of the CdSe -ZnS core-shell QDs (C0, C1, C2, and C3)

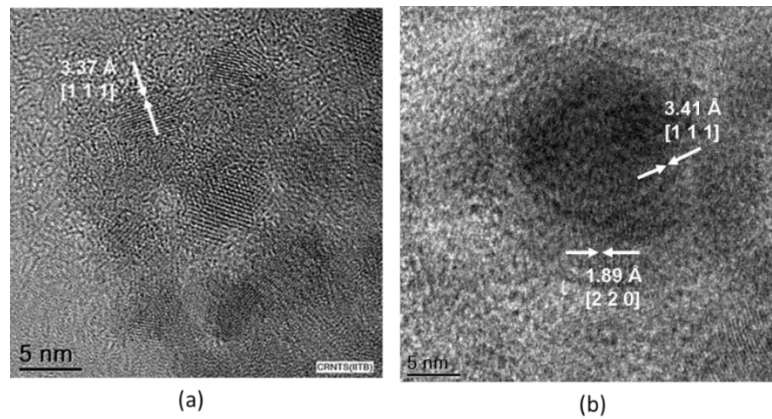


Figure 6.7: A typical HRTEM micrographs (scale bar = 5 nm) for (a)CdSe and CdSe-ZnS QDs

Figure. 6.7 shows HRTEM micrographs (scale bar = 5 nm) for CdSe (a), and CdSe-ZnS (b) clearly showing the lattice fringes for the core and shell materials.

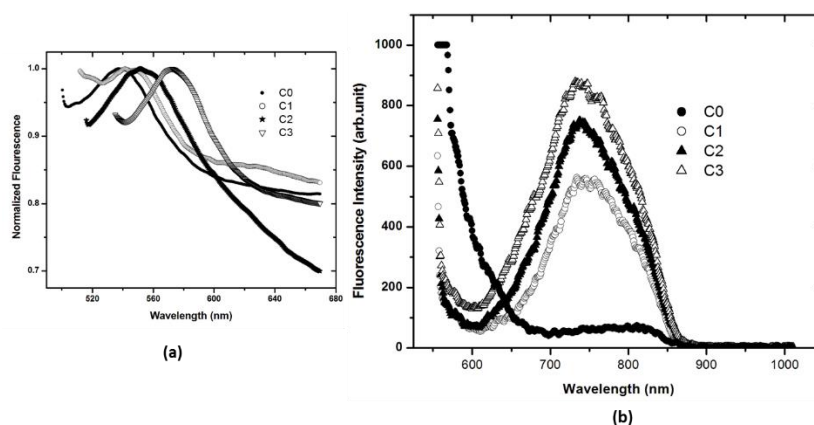


Figure 6.8: (a) Emission peak shift of CdSe-ZnS QDs with increase in shell thickness under excitation wavelength 390nm (b) Emission band of CdSe-ZnS QDs with increase in thickness of ZnS shell under excitation 532nm

Figure 6.8(a) shows the fluorescence spectrum of these CdSe-ZnS core-shell QDs under excitation of 390nm using Cary Eclipse fluorescence spectrophotometer. The emission peak of C0 is at 537 nm, which is shifted to 541nm for C1 sample and which is again shifted to 551nm in the case of C2. Hence a shift of 4nm when the shell is introduced to the CdSe QDs. For C2 QDs a shift of 10nm occurred in comparison with the C1 QDs. Thus there is a red shift of emission peaks as the shell thickness of these core-shell QDs increases. For C3 QDs, there is a peak around 572nm. The emissions of these QDs are assigned to excitonic emissions corresponding to that reported for the 1se-1sh excitonic state of the CdSe QDs. The emission is solely band-edge photoluminescence with nearly symmetric and narrow emission band shifting from bluish-green to red with increasing particle size. Thus the red shift of the emission wavelength with increase of particle size reveals the quantum confinement effect which is already reported in the case of CdSe-ZnS quantum dots [23].

Figure 6.8(b) shows the emission spectra of these QDs under the excitation of 532nm. It shows an emission around 745nm which is getting enhanced with the increase of shell thickness. This is a clear sign of the effect of

ZnS shell around CdSe QDs. This emission is asymmetric and can be resolved into two emission bands. Introduction of ZnS will enhance the defect structure of CdSe thereby increases the emission intensity. The 700-800nm region is in the water dip so that this light can be useful in the biomedical field.

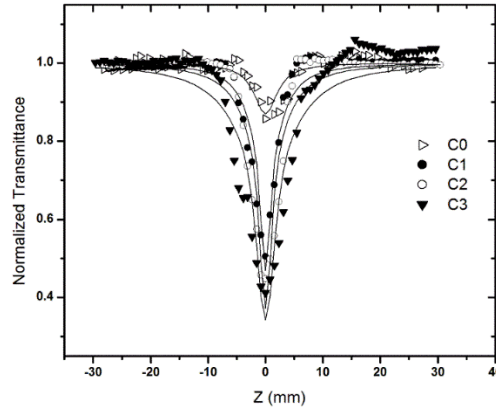


Figure 6.9: Open aperture Z-scan traces of C0, C1, C2, and C3 QDs

Figure 6.9 gives open aperture Z-scan traces of these QDs (C0, C1, C2, and C3) at a typical fluence of $371\text{MW}/\text{cm}^2$. The open-aperture curve exhibits a normalized transmittance valley, indicating the presence of a reverse saturable absorption in these QDs. The data are analyzed by using the procedure described by Bahae *et al.*[24] for a two photon absorption process; the nonlinear absorption coefficient is obtained by fitting the experimental Z-scan plot to equation (6.2),

$$T(z) = \frac{c}{q_0\pi} \int_{-\infty}^{\infty} \ln(1 + q_0 e^{-t^2}) dt \quad (6.2)$$

where $q_0(z, r, t) = \frac{\beta I_0 L_{\text{eff}}}{\left(1 + \frac{z^2}{z_0^2}\right)}$ and $L_{\text{eff}} = \frac{(1 - e^{-\alpha l})}{\alpha}$ is the effective thickness

with linear absorption coefficient, α and I_0 is the irradiance at the focus. The solid curves in Figure 6.9 are the theoretical fit to the experimental data. The open-

aperture Z-scan scheme was used to measure β and $\text{Im } \chi^{(3)}$. The imaginary part of the third-order susceptibility, $\text{Im } \chi^{(3)}$ is related to β through the equation $\text{Im } \chi^{(3)} = n_0^2 c^2 \beta / (240 \pi^2 \omega)$ (in esu.) where $n_0=2.34$ is the linear refractive index of CdSe, ϵ_0 is the permittivity of free space, c is the velocity of light in vacuum, ω is the angular frequency of the radiation used.

It is clear from table.1 that the formation of ZnS shell around CdSe QDs makes an increase in nonlinear absorption. Also when the core-shell thickness is increased, the nonlinear optical absorption gets enhanced.

Table.6.1: Linear and nonlinear optical absorption

Samples	Linear absorption at 532nm(cm^{-1})	Nonlinear absorption (β) $\times 10^{-10}$ (m/W)	Imaginary part of $\chi^{(3)}$ $\times 10^{-11}$ (e.s.u)
C0	0.151	2.69	1.58
C1	0.032	3.56	2.1
C2	0.036	3.78	2.21
C3	0.033	3.83	2.25

This enhancement in nonlinear optical absorption can be explained as below. Generally, optical response of nanoparticles consists of absorption, refraction and scattering. In this case, scattering does not play any significant role as the size of these QDs is much less and hence can be neglected. In order to explain the optical nonlinearity of these QDs, the system can be considered as a two level system. As the excitation wavelength is 532nm, which is in the range of band gap of these QDs, we can consider the nonlinear absorption to be mainly contributed by an excited-state absorption or free carrier absorption process, in which electrons in the ground state level are excited to intermediate energy states because of the linear absorption tail. Thus a large number of free carriers are

generated by one-photon excitation under a 532nm laser pulse. Subsequently, the free carriers thus generated could further absorb another photon and get excited to a higher excitonic level, resulting in the transient absorption. In this process, we suggest the lower level of higher excited state level may act as an intermediate state to generate the reverse saturable absorption. Considering that the absorption tail is mainly related to the core of CdSe QDs, it is almost of the same value for these Quantum dots. So the contribution from the core of the QDs for the optical nonlinear absorption can be treated as the same.

From intermediate level, electron-hole pair recombination occur yielding emission from 537nm to 572nm for these QDs. This intermediate level also acts as a source of excited state absorption. In addition to the emission of 537nm-572nm, there is a strong emission around 745nm arising from deep trap state levels in the CdSe-ZnS interface. This indicate the presence of free electron hole pairs which can recombine to give 745nm and also act as the source of free-carrier absorption.

Thus two types of free-carrier absorption can occur. One is due to the tail of absorption edge and other is due to the deep trap state level. In the case of bare CdSe QDs, the nonlinear absorption is mainly due to the excited state absorption involving the intermediate state due to the absorption tail. In the case of CdSe-ZnS core-shell case, the nonlinear absorption is enhanced. CdSe core has got spherical symmetry. As the ZnS shell is formed around CdSe core, it is distorted so as to reduce the spherical symmetry, thereby enhancing the nonlinearity in the interaction between light and sample. This can be explained considering the emission of 745 nm which is due to the deep trap states. So in addition to the intermediate excitonic level, these deep trap states also act as the source of free carriers. As the thickness of the shell increases, from Figure 6.8(b) it is clear that 745nm emission also gets enhanced. i.e., the density of free carriers is also increased, causing an enhancement in the nonlinear absorption. The contribution

from the free carrier can also be confirmed by the enhancement in fluorescence intensity as observed in Figure 6.8(b). The involvement of intermediate state level and deep trap state level are the source of free-carriers. This increase in the free carriers contributes to the enhancement of optical non-linearity in the case of CdSe-ZnS core-shell QDs.

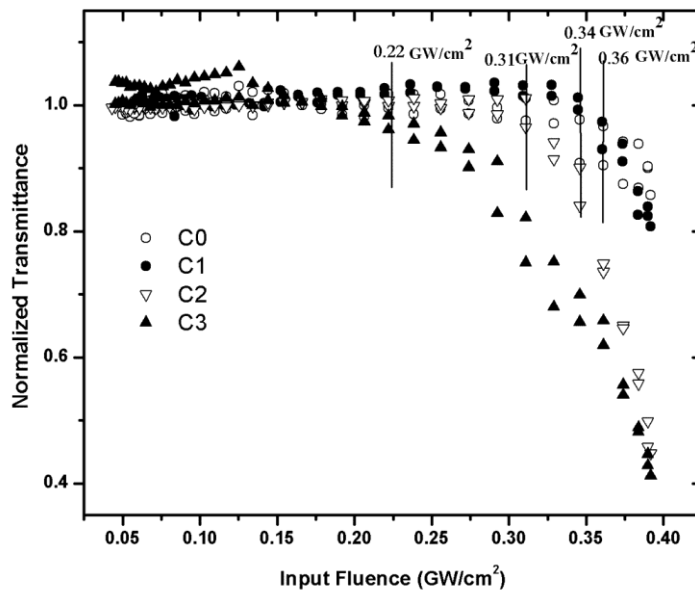


Figure 6.10: Optical limiting curves for C0, C1, C2, and C3 QDs

The optical limiting phenomenon with samples could be of interest in this context. To study the optical limiting property of the samples, the nonlinear transmission of the sample is measured as a function of input fluence. The optical limiting property mainly arises from absorptive nonlinearity, which corresponds to the imaginary part of third-order optical susceptibility [25]. From the value of fluence at focus, the fluence values at other positions could be calculated using the standard equations for Gaussian beam waist. Such plots (fluence vs transmittance) generated from Z-scan trace give a much better representation of intensity dependent transmission of the light in the sample. Figure 6.10 illustrates

the optical limiting response of the core-shell QDs. The continuous line in the figure indicates the approximate fluence at which the normalized transmission begins to deviate from linearity. The fluence value corresponding to the onset of optical limiting (optical limiting threshold) is found to be varying from 0.345 GW/cm² to 0.298GW/cm². As a result the limiting threshold is decreased as the shell thickness is increased in respect of CdSe QDs. Thus the core-shell QDs in the strong confinement regime can be used for optical power limiting of high intensity laser pulses.

6.3.2 Conclusions

CdSe-CdS and CdSe-ZnS core-shell QDs with varying shell size were characterized using UV–VIS spectroscopy. Optical absorption and TEM analysis of these QDs suggested a particle size around 5 nm. It is clearly shown that the surface coating influences the optical properties of QDs in terms of their size. Fluorescence studies reveal the presence of trap states in CdSe-CdS and CdSe-ZnS QDs. Trap states are increased as the shell of CdS introduced and increasing the shell size of CdS thereafter found to be decreased the trapstate emission. There is no sizeable nonlinear optical absorption observed. In the case of CdSe-ZnS QDs, the trap state emission gets enhanced with the increase in ZnS shell thickness. The enhancement of emission from trap states transition due to the increase in thickness of ZnS shell gives a clear indication of distortion occurring in the spherical symmetry of CdSe quantum dots. Consequently the nonlinear optical absorption of CdSe-ZnS QDs gets increased and the optical limiting threshold is decreased as the shell thickness is increased in respect of CdSe QDs. In comparison with CdSe-CdS QDs, CdSe-ZnS QDs possess much better optical property and thereby CdSe-ZnS is a strong candidate for nonlinear as well as linear optical applications.

References

- [1] H. Weller, "Quantum size colloids: From size-dependent properties of discrete particles to self-organized superstructures," *Current Opinion in Colloid & Interface Science*, vol. 3, pp. 194-199, 1998.
- [2] L. Irimpan, V. P. N. Nampoore, P. Radhakrishnan, a. Deepthy and B. Krishnan, "Size dependent fluorescence spectroscopy of nanocolloids of ZnO," *J. Appl. Phys.*, vol. 102, pp. 063524-063524, 2007.
- [3] N. Venkatram, R. Sathyavathi and D. N. Rao, "Size dependent multiphoton absorption and refraction of CdSe nanoparticles," *Optics Express*, vol. 15, pp. 12258-63, 09, 2007.
- [4] B. Luther-Davies, D. Choi, a. Prasad, R. Wang, D. Bulla, C. Zha, M. Pelusi, V. Ta'eed, M. R. E. Lamont, L. Fu, D. J. Moss, K. Finsterbusch, H. C. Nguyen and B. J. Eggleton, "Nonlinear materials for integrated ultra-fast all-optical devices," 2008 IEEE/LEOS Winter Topical Meeting Series, pp. 2-3, 2008.
- [5] S. Wang, B. R. Jarrett, S. M. Kauzlarich and A. Y. Louie, "Core/shell quantum dots with high relaxivity and photoluminescence for multimodality imaging," *J. Am. Chem. Soc.*, vol. 129, pp. 3848-56, 04, 2007.
- [6] B. Karthikeyan, M. Anija and R. Philip, "In situ synthesis and nonlinear optical properties of Au:Ag nanocomposite polymer films," *Appl. Phys. Lett.*, vol. 88, pp. 053104-053104, 2006.
- [7] X. Liu, Y. Adachi, Y. Tomita, J. Oshima, T. Nakashima and T. Kawai, "High-order nonlinear optical response of a polymer nanocomposite film incorporating semiconductor CdSe quantum dots," *Optics Express*, vol. 20, pp. 13457-69, 06, 2012.
- [8] L. Irimpan, B. Krishnan, V. P. N. Nampoore and P. Radhakrishnan, "Linear and nonlinear optical characteristics of ZnO-SiO₂ nanocomposites," *Appl. Opt.*, vol. 47, pp. 4345-51, 08, 2008.

- [9] M. Feng, R. Sun, H. Zhan and Y. Chen, "Lossless synthesis of graphene nanosheets decorated with tiny cadmium sulfide quantum dots with excellent nonlinear optical properties," *Nanotechnology*, vol. 21, pp. 75601-75601, 02, 2010.
- [10] P. O. Anikeeva, J. E. Halpert, M. G. Bawendi and V. Bulovic, "Quantum Dot Light-Emitting Devices with Electroluminescence Tunable over the Entire Visible Spectrum", *Nano Lett.*, vol.9 (7), pp 2532–2536, 2009.
- [11] A. D. Aprano, G. D. Amgo and A. Paparellit, "Volumetric and Transport Properties of Water/AOT/n-Heptane Microemulsions," *J. Phys. Chem.* vol. 97, pp.3614-3618, 1993.
- [12] D. R. Baker and P. V. Kamat, "Tuning the emission of CdSe quantum dots by controlled trap enhancement," *Langmuir : The ACS Journal of Surfaces and Colloids*, *Langmuir*, vol.26 (13), pp 11272–11276, 2010.
- [13] A.I L. Efros and A.L.Efros, "Interband Absorption of Light in a Semiconductor Sphere," *Sov. Phys. Semicond*, vol. 16, pp. 772-775, 1982.
- [14] S. Schmitt-Rink, D. Miller and D. S. Chemla, "Theory of the linear and nonlinear optical properties of semiconductor microcrystallites," *Physical Review B*, vol. 35, pp. 8113, 1987.
- [15] M. Al-Mossawi, A. Al-Shatravi and A. Al-Khursan, "CdSe/ZnSe Quantum-Dot Semiconductor Optical Amplifiers," *Insciences Journal*, vol. 2, pp. 52-62, 04, 2012.
- [16] J. J. Angell, "Synthesis and characterization of CdSe-ZnS core-shell quantum dots for increased quantum yield “, 2011.
- [17] U. Banin, M. Bruchez, a. P. Alivisatos, T. Ha, S. Weiss and D. S. Chemla, "Evidence for a thermal contribution to emission intermittency in single CdSe/CdS core/shell nanocrystals," *J. Chem. Phys.*, vol. 110, pp. 1195-1195, 1999.
- [18] S. Changyu, "CdSe/ZnS/CdS core/shell quantum dots for white LEDs," *Proc. SPIE 7138, Photonics, Devices, and Systems IV*, 71382E, 2008.

- [19] S. Mathew, A. D. Saran, B. S. Bhardwaj, S. A. Joseph, P. Radhakrishnan, V. Nampoory, C. Vallabhan and J. R. Bellare, "Size dependent optical properties of the CdSe-CdS core-shell quantum dots in the strong confinement regime," *J. Appl. Phys.*, vol. 111, pp. 074312, 2012.
- [20] A. D. Saran and J. R. Bellare, "Green engineering for large-scale synthesis of water-soluble and bio-tagable CdSe and CdSe-CdS quantum dots from microemulsion by double-capping," *Colloids Surf. Physicochem. Eng. Aspects*, vol. 369, pp. 165-175, 10, 2010.
- [21] L. E. Brus. "Electron-electron and electron-hole interactions in small semiconductor crystallites: The size dependence of the lowest excited electronic state". *J. Chem. Phys.* 80(9), pp. 4403-4409. 1984.
- [22] D. R. Lide, *CRC Handbook of Chemistry and Physics 2004-2005: A Ready-Reference Book of Chemical and Physical Data*. CRC press, 2004.
- [23] B. Dabbousi, J. Rodriguez-Viejo, F. V. Mikulec, J. Heine, H. Mattoussi, R. Ober, K. Jensen and M. Bawendi, "(CdSe) ZnS core-shell quantum dots: synthesis and characterization of a size series of highly luminescent nanocrystallites," *The Journal of Physical Chemistry B*, vol. 101, pp. 9463-9475, 1997.
- [24] M. Sheik-Bahae, a. a. Said, T. -. Wei, D. J. Hagan and E. W. Van Stryland, "Sensitive measurement of optical nonlinearities using a single beam," *IEEE J. Quant. Electron.*, vol. 26, pp. 760-769, 1990.
- [25] S. Shi, W. Ji, S. H. Tang, J. P. Lang and X. Q. Xin "Synthesis and Optical Limiting Capability of Cubane-like Mixed Metal Clusters $(n\text{-Bu}_4\text{N})_3[\text{MoAg}_3\text{BrX}_3\text{S}_4]$ (X = Cl and I), *J. Am. Chem. Soc.*, vol. 116 (8), pp. 3615-3616, 1994.

Chapter 7

Conclusion and Future prospects

General Conclusions

Nanophotonics is an exciting research field which merges lasers, nanomaterials as well as optics and electronics. Semiconductor nanoparticles are of much interest in this field as quantum confinement effect provides a means to manipulate its bandgap and consequently the optical properties. In the present investigations, various types of nanomaterials suitable for photonics applications have been investigated. The results which have emerged out of these studies are also presented.

Preparation and characterization methods and experimental techniques adopted for the investigations were illustrated in chapter 2 of this thesis.

Chapter 3 discusses the preparation of CdS, TiO₂ and Au nanoparticles. We observed that the fluorescence behaviour of the CdS nanoparticles, prepared by precipitation technique, depends on excitation wavelength. It was found that the peak emission wavelength can be shifted by as much as 147nm by varying

the excitation wavelengths and the reason for this phenomenon is the selective excitation of the surface states in the nanoparticles. This provided certain amount of tunability for the emission which results from surface states. TiO₂ nanoparticle colloids were prepared by hydrothermal method. The optical absorption study showed a blue shift of absorption edge, indicating quantum confinement effect. The large spectral range investigated allows observing simultaneously direct and indirect band gap optical recombination. The emission studies carried out show four peaks, which are found to be generated from excitonic as well as surface state transitions. It was found that the emission wavelengths of these colloidal nanoparticles and annealed nanoparticles showed two category of surface state emission in addition to the excitonic emission. Au nanoparticles prepared by Turkevich method showed nanoparticles of size below 5nm using plasmonic absorption calculation. It was also found that there was almost no variation in size as the concentration of precursor was changed from 0.2mM to 0.4mM.

We have observed SHG from CdS nanostructured thin film prepared on glass substrate by chemical bath deposition technique. The results point out that studied sample has in-plane isotropy. The relative values of tensor components of the second-order susceptibility were determined to be $\chi_{zzz} = 1$, $\chi_{xxz} = 0.14$, and $\chi_{zxx} = 0.07$. These values suggest that the nanocrystals are oriented along the normal direction. However, the origin of such orientation remains unknown at present. Thus CdS is a promising nonlinear optical material for photonic applications, particularly for integrated photonic devices.

CdS Au nanocomposite particles were prepared by mixing CdS nanoparticles with Au colloidal nanoparticles. Optical absorption study of these nanoparticles in PVA solution suggests that absorption tail was red shifted compared to CdS nanoparticles. TEM and EDS analysis suggested that the


amount of Au nanoparticles present on CdS nanoparticles is very small. Fluorescence emission is unaffected indicating the presence of low level of Au nanoparticles. CdS:Au PVA and CdS PVA nanocomposite films were fabricated and optically characterized. The results showed a red-shift for CdS:Au PVA film for absorption tail compared to CdS PVA film. Nonlinear optical analysis showed a huge nonlinear optical absorption for CdS:Au PVA nanocomposite and CdS:PVA films. Also an enhancement in nonlinear optical absorption is found for CdS:Au PVA thin film compared to the CdS PVA thin film. This enhancement is due to the combined effect of plasmonic as well as excitonic contribution at high input intensity. Samples of CdS doped with TiO₂ were also prepared and the linear optical absorption spectra of these nanocomposite particles clearly indicated the influence of TiO₂ nanoparticles. TEM and EDS studies have confirmed the presence of TiO₂ on CdS nanoparticles. Fluorescence studies showed that there is an increase in emission peak around 532nm for CdS nanoparticles. Nonlinear optical analysis of CdS:TiO₂ PVA nanocomposite films indicated a large nonlinear optical absorption compared to that of CdS:PVA nanocomposite film. The values of nonlinear optical absorption suggests that these nanocomposite particles can be employed for optical limiting applications.

CdSe-CdS and CdSe-ZnS core-shell QDs with varying shell size were characterized using UV–VIS spectroscopy. Optical absorption and TEM analysis of these QDs suggested a particle size around 5 nm. It is clearly shown that the surface coating influences the optical properties of QDs in terms of their size. Fluorescence studies reveal the presence of trap states in CdSe-CdS and CdSe-ZnS QDs. Trap states showed an increase as a shell for CdS is introduced and increasing the shell size of CdS beyond a certain value leads to a decrease in the trap state emission. There is no sizeable nonlinear optical absorption observed. In the case of CdSe- ZnS QDs, the trap state emission gets enhanced with the

increase in ZnS shell thickness. The enhancement of emission from trap states transition due to the increase in thickness of ZnS shell gives a clear indication of distortion occurring in the spherical symmetry of CdSe quantum dots. Consequently the nonlinear optical absorption of CdSe-ZnS QDs gets increased and the optical limiting threshold is decreased as the shell thickness is increased in respect of CdSe QDs. In comparison with CdSe-CdS QDs, CdSe-ZnS QDs possess much better optical properties and thereby CdSe-ZnS is a strong candidate for nonlinear as well as linear optical applications

Future prospects:

From results of the optical studies reported in the present thesis, it is clear that CdS has optical properties which are very interesting with respect to photonic applications. It requires further research to understand the mechanism of CdS based photonic devices completely. The shifting of fluorescence peak can be used in photonic applications for tuning purposes. Chemical bath deposited films of CdS needs further study in view of better nonlinear optical properties. Multipolar nonlinear optical studies can be carried out in CdS films with a view of finding the origin of second order nonlinearity in the CdS nanostructured thin film. SHG generation can be utilized in all optical devices. The significant enhancement in nonlinear optical properties observed in CdS: Au PVA , CdS:TiO₂ PVA and CdS PVA nanocomposite films can be explored in detail. Much research on the basic electroluminescence properties of CdS based nanocomposites in display devices will be a potential field of future research. Band gap engineering can be explored in CdS based nanocomposites as it gives a behavior of red-shift in the linear optical absorption. CdS:TiO₂ nanocomposite particles can be used in solar cells or in photocatalytic process. These nanocomposite materials can be used to increase the refractive index of the system in designing optical waveguides. On further increasing the size of these nanocomposites, they can be used in random lasing media.



International School of Photonics
Cochin University of Science and Technology
Kochi - 682 022
Kerala, India